



# Tomas Bata University in Zlín

## Faculty of Technology

Doctoral thesis

### **Electronic properties of polysilylenes studied *in silico* on oligomers in various conformations**

**Elektronové vlastnosti polysilylenů studované výpočty na  
oligomerech v různých konformacích**

Author: **Ing. Barbora Hanulíková**

Study programme: Chemistry and materials technology P2808

Study course: Technology of macromolecular compounds 2808V006

Supervisor: doc. Ing. et Ing. Ivo Kuřitka Ph.D. et Ph.D.

Zlín, June 2016



## **ACKNOWLEDGEMENT**

First of all, I would like to express my sincere gratitude to my supervisor assoc. prof. Ing. et Ing. Ivo Kuřitka Ph.D. et Ph.D. for his guidance and advices during my study.

I am grateful to prof. Ing. Petr Sáha, CSc. for creation of excellent academic and social environment and for giving me the opportunity to participate on the project of Centre of Polymer Systems.

My thanks also belong to my colleagues, friends, my family and every single person who helped me during my doctoral study.

The financial support granted to my research work by the funding providers is partially addressed and acknowledged in the respective places in my published or submitted papers whenever the opportunity to do so was. Here, I would like to thank the Centre of Polymer Systems at the University Institute of the Tomas Bata University in Zlín for support during my studies.

# TABLE OF CONTENTS

ABSTRACT .....	i
ABSTRAKT .....	ii
1. INTRODUCTION .....	1
2. POLYSILYLENES .....	2
3. COMPUTATIONAL CHEMISTRY .....	6
3.1 Computational theory .....	6
3.1.1 <i>Hartree-Fock theory</i> .....	7
3.1.2 <i>Density functional theory</i> .....	7
3.1.3 <i>Calculated properties</i> .....	8
4. THEORY AND EXPERIMENTS .....	9
4.1 Equilibrium geometry .....	9
4.2 Excitation process .....	10
5. AIMS OF WORK .....	12
6. COMPUTATIONAL METHODS .....	13
6.1 Geometry optimization .....	13
6.2 Energy of excitation transitions .....	14
6.3 Energy of non-bonding interactions .....	14
7. SUMMARY OF RESULTS .....	15
7.1 Conformational defect in oligosilylene backbone .....	15
7.2 Oligo[methyl(phenyl)silylene] conformation .....	18
7.3 Stabilization of conformational defect by non-bonding interactions .....	19
7.4 Conformational defect in oligosilylene ions – A model for polarons on polysilylene chain .....	24
8. CONCLUSIONS .....	27
9. CLOSING REMARKS .....	29
9.1 Contributions to science and technology .....	29
9.2 Ongoing research and future prospective .....	29
REFERENCES .....	30
LIST OF FIGURES .....	38
LIST OF ABBREVIATIONS .....	39

LIST OF PUBLICATIONS .....	41
CONFERENCE LIST .....	42
CURRICULUM VITAE .....	43
APPENDIX .....	44



## ABSTRACT

Polysilylenes are materials that have potential application as active layers in electronics, active optical elements, photo- and electron resists, macroinitiators, ceramic precursors etc. Their properties are significantly affected by conformation of their backbones because their  $\sigma$ -electrons are conjugated and thus any modification of a backbone arrangement involves corresponding response in  $\sigma$ -conjugation extent and any change on the electron level naturally causes an alteration in final material properties. One of the causes definitely influencing the  $\sigma$ -conjugation is a conformational defect in the backbone that can be represented by some kind of a bend. However, bends are inevitable parts of chains of any polymers as they can be regarded as sites, which enable backbone folding into a regular arrangement or to the contrary can increase random disorder.

This doctoral thesis is focused on the theoretical description of electronic properties of alkyl- and aryl-substituted oligosilylenes which are significantly dependent on the structural arrangement of their silicon backbone. The main aim of the work is modelling of a conformational defect, which comprises a kink in the chain. The excitation process was evaluated in such disrupted structures in neutral and charged (polaron modelling) molecules. Furthermore, stabilization of a kink by non-bonding interactions was also considered. The goal was to discover if this kink is viable type of defect, which can occur in real polysilylene chains.

Density functional theory was used as a tool for investigation of geometry and electronic properties of several sets of oligosilylene structures up to tridecamers with and without an introduced kink. Conformational studies, which were performed mainly on tetrasilylenes with various side groups, were indispensable part of the work. The choice of model side groups was pointed towards selection of practically relevant and most reported polysilylene materials in experimental literature as poly(dimethyl)silylene, poly[cyclohexyl(methyl)silylene] and namely poly[methyl(phenyl)silylene].

The thesis has been prepared as a thematically arranged collection of papers published with accompanying texts.

### **Keywords:**

Conformation, DFT (density functional theory), defect, kink, oligosilylenes, polaron

## ABSTRAKT

Polysilyleny jsou materiály, které mají aplikační potenciál jako aktivní vrstvy v elektronice, opticky aktivní elementy, foto- a elektronové rezisty, makroiniciátory, prekurzory v keramice apod. Jejich vlastnosti jsou značně ovlivněny konformací hlavních řetězců, protože jejich  $\sigma$ -elektrony jsou konjugovány, a proto jakákoliv změna v konformaci vyvolá odpovídající změnu v  $\sigma$ -konjugaci a tím změnu v celkových elektronových vlastnostech materiálu. Jedním z faktorů, který dozajista způsobuje tyto změny, je konformační defekt na řetězci, který může být tvořen například jeho ohybem. Ohyby hlavních řetězců jsou nevyhnutelnou součástí polymerů a slouží jako místa, která umožňují poskládání řetězců do uspořádaných struktur nebo naopak, zvětšují nahodilou neuspořádanost.

Disertační práce se zabývá teoretickým popisem elektronových vlastností alkyl- a aryl-substituovaných oligosilylenů, které jsou značně závislé na strukturním uspořádání jejich křemíkového řetězce. Hlavním cílem práce je modelování konformačního defektu, který je reprezentován ohybem v řetězci. Konformačně narušené řetězce byly studovány z hlediska excitačního procesu, a to v neutrálních molekulách a ionech (modelujících polarony). Dále byl uvažován příspěvek nevazebných interakcí ke stabilizaci ohybu, čímž bylo posouzeno, zda je možné, aby se tento ohyb vyskytoval v reálných řetězcích polysilylenů.

Pro popis geometrie a elektronových vlastností byla použita teorie funkcionalu hustoty, přičemž výpočty byly aplikovány na několik sad oligosilylenových struktur až do velikosti tridekameru a to s vloženým ohybem řetězce i bez něj. Nezbytnou součástí práce byly také studie konformací, které byly provedeny na tetrasilylenech s různými vedlejšími skupinami, jejichž výběr směřoval k polydimethylsilylenu, polycyklohexylmethylsilylenu a především k polyfenylmethylsilylenu, jakožto k nejčastěji experimentálně studovaným polysilylenům.

Tato disertační práce byla vypracována jako tematicky uspořádaný soubor uveřejněných prací s průvodním textem.

### **Klíčová slova:**

Konformace, DFT (density functional theory – teorie funkcionalů hustoty), defekt, ohyb, oligosilyleny, polaron



# 1. INTRODUCTION

Computational chemistry, which is used for modelling of molecular systems and calculation of their properties, has undergone development on two different levels. The first was the development of theories of quantum chemistry (QC) in the beginning of 20<sup>th</sup> century, from which models used in present days have been subsequently established. However, until the 1990s computational chemistry was significantly limited by capabilities of personal computers used at that time, and it was also a privilege of scientists, who were skilled in programming of software and operational systems. Therefore, true development has started in 1990s and followed the evolution of computers and computational software. This has led to present situation that offers various computational software available for general scientific public. Computational chemistry has become an important part of research and gained a stable position in the scientific areas such as chemistry, physics and biology. The significance of various modelling methods has also been supported by the rise of special term *in silico* (analogous to *in vivo*, *in vitro*) that describes studies performed with modelling, calculation and computer simulation. Main advantages of computational chemistry lie in the opportunity to model various systems and situations that would consume significant time and resources in laboratory experiment. For example, if new derivatives of substance are to be synthesized, calculation of several molecules can be done first and only the derivatives with required properties thus can be chosen for preparation. For example, calculations of various spectra performed with organic compounds are given in refs. [1, 2, 3, 4].

Polysilylenes are materials with interesting electrical properties that are crucial for all of their electrical, optical and optoelectrical applications due to their electronic structure and photoelectrical properties caused by the effect of  $\sigma$ -electron delocalization along the main chain composed from single bonded silicon (Si) atoms. An extent of delocalization is given by overlapping of  $\sigma$ -orbital lobes and that is strongly dependent on the conformation of backbone, as was shown by experimental measurements.

Therefore, the thesis is focused on the description of conformational defect in polysilylene backbones and considers a defect – a kink – and its properties and stability in neutral and charged state by methods of computational chemistry, precisely by density functional theory (DFT). Such investigation can contribute to interpretation of experimentally observed phenomena as well as to prediction of new features in virtual (logical) experiments.

The thesis has been prepared as a thematically arranged collection of three already published papers and two papers at the stage of manuscript with accompanying texts, whose full texts can be found in Appendix.

## 2. POLYSILYLENES

Polysilylenes (also called linear polysilanes, polyorganosilylenes) consist of silicon atoms, which are bonded through interaction of  $\sigma$ -electrons in  $sp^3$  hybridized orbitals. In fact, several types of interactions, which are depicted in Fig. 1A, can be found in these structures. The first involves interaction of two  $sp^3$  orbital lobes of adjacent Si atoms. Their overlapping enables formation of  $\sigma$ -bonds and it is characterized by vicinal resonance integral ( $\beta_{vic}$ ). Another interaction is provided by  $sp^3$  orbital lobes of the same atom and it is responsible for  $\sigma$ -electron delocalization along the backbone and formation of  $\sigma$ -conjugated structure. This interaction is described by geminal resonance integral ( $\beta_{gem}$ ). Moreover, the ratio  $\beta_{vic}/\beta_{gem}$  serves to evaluation of an extent of the delocalization with maximum in the value of 1. On the contrary, strong localization is expressed by  $\beta_{vic}/\beta_{gem}$  value close to 0. This description has been adopted and applied on polysilylenes from Sandorfy C and Sandorfy H model that was originally defined for alkane chains [5]. However, as can be seen in Fig. 1A, other integrals  $\beta_{1,3}$  and  $\beta_{1,4}$  are presented. These interactions express the conformational dependence of the orbitals arrangement and are described by ladder C and ladder H models [6, 7, 8, 9, 10]. In spite of the often used comparison of polysilylenes with  $\pi$ -conjugated carbon backbones, such as polyacetylenes, their real carbon analogues are polymers with single  $\sigma$ -bonds between carbon (C) atoms. However, carbon-based structures do not evince  $\sigma$ -conjugation and their properties are different, for instance, Si-Si bond distances are longer, photostability of Si-structures is lower and charge carrier mobility is higher than those of C-polymers [10].

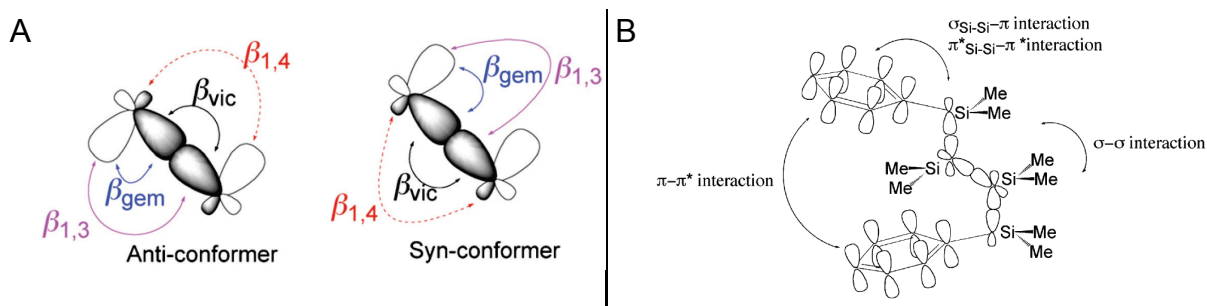


Fig. 1: Orbitals (A) and their intramolecular interaction (B) in polysilylene chain [10]

In addition, Fig. 1B illustrates several types of intramolecular interactions which occur in polysilylenes. These interactions are dependent on the attached functional groups, which strongly influence final material properties. The role of alkyl and aryl substituents has been thoroughly examined for poly[methyl(phenyl)silane] (PMPSi). This polymer is interesting for investigation since it contains combination of  $\sigma$ - as well as  $\pi$ -bonds and it is processable and accessible for production [11, 12].



520–540 nm, respectively [8, 9, 13, 17]. Energy of  $(\sigma\text{-}\sigma^*)$  and  ${}^1(\sigma\text{-}\pi^*)^{\text{CT}}$  states is influenced by conformational changes, while  ${}^1(\sigma\text{-}\sigma^*)^{\text{CT}}$  is temperature-dependent and with higher temperature shifts to higher wavelengths [18].

CT states characterise result of charge transport process that is accompanied by polaron quasiparticle formation in PMPSi. As was described in ref. [19], polaron quasiparticle is here described as charged molecule (cation or anion), whose atoms are shifted to another equilibrium position due to presence of charge and its potential energy minimum (with respect to neutral state) is characterised by polaron binding energy  $E_p$  as depicted in Fig. 3 [20, 21, 22, 23, 24].

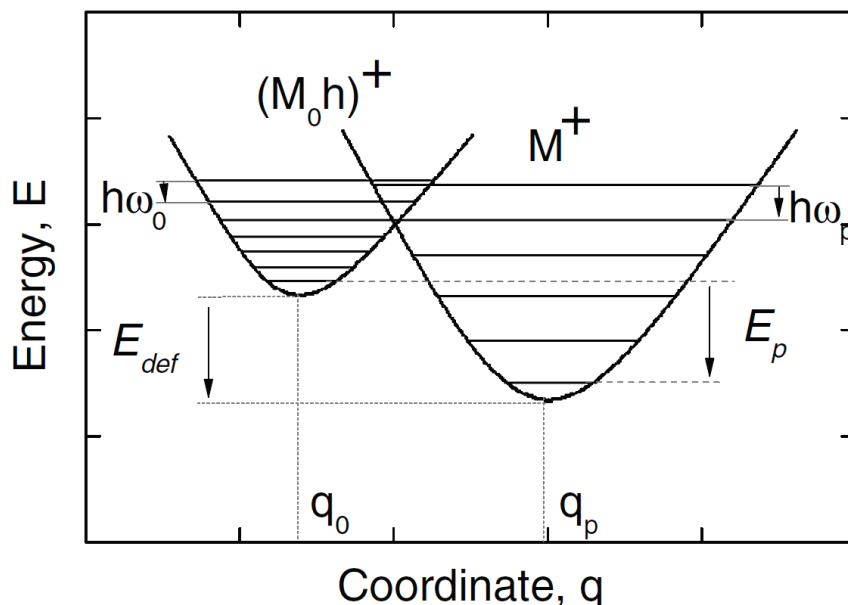


Fig. 3: Potential energy curves of neutral and polaron geometry [20]

An influence of conformational changes on CT and  $\sigma$ -conjugation is often studied by means of QC calculations, which allow to better understand to unique properties of polysilylenes (photosensitivity, photoconductivity). A few examples of theoretical works concerning PMPSi are given in ref. [25, 26] and alkyl-substituted analogues in various conformations in [27, 28]. Excited states and geometries were described theoretically in a study of peralkylated oligosilylenes [29, 30], which describes the excitation and emission mechanism up to the backbone length of 16 repeating units. Even though that long backbones of polysilylenes enable clear emission behaviour, short chains of di- or trisilylenes do not fluoresce at all. This issue was studied in [31, 32] and revealed shallow energy minima of excited singlet states and funnels that enable efficient deactivation of excited states. Currency of the research, such as above mentioned [28, 29], has proven that this topic is still at the forefront of scientific interest.

As stated above, conformation of Si backbone has direct influence on  $\sigma$ -conjugation and electronic properties related to it as was studied on permethylated oligosilylenes, for instance, in [2, 33]. In addition, other than linear

backbones were described in [34], which is dedicated to branched, network and dendrimer polysilanes. Further, chemical character of side groups and their size affect conformation and also polysilylene properties [35, 36 37], as in case of optically active side groups [38]. The crucial parameter that affects the final conformation and thus properties is the value of a dihedral angle of four consecutive Si atoms ( $\omega$ ). Molecular energy dependence on  $\omega$  was published in many papers and the first complex nomenclature was suggested by Michl and West in ref. [39]. Conformations were previously often investigated for tetrasilylene and it was found that  $\omega = 40^\circ \rightarrow$  *cisoid*,  $\omega = 60^\circ \rightarrow$  *gauche*,  $\omega = 90^\circ \rightarrow$  *ortho*,  $\omega = 150^\circ \rightarrow$  *deviant* and  $\omega = 165^\circ \rightarrow$  *transoid* are stable arrangements. The preferred ordering in polymer-size chains with bulky substituents, such as phenyl groups, is of *deviant* or *transoid* type along the backbone, which is thus twisted into the helix of 7/3 or 15/7 size, respectively [40]. Other conformers, where  $\omega = 0^\circ \rightarrow$  *syn*,  $\omega = 120^\circ \rightarrow$  *eclipsed* and  $\omega = 180^\circ \rightarrow$  *anti*, are not energetically favourable even though all-*anti* chain provides maximum of the  $\sigma$ -conjugation [10, 12, 41]. On the other hand, all-*anti* arrangement is not completely unavailable and can be found in polysilylenes with small side groups, for example in permethylated backbones [42].

### 3. COMPUTATIONAL CHEMISTRY

The large number of molecular quantum chemical investigations is based on theories assembled by Hartree and Fock (Hartree-Fock theory, HF) and by Hohenberg, Kohn, Sham (Density Functional Theory, DFT). These theories have become a stable base for computational chemists because they are able to treat quite large systems and provide good agreement with experimental results with satisfactory computational time, especially DFT [43, 44, 45].

#### 3.1 Computational theory

Eq. 1 is general expression of Schrödinger equation, which is defined by Hamiltonian operator ( $\hat{H}$ ), wavefunction ( $\Psi$ ) and numerical value of energy ( $E$ ) of the state that is defined by  $\Psi$  [46, 47, 48, 49].

$$\hat{H}\Psi = E\Psi \quad (1)$$

$\hat{H}$  corresponds to the total energy of the molecules, and can be divided into several components that are given in eq. 2. It comprises kinetic energy of electrons  $i$  and  $j$  and nuclei  $A$  and  $B$ , where  $M_A$  is mass of nucleus and three coulomb terms, where  $Z_A, Z_B$  are nuclear charges. These terms describe as follows electrons-nuclei attractive interaction and repulsive interaction between electrons and nuclei and these interactions are dependent on the distance between electron and nucleus ( $x_{iA}$ ), electrons ( $x_{ij}$ ) and nuclei ( $X_{AB}$ ), respectively [45, 46, 47, 48].

$$\hat{H} = -\frac{1}{2} \sum_i^{electrons} \nabla_i^2 - \frac{1}{2} \sum_A^{nuclei} \frac{1}{M_A} \nabla_A^2 - \sum_i^{electrons} \sum_A^{nuclei} \frac{Z_A}{x_{iA}} + \sum_{i<j}^{electrons} \frac{1}{x_{ij}} + \sum_{A<B}^{nuclei} \frac{Z_A Z_B}{X_{AB}} \quad (2)$$

$\Psi$  describes a state of the system and it is dependent on  $3N$  of spatial coordinates,  $N$  spin coordinates of electrons and  $3M$  spatial coordinates of nuclei, where  $N$  and  $M$  is the number of electrons and nuclei of the system, respectively [50].

Schrödinger equation cannot be solved exactly for many-electron systems and therefore, approximations must be done. This is the point where differences between theoretically calculated values and results from experiment originate.

Born-Oppenheimer (frozen core) approximation excludes the influence of nuclear motion from Hamiltonian, because nuclei are much heavier than electrons. Since distance between nuclei  $X_{AB}$  does not alter in this approximation, the term in eq. 2 describing electrostatic interaction of nuclei is constant and can be designed as  $E^{nuc}$ . Hamiltonian and thus Schrödinger equation is transformed to the electronic form by this approximation and provides energy of electrons ( $E^{el}$ ) as a result. However, total energy of system consists of  $E^{el}$  and  $E^{nuc}$  [51].

### 3.1.1 Hartree-Fock theory

HF theory simplifies the complexity of N-electron wavefunction  $\Psi$ . It is here replaced by N one-electron wavefunctions – spin orbitals, which are arranged into antisymmetrical Slater determinant. Through steps of variational principle, the energy of Slater determinant is minimized and thus energy of system (HF energy,  $E_{HF}$ ) is minimized too.  $E_{HF}$  is dependent on the spin orbitals, whose definition that leads to minimal  $E_{HF}$ , is given by Hartree-Fock equations. These equations involve Fock operator  $\hat{f}$  (given in eq. 3) that similarly as  $\hat{H}$  describes kinetic and potential energy, however of one electron and nuclei [50].

$$\hat{f}_i = -\frac{1}{2}\nabla_i^2 - \sum_A^{nuclei} \frac{Z_A}{x_{iA}} + V_{HF}(i) \quad (3)$$

A problem that arises from the description of repulsive interactions between two electrons as given by  $1/x_{ij}$  in eq. 2 is in eq. 3 solved with introduction of  $V_{HF}(i)$  that is time-averaged repulsive potential of one electron due to other remaining electrons. HF approximation thus assumes that particular electron moves in the average field formed by other electrons. However, electron motions are in fact interdependent and thus correlated and resulted  $E_{HF}$  value is higher than would be the energy calculated from Schrödinger equation, in which electron motions are fully correlated. This difference is the direct result of the ignorance of electron correlation, which is the weak point of this theory [45, 50].

On the other hand, HF theory level offers its specific benefits. Contributions to  $E_{HF}$  are summarized by three operators – kinetic, Coulomb and exchange and the exchange operator is the advantage of HF theory as it solves the problem of self-interaction of electron and thus  $E_{HF}$  is not influenced by this. Detailed definition can be found in ref. [50].

### 3.1.2 Density functional theory

Density functional theory is established on the work of Hohenberg, Kohn and Sham [52, 53]. The main idea that ground state properties of the many electron system can be described by electron density was presented in Hohenberg-Kohn's first theorem, which states that ground state properties of many-electron system can be determined as a functional only of ground state electron density. Further, the second Hohenberg-Kohn's theorem explains how the true ground state density is obtained by application of variational principle [53].

Total electronic energy in DFT is treated as a sum of electron-nuclear interaction, electron-electron repulsion and kinetic energy. These terms are here described with electron density ( $\rho_0$ ) as they are functionals of electron density  $V_{en}[\rho_0]$ ,  $V_{ee}[\rho_0]$  and  $T[\rho_0]$ , respectively.  $V_{ee}[\rho_0]$  and  $T[\rho_0]$  operators are system

independent and are expressed by Hohenberg-Kohn functional  $F_{HK}[\rho_0]$ . Thus, exact knowledge of  $F_{HK}[\rho_0]$  would lead to exact ground state energy of any kind of molecule. However, exact  $F_{HK}[\rho_0]$  is unknown [50, 51, 54, 55].

The above described density functionals represents the main difference from HF theory, where these energies are based on many-electron wavefunction  $\Psi$ . Moreover, DFT also takes into account electron correlation, which was completely neglected in HF theory. The exact solution of exchange-correlation term is, however unknown, and it is approximated by various DFT functionals and results are thus often dependent on the type of the used exchange-correlation functional. DFT functionals can be divided into local density functionals [52], which rely on local spin density and functionals emerging from generalized gradient approximations [56, 57] and non-local, so-called hybrid functionals, which incorporates the part of exact (Hartree-Fock) exchange [58, 59].

To summarize HF theory and DFT, DFT considers the correlation of electrons that is advantageous in comparison with HF theory. On the other hand, exchange-correlation functional is not exactly known and it is approximated by various types of functionals that influence the final results. Hybrid functionals, which combine correlation part of DFT and exact exchange from HF, are very good performing as they prevent the most significant weaknesses of both HF and DFT.

### 3.1.3 Calculated properties

Quantum chemical theories are able to deal with many different tasks. Information on energy of molecule and orbitals energies, equilibrium geometry and transition state geometry, energy profiles and conformer search, reaction mechanisms including reaction products and reactants, various spectra (IR, UV-Vis, Raman, NMR), atomic charges, orbital occupancies, dipole moments and many others can be obtained from calculations [60].



## 4. THEORY AND EXPERIMENTS

Theoretical results of calculations are often compared with experiments. The reasons are different but their main goal is to describe chemical systems as deeply as possible and confirm this information by fundamental theories. For instance, results from experiments can serve as initial and valid references that enable to find the most proper theoretical approach. This assumption is based on the fact that all computational theories, which are used in practice, are various approximations of Schrödinger equation and therefore the perfect match between theory and experiment cannot be reached. On the other hand, predictive and explanatory power of QC can be used for prediction of experimental data and their analysis. Pure theoretical investigations have also their stable place in the molecular characterization field because they can reveal the trends of molecular behaviour considering any conceivable influences.

### 4.1 Equilibrium geometry

Bond between two nuclei is provided by an interaction of electrons from individual atomic orbitals (AO). The lobes of AO overlap and form space that is shared by two electrons. For diatomic molecule, a bond length is given as an equilibrium distance of nuclei ( $r$ ) when potential energy reaches minimum as can be seen in Fig. 4.

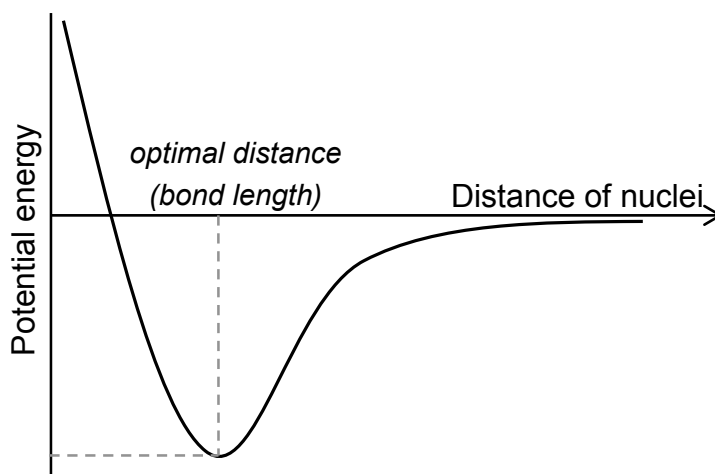


Fig. 4: One-dimensional potential energy curve for diatomic molecule

Equilibrium geometry of many-atomic molecules can therefore be regarded as optimal position of each nucleus. Energy minima or maxima of such systems are described with force constants ( $\kappa$ ) together with frequency of vibration [45]. Eq. 4 reflects the way of energy minimum and maximum differentiation using derivation rules. Eq. 5 (where  $\tilde{\nu}$  is wavenumber and  $m_1$  and  $m_2$  are atomic masses) then complements relation between force constant and wavenumber, whose values are used for construction of calculated vibrational spectra [61, 62, 63, 64].

It is confirmed in various publications that differences in experimentally obtained results by X-ray diffraction (XRD) [65, 66] and theoretically determined geometries are in hundredths of Ångströms (Å) for lengths and up to several degrees (°) for angles [45, 67, 68, 69]. These differences mainly origin in inability to simulate exactly same conditions in the model as in the experiment, especially the effect of crystal packing, which can be solved e. g. by the introduction of periodic boundary conditions into used system of equations describing the problem. Thus, calculations are usually set for isolated molecules that are more similar to molecules in gaseous phase, whose geometry is experimentally studied by microwave spectroscopy or electron diffraction [70, 70, 72]. However, studied systems are often large molecules of organic character (polymers, oligomers, proteins), not available in gas phase and therefore calculation of such large molecules on the proper level of theory or alternatively modelling of crystal lattice require advanced software and hardware equipment and long computational time.

$$\kappa = \frac{\partial^2 E}{\partial r^2} > 0 \rightarrow \text{energy minimum}; \quad \frac{\partial E}{\partial r} = 0 \rightarrow \text{minimum or maximum} \quad (4)$$

$$\tilde{\nu} = \frac{1}{2\pi} \sqrt{\frac{\kappa}{\mu}}, \quad \text{where } \mu = \frac{m_1 m_2}{m_1 + m_2} \quad (5)$$

## 4.2 Excitation process

An exposition to ultraviolet and visible (UV-Vis) radiation affects molecules to a significant extent. Electrons, which are in ground state, are excited to higher energy levels – singlet or triplet, according to presence of spin-paired or spin-unpaired electrons in a molecule (i.e. according to electronic configuration of atoms and molecules). Further, electrons are considered as occupants of molecular orbitals (MO), and excitation can therefore be regarded as transition from one MO to another, e.g. from highest occupied molecular orbital (HOMO) to lowest unoccupied molecular orbital (LUMO). Received energy is subsequently emitted by fluorescence ( $10^{-5}$ – $10^{-10}$  s) or phosphorescence ( $10^{-2}$ –days) mechanism. The first process is immediate and involves transition from excited to ground singlet state, while the latter is longer in time as it is related with transition from excited singlet to triplet state and then to ground state [25, 73, 74]. Every molecule has its own characteristic absorption behaviour that is complementary to its emission profile. These spectra consist of broad bands located at particular wavelengths, which carry information about electron transition. Transitions are realized from bonding ( $\sigma$ ,  $\pi$ ) or non-bonding (n) orbital to anti-bonding orbital ( $\sigma^*$ ,  $\pi^*$ ) and can be of  $\sigma \rightarrow \sigma^*$ ,  $\pi \rightarrow \pi^*$ ,  $n \rightarrow \pi^*$ ,  $n \rightarrow \sigma^*$  character [75, 76].

A contribution of theoretically calculated absorption/emission spectra does not lie only in the values of wavelengths and intensities, but also in the description of the whole excitation process. It means that energy and identification of all MO which are involved in particular transitions is available together with respect to amount each MO involvement. Distribution of MO indicates locations of electrons and effects, such as electron transfer. Difference in absorption wavelengths between theoretical calculation and experimental values is inevitably experienced, however, it is relatively small and can be refined by certain procedures, for example, for B3LYP/6-311G calculation of organic acids it is around 0.1–0.5 eV, as quoted in ref. [77, 78].

## 5. AIMS OF WORK

The doctoral thesis is mainly focused on a theoretical description of the influence of conformational defects on electronic structure and processes occurring during the electron excitation in two types of oligosilylene molecules; oligo[(dimethyl)silylene] and oligo[methyl(phenyl)silylene] which have been selected as representatives for alkyl and aryl substituted polysilylenes. Relaxation processes in excited state are studied as well, however the scope of these calculations is limited due to excessive demand for computational time.

The electronic structure of  $\sigma$ -conjugated linear polysilylenes is extremely sensitive to conformational disorder. The simplest conformational defect plausible on linear silicon chain is a kink formed by four consecutive silicon atoms in other than ideal conformation for maximal  $\sigma$ -conjugation. Therefore, the crucial part of the work is investigation of influence of the kink on electronic behaviour and molecular stability (total energy) of given oligomers in neutral or charged state (ions). The basic questions of kink stabilization by non-bonding interactions between polymer side groups are elucidated with conformational studies. Results, obtained for series of oligomers are further extrapolated and generalized for long polymer chains. These theoretical findings are corroborated with experimental spectroscopic data available partially from previous work and partially from the literature. Chosen polymers belongs mainly to the family of processable polysilylenes with alkyl and/or aryl side groups imparting solubility as well as many other structural and functional properties. The study contributes to explanation of features observable namely in thin polymer films which is the main polysilylene form used to electronic and resist applications. The properties relevant for making of silicon carbide ceramics are not in the focus of this study.

## 6. COMPUTATIONAL METHODS

Spartan software v. 08 and 14 (Wavefunction, Inc., Irvine, CA) was used in all cases of calculations [79].

### 6.1 Geometry optimization

Equilibrium geometries of studied oligo[(dimethyl)silylene]s (ODMSi<sub>n</sub>, n is the number of repeating units, n = 1–13) and oligo[methyl(phenyl)silylene]s (OMPSi<sub>n</sub>, n = 1–10) were calculated firstly at semi-empirical level with PM3 model and then using DFT and B3LYP functional. The 6-31G\* basis set was used overall the work, as it is appropriate for involved elements (H, C, Si). Calculations were set in vacuum. Geometry specifications for all presented studies are described below.

**Paper I** has been focused on the modelling of conformational defect, whose geometry was obtained according to following steps. First, an energy profile of oligosilylene conformers with  $n \geq 4$  was calculated at PM3 level. An observed property was the value of dihedral angle that consists from four subsequent Si atoms and thus forms a kink in a chain. The most convenient kinks were approximately of *gauche* conformation and were chosen as an initial guess for DFT optimization of OMPSi<sub>4-10</sub> and ODMSi<sub>4-13</sub> with an introduced kink. As the number of Si atoms in backbone increased, the kink could have been modelled in more positions on the backbone. Therefore, five sets of oligosilylenes (four with a kink in different backbone position and one without any kink) were obtained and used for following investigation. Equilibrium geometries of OMPSi<sub>n</sub> obtained by this way were also used for study of charged oligomers described in **Paper V**.

OMPSi<sub>10</sub> with all Si dihedral angles locked have been investigated in **Paper II**. Backbone geometries were constrained with  $\omega = 120^\circ\text{--}180^\circ$  and the kink dihedral angle was set to  $60^\circ$ . Molecules, which were virtually prepared according to these requirements, were then optimized. Thus, the main contribution to geometry optimization was related with rotation of phenyl rings.

Five different tetramers, represented by OMPSi<sub>4</sub>, ODMSi<sub>4</sub>, tetra(silylene) (OSi<sub>4</sub>), tetra[cyclohexyl(methyl)silylene] (cyc-HMSi<sub>4</sub>) and carbonaceous analogue of OMPSi<sub>4</sub> (MPC<sub>4</sub>) have been the main aim of the **Paper III** and **Paper IV**. Equilibrium geometries were obtained with constrained dihedral angles  $\omega$  in the range of  $180^\circ$  for ODMSi<sub>4</sub>, OSi<sub>4</sub>, cyc-HMSi<sub>4</sub> and MPC<sub>4</sub> with a step of  $10^\circ$  and  $20^\circ$ , respectively. The range of studied  $\omega$  was  $360^\circ$  for OMPSi<sub>4</sub> with a  $10^\circ$  step, i.e. from  $0^\circ$  (modelling ideal kink *syn*) through  $180^\circ$  (modelling ideal linear *anti*) back to  $-0^\circ$ . These geometries served for conformational studies that led to further characterisation of a kink from the viewpoint of its stabilization by non-bonding interaction.

## 6.2 Energy of excitation transitions

Excitation properties including mainly absorption spectra, which are involved in **Paper I** and **Paper II**, were calculated with time dependent DFT method [80, 81] with B3LYP functional and 6-31G\* basis set, according to ref. [82, 83, 84]. Optimal geometries of excited states were not determined with the use of chosen functional therefore the relaxation processes and luminescence in studied molecules were not investigated although experimental data on fluorescence were available.

## 6.3 Energy of non-bonding interactions

Investigation of non-bonding interactions involvement into molecular energy of studied conformers of OMPSi<sub>10</sub> and several tetrasilylenes as described in **Paper II**, **Paper III** and **Paper IV** was also performed with DFT and 6-31G\* basis set, however density functionals were chosen with the respect of involvement of the dispersion term. B3LYP hybrid functional is considered among computational chemist as a reliable tool for calculations; however it significantly underestimates long range (non-bonding) interactions and treats them poorly. From this reason, M06 functional, which has a very good response under dispersion forces, was used [85] and compared with long-range corrected  $\omega$ B97X-D functional that involves empirical dispersion[86].

These specific functionals were chosen as they are available in used Spartan software, despite the awareness that some other functionals could serve better for comparison with B3LYP, namely CAM-B3LYP or B3LYP-D [87, 88].

The above described selection of functionals allows a virtual experiment based on comparison of three calculated conformational energy profiles with different extent of long range interactions involvement. Hence, it is expected that the increasing contribution of non-bonding interactions will be manifested as increasing either positive or negative energy difference for each conformer enabling thus conformational analysis and comparison between tested model molecules with different chemical structure.

## 7. SUMMARY OF RESULTS

Properties of polysilylene materials are considerably dependent on the degree of  $\sigma$ -electron delocalization, which is provided by overlapping of lobes belonging to Si orbitals. The degree of delocalization (or  $\sigma$ -conjugation) is significantly affected by the backbone conformation. The maximal rate of the  $\sigma$ -conjugation would be reached with all-*anti* conformation of the silicon chain. However, several defects, which disrupt the ideal all-*anti* arrangement, may appear in the real polymer system. The research performed with the aim to clarify these issues has been reported in a series of **Papers I to V** that have been attached to this Doctoral thesis and are available in Appendix.

### 7.1 Conformational defect in oligosilylene backbone

*This chapter summarizes findings published in Paper I.*

One of the conformational defects can be a kink on the polymer backbone that assures, for instance, folding of backbone chains in the semi-crystalline structures. Four consecutive silicon atoms form the kink by rotation along the bond between the second and third Si atom, i.e. by the change of the dihedral angle from the value  $180^\circ$  for all-*anti* conformation (ideal for polysilylenes with small side groups only, polymers with bulky substituents adopt helical arrangement of the chain, see below). In this theoretical work, changes in electronic properties of ODMSi<sub>1-13</sub> and OMPSi<sub>1-10</sub> caused by an introduced kink of approximately *gauche* conformation have been investigated. Obtained equilibrium geometry of defect-less OMPSi<sub>10</sub> corresponds to helical *transoid–deviant* (dihedral angle in the range approx.  $155\text{--}165^\circ$ ) conformation, just due to presence of bulky phenyl side groups that would lead to helical structure in case of polymer with a long backbone chain. The defect-less structure together with oligomers having the kink on various positions are depicted in Fig. 5.

Oligosilylene labels here and through the whole text consist of a figure (10) and a letter (A-D), where the first represents the number of silicon atoms in the backbone (this case “decamer”) and the latter is the kink location. The kink was investigated in as many locations as possible in accordance with the backbone length. The purpose of this was to describe the influence of a kink on the properties regarding its location moving from the edge (Si10–Si7) up to the centre (Si7–Si4) of the backbone. Carbon atoms are coloured in grey, silicon atoms in cyan and hydrogen atom are omitted. The kink is highlighted by red. The structure 10 illustrates the defect-less molecule with disrupted all-*anti* arrangement and the effect of kink introduction to positions from 10A to 10D is clearly visible too. On the contrary, ODMSi<sub>n</sub> structures kept the all-*anti* arrangement with optimal (no kink) case, which can be also found in the Fig. 5.

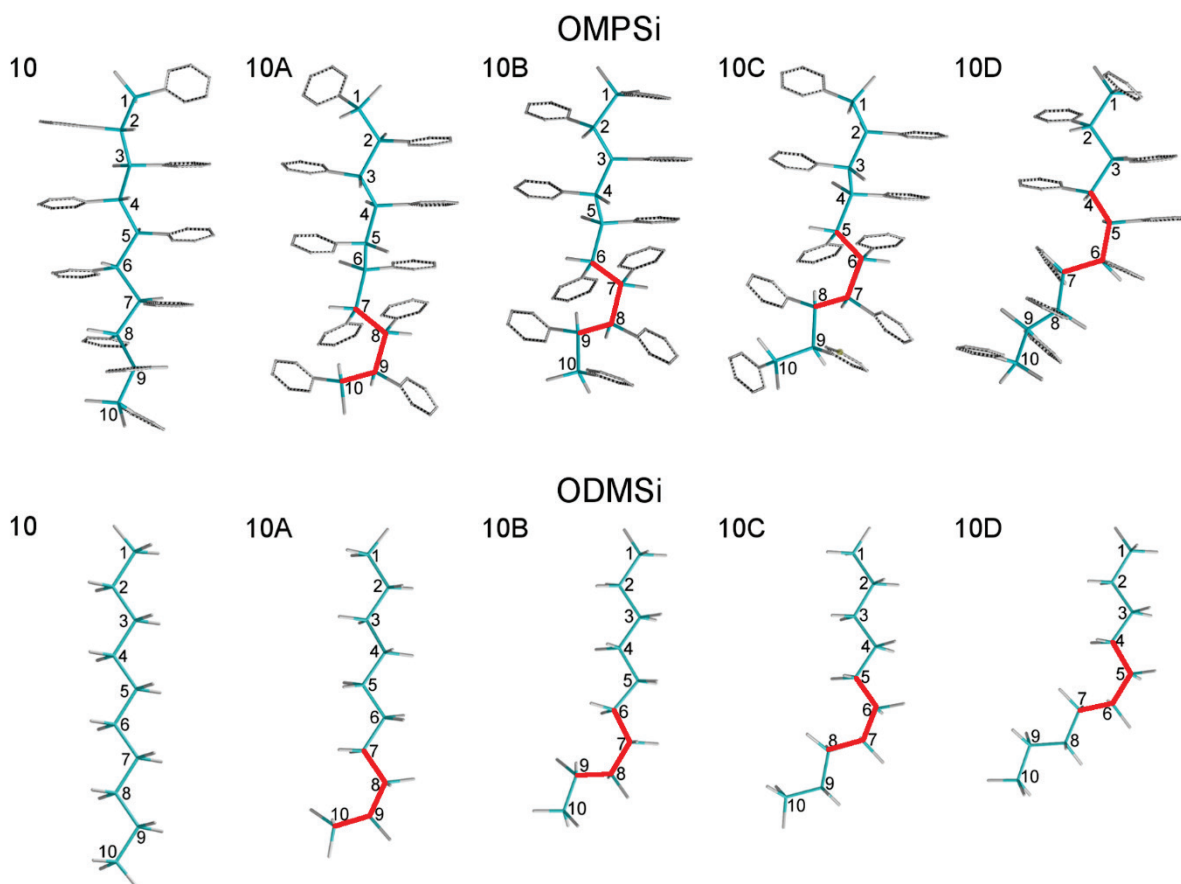


Fig. 5: Optimized helical structures of  $OMPSi_{10}$  without (10) and with a kink (10A–D)

It was discovered that the energy gap between HOMO and LUMO decreases with an increasing length of the backbone chain and therefore  $\lambda_{max}$  evinces bathochromic shift. This dependence is graphically shown in Fig. 6, where the evolution of frontier molecular orbital (FMO) energies with increasing number of backbone units can be seen. Generally, the kink divides the chain into two parts and it can be located at several positions on the backbone (see Fig. 5). Therefore, as the kink alters its position closer to the centre of the particular chain,  $\lambda_{max}$  shifts to lower wavelengths and at the same time energy of HOMO decreases and LUMO energy increases (in other words the bandgap becomes wider).



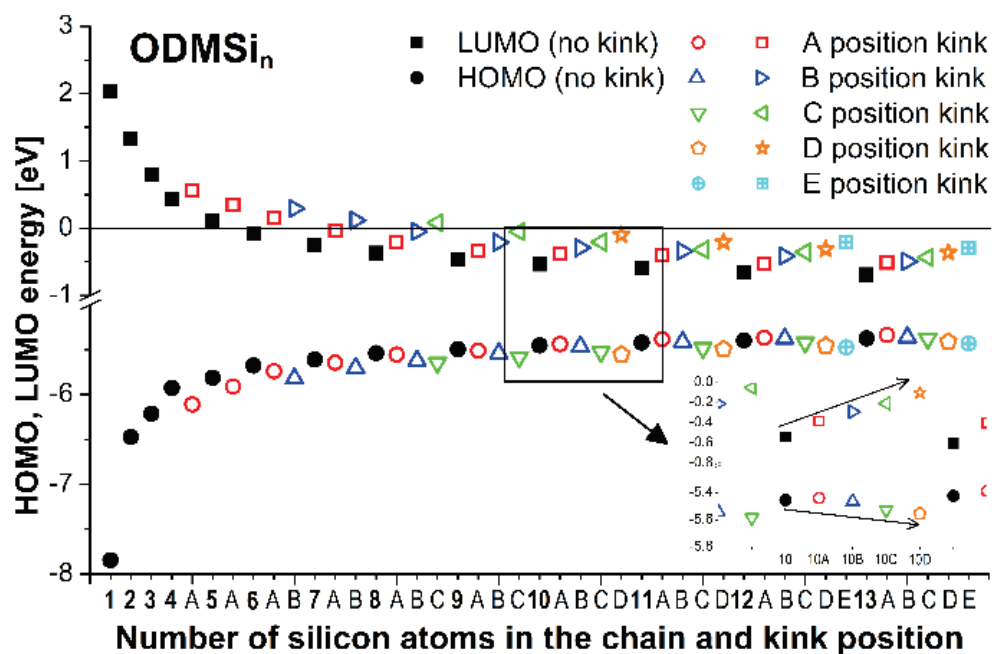
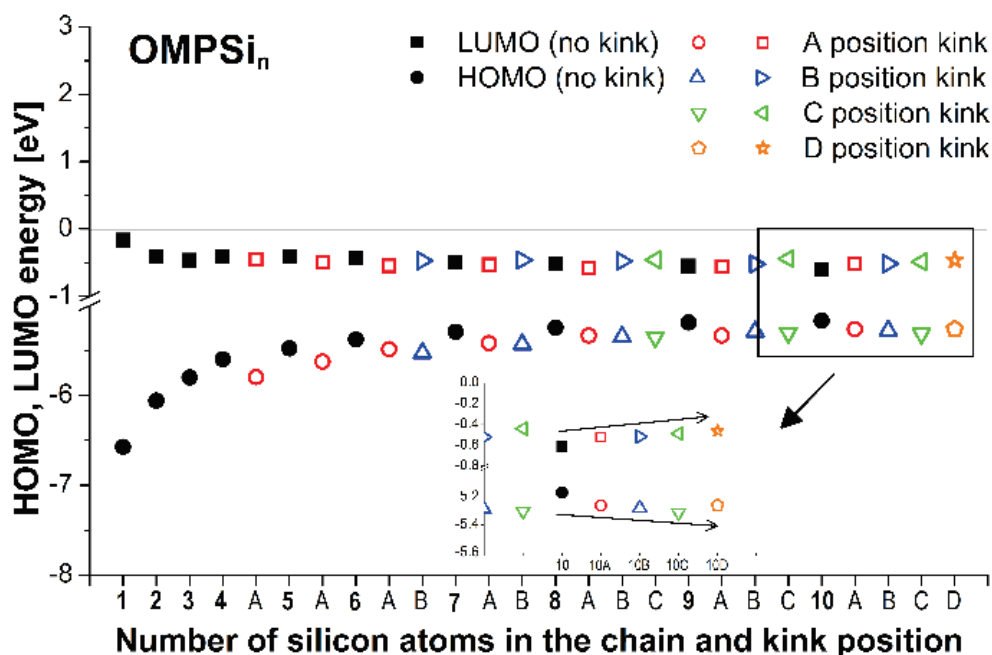


Fig. 6: FMO energies of  $OMPSi_n$  and  $ODMSi_n$  structures

Further, distribution of molecular orbitals was examined. It was found that HOMO and LUMO are distributed symmetrically along backbone in chains without the defect. This is depicted in Fig. 7, where FMO of three molecules of  $OMPSi_n$  are displayed and they represent the symmetrical and asymmetrical cases of FMO distribution along the backbone caused by the presence of a kink in non-central part of the chain and also by phenyl groups. The regularity of FMO distribution is disrupted in chains, where the kink divides the backbone into a two length-unequal parts (chains segments). FMO are in these cases shifted to longer chain segments. This situation is slightly different in  $OMPSi_n$ , where the trend of

$\lambda_{max}$  shift is not so clear. Energies of FMO and their delocalization are, beside the kink, affected also by the presence of phenyl substituents. This influence is more evident for LUMO. This orbital is somewhat contra-intuitively (one would expect its location on phenyl groups) delocalised along the Si chain in case of defect-less chain while strongly located at attached phenyl rings neighbouring the kink introduced to the backbone.

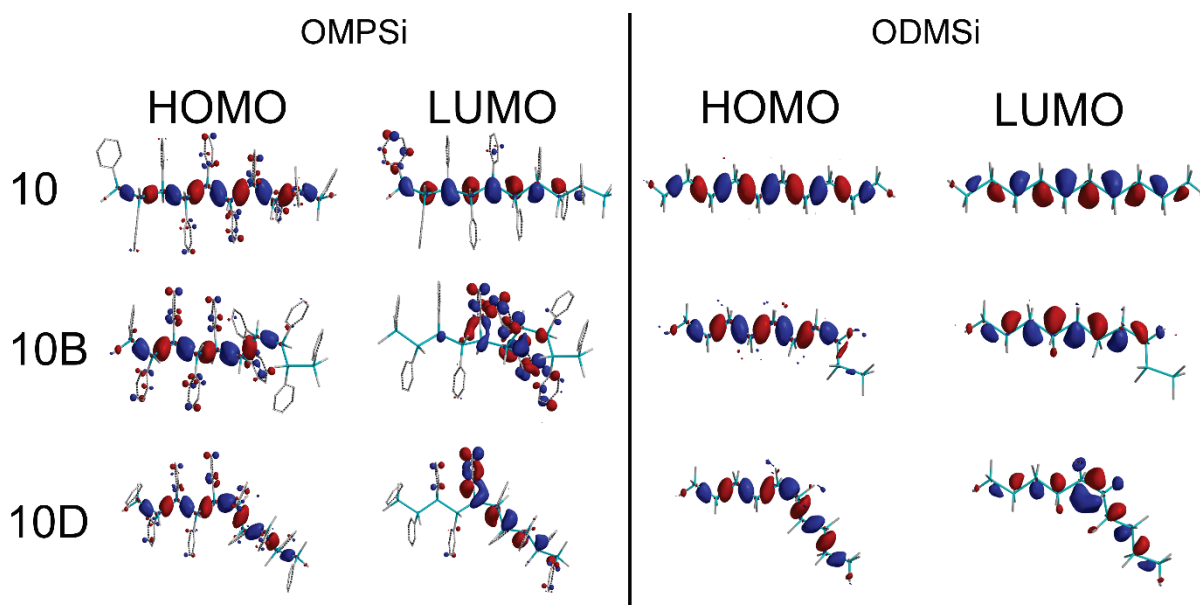


Fig. 7: HOMO and LUMO of OMPSi<sub>10</sub>– 10, 10B and 10D

In addition, a prediction of behaviour of HOMO/LUMO energies for polymer-size backbones of poly[(dimethyl)silylene] (PDMSi) and PMPSi was done with linear regression. HOMO and LUMO energies plotted against  $1/N$  ( $N$  is number of Si atoms in the backbone) were fitted with line. It was found that the introduced kink has negligible effect on FMO energies of substantially long chains. This is expectable because the kink located at A, B, C or D position on the backbone is in the very edge part of chain for  $N \rightarrow \infty$  in this virtual experiment. On the other hand, more than one kink can be present on one chain dividing thus the long chain into segments.

## 7.2 Oligo[methyl(phenyl)silylene] conformation

*This chapter summarizes findings published in Paper II.*

Another part of theoretical description of electronic behaviour of polysilylenes was dedicated only to OMPSi<sub>n</sub> ( $n = 10$ ) which was selected as the most suitable model molecule. The kink of given dihedral angle  $\omega = 60^\circ$  was introduced in the backbone, as described in previous chapter (positions A...D), but moreover all backbone dihedral angles were locked to  $120^\circ, 130^\circ \dots 180^\circ$ , so the conformation from helical to all-*anti* arrangement was investigated. Geometry optimization was thus performed with these dihedral angle constraints.

Fig. 8A depicts the dependence of  $\lambda_{max}$  on the OMPSi<sub>10</sub> backbone dihedral angles. It can be considered that with increasing extent of  $\sigma$ -delocalization the  $\lambda_{max}$  shifts to higher wavelengths. Indeed, a maximum was found at  $\omega=180^\circ$  corresponding to all-*anti* conformation and another local maximum at about  $130\text{--}140^\circ$  corresponding to *eclipsed* conformation. The  $\lambda_{max}$  dependence has a local minimum in the  $\omega$  range of  $140\text{--}160^\circ$ , which means that the delocalization is somewhat disturbed. On the contrary, this range represents the most favourable backbone conformation among tested geometries (see Fig. 8B) and the equilibrium geometry of non-constrained OMPSi<sub>10</sub> molecules too. Hence, it was confirmed that the most stable conformation is the helix with  $\omega = 160\text{--}165^\circ$  regardless the presence of a kink as can be further found in Fig. 8B. The energy gain from conjugation cannot overbalance the steric effect (conformational barrier) and other possible non-bonding interactions of the bulky phenyl substituents imparting thus the helical *transoid-deviant* geometry to the molecule as discussed above. These results have strong implications towards experimentally obtained UV-Vis of PMPSi that have been reinterpreted in the **Paper II**.

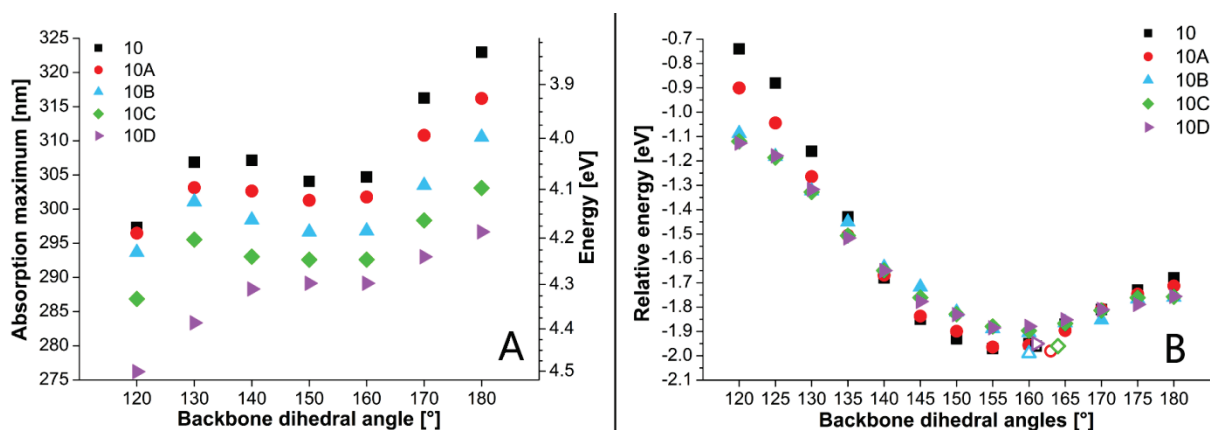


Fig. 8: Absorption maximum (graph panel A) and oligomer energy (B3LYP/6-31G\*) (graph panel B) reported vs. conformation of OMPSi<sub>10</sub> (empty symbols are non-constrained equilibrium geometries of OMPSi<sub>10</sub>)

### 7.3 Stabilization of conformational defect by non-bonding interactions

This chapter summarizes findings published in Paper II, Paper III and Paper IV.

The presumption that a kink in OMPSi<sub>10</sub> structure does not bring any impassable energy disadvantage and therefore it is probably stabilized by phenyl ring non-bonding interactions has been stated previously. Optimized geometries were analysed from the viewpoint of mutual phenyl group distances and angles between their planes. Four phenyl groups in the vicinity of a kink (see Fig. 9A) were analysed. An angle was measured between two phenyl planes and a distance was measured between two plane central points. In total, six pairs of

phenyl groups have been investigated for each decamer (120–180° and A–D). The values were plotted in the form of angle-distance dependence in Fig. 9B, according to ref. [89]. This revealed that adjacent phenyl groups (pair I-II and III-IV, in the figure highlighted by encircling) are in the mutual position suitable for employment of attractive  $\pi$ - $\pi$  interactions. It is possible to find two pairs of phenyl groups in suitable geometry for positive interaction on each sequence of four consecutive Si atoms on an ideal PMPSi chain. Due to its relatively sterically constrained helical *transoid-deviant* geometry, the phenyl groups have alternating orientation along the chain axis hence the pairs are formed by phenyl groups joined to evenly numbered Si atoms and by phenyls joined to odd numbered Si atoms. This arrangement can be seen in Fig. 9A on the sequence of first six Si atoms of the molecule 10B\_180 (left part of the figure). However, the formation of a kink passes over a conformational energy barrier and new order of pairs is arranged so phenyl rings joined to the first and fourth Si atom and phenyl rings joined to the second and third Si atom of the kink occupy positions suitable for attractive  $\pi$ - $\pi$  interaction stabilizing thus the kink conformation.

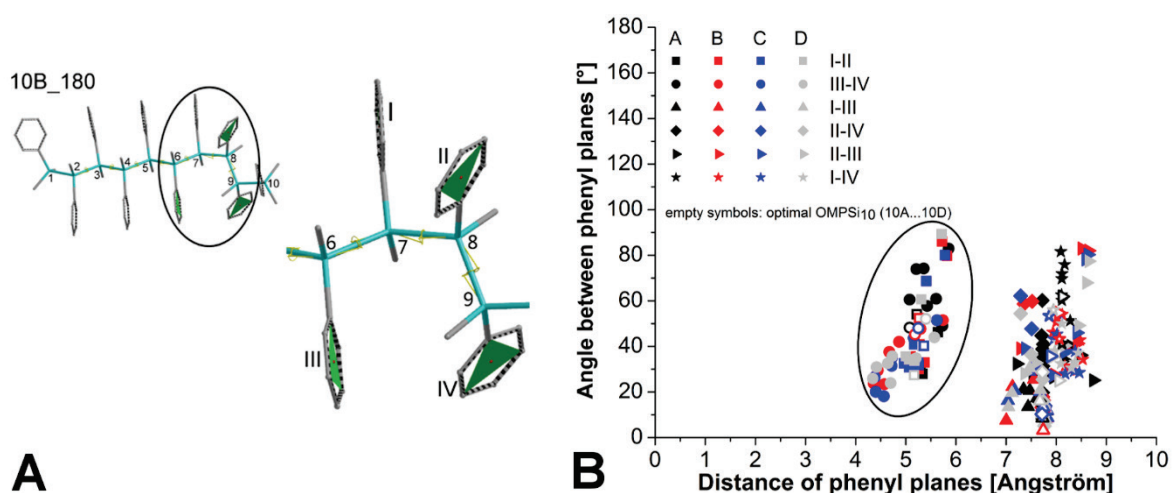


Fig. 9: Kink and designation of phenyl groups (A) and angle-distance dependence (B) in  $OMPSi_{10}$

Moreover, energy of  $OMPSi_{10}$  structures was calculated with functionals M06 and  $\omega$ B97X-D (all employing 6-31G\* basis set) describing the dispersion interaction better than B3LYP and therefore the value of molecular energy obtained with these functionals covers also employment of non-bonding interactions. (Details on functional and basis selection can be found in Computational methods section.) B3LYP energies then stand for situation where phenyl ring interactions are not involved into result and thus describe energy contribution of Si backbone. Graphically expressed comparison of B3LYP and M06 and  $\omega$ B97X-D energies of all studied  $OMPSi_{10}$  is given in Fig. 10. The results indicate which conformation is mostly influenced by dispersion term and therefore phenyl interactions.

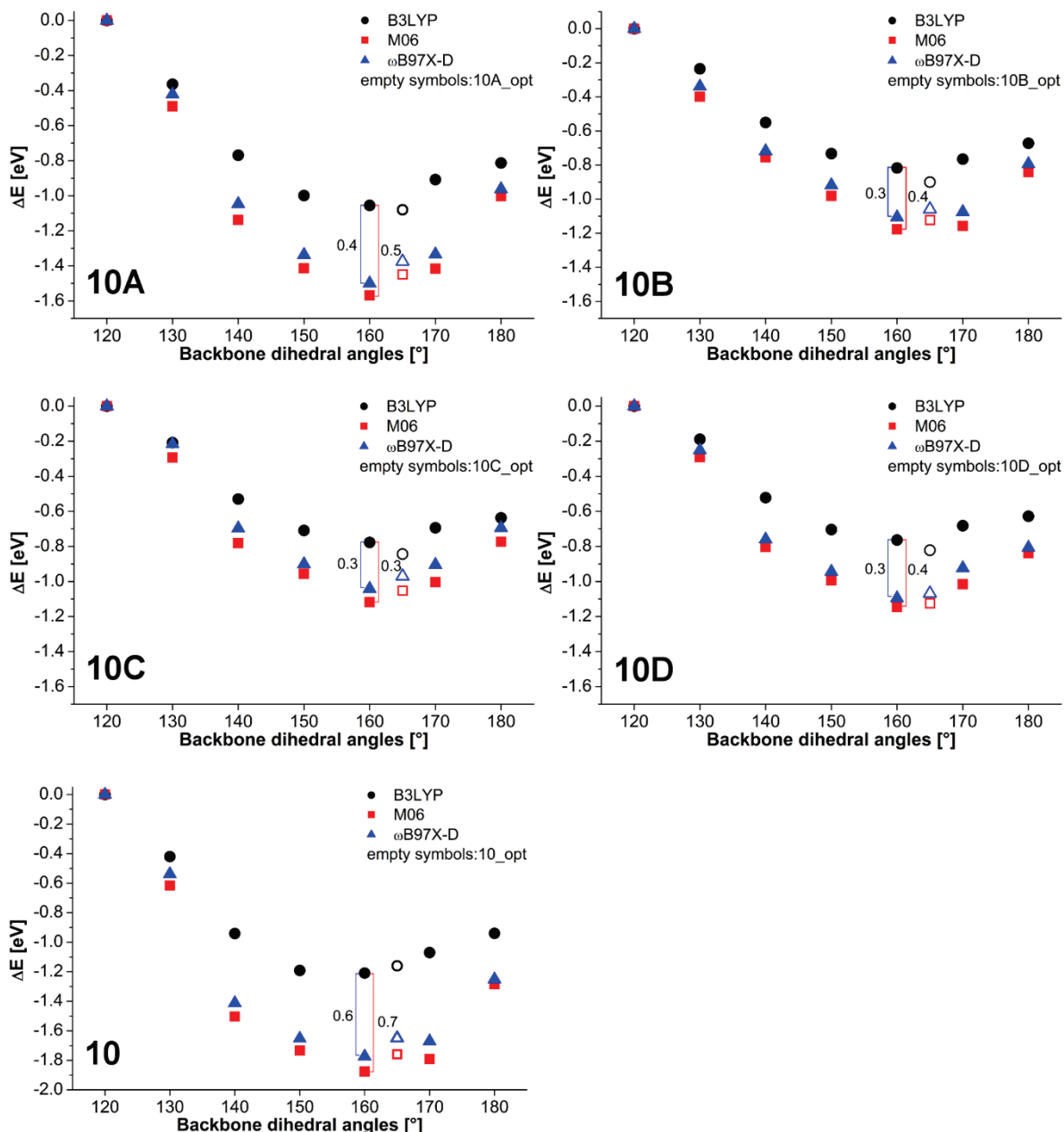


Fig. 10: Energy profile of OMPSi<sub>10</sub> obtained by B3LYP, M06 and ωB97X-D with 6-31G\* basis set (empty symbols: equilibrium non-constrained geometries)

The largest difference between B3LYP and M06/ωB97X-D energies was found for  $\omega = 160^\circ$  in all studied decamers. The energy difference decreases from 0.6–0.7 eV for 10 (OMPSi<sub>10</sub> without a kink) through 10A, 10B, 10C up to 0.3 eV for 10D (OMPSi<sub>10</sub> with a kink in the centre of chain). This finding can be explained with an assistance of previous Fig. 9 and by phenyl interactions, however between different phenyl planes in molecule 10 than in molecules 10A–10D. Helical conformation of 10 ( $\omega = 160^\circ$ ) offers the employment of phenyl planes that are attached to alternate Si atoms (from Fig. 9 planes II-III and I-IV) and without a kink defect, these interactions are kept along the whole backbone therefore providing maximally dispersion stabilized molecule. On the

other hand, the kink causes disruption of the helical arrangement and employs phenyl interactions between planes I-II and III-IV. It can be deduced from these results that non-bonding stabilization by phenyl rings attached to kink Si atoms is weaker than that of phenyl rings attached to Si atoms of helix as the energy differences are lower in molecules with the kink. 10A molecule with the kink at the edge part of the backbone is influenced the least significantly as it is actually helix with the kink defect at the very edge part. This means that an equilibrium geometry of OMPSi<sub>10</sub> (in Fig. 10 depicted at  $\omega = 165^\circ$ ) is supported by phenyl interactions and that a kink in the backbone is stabilized too and thus it is viable conformational defect in real PMPSi chains.

Another part of oligosilylene conformational research was focused only on tetrasilylene geometrical arrangement, first of OMPSi<sub>4</sub> (in **Paper III**) and then of the other tetramers, namely ODMSi<sub>4</sub>, OSi<sub>4</sub>, cyc-HMSi<sub>4</sub> and MPC<sub>4</sub> (in **Paper IV**). As a kink defect consists of four Si atoms, tetrasilylene can serve as a suitable model for such kink. Geometries were optimized and palette of conformers with  $\omega$  varying with  $10^\circ$  or  $20^\circ$  step was obtained. These (sub)optimal structures with energies calculated by B3LYP were then subjected to additional energy calculation using M06 and  $\omega$ B97X-D functionals as described above. The purpose of this investigation was to discover which geometry of a kink is the most influenced by non-bonding interactions and to consider if this conformation corresponds to those obtained in optimal geometries of other oligosilylenes. Fig. 11 shows energy profile of OMPSi<sub>4</sub> as the energy difference between particular computational methods.

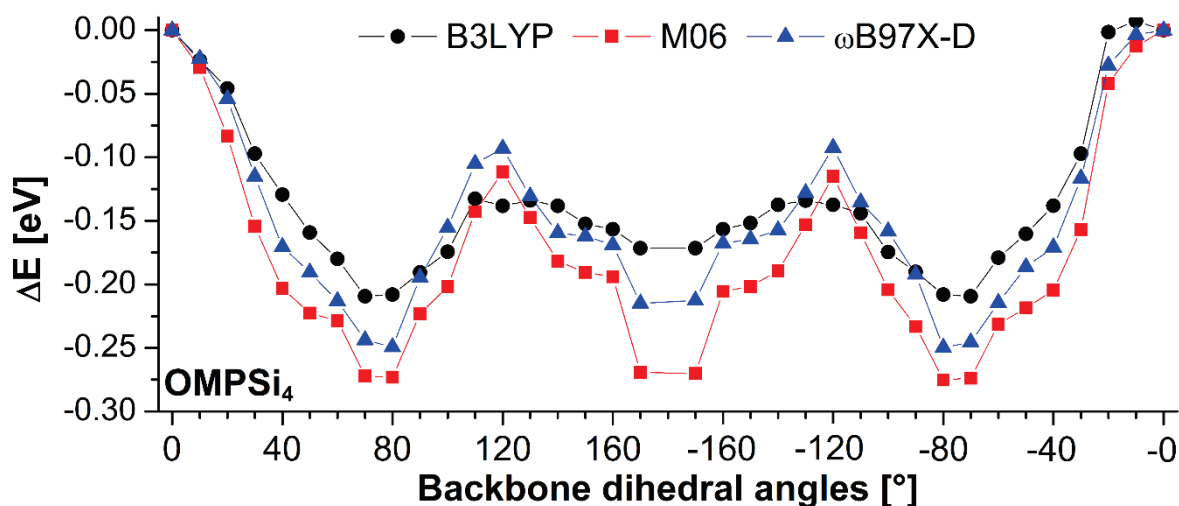


Fig. 11: Energy profile of OMPSi<sub>4</sub> obtained by B3LYP, M06 and  $\omega$ B97X-D with 6-31G\* basis set

Conformation with  $\omega = 0^\circ$  has the highest energy, therefore, it has been set as the reference level for all obtained energy profiles which are then expressed as differences  $\Delta E$ . The main result is that the most stable conformation belongs to molecule with  $\omega$  value  $70^\circ$ ,  $-70^\circ$  and  $80^\circ$ ,  $-80^\circ$  and at the same time these are the

conformations in which phenyl interactions are the most dispersion stabilized. This also supports previous results that four atom kink is stable in approximately *gauche* conformation and that it is stabilized by phenyl interactions. Furthermore, it can be seen in the graph, that phenyl-phenyl interactions have not only stabilizing effect but contribute also to an increase of conformational energy barriers between local minima which can be explained by mutual positions of phenyl rings where the repulsive interactions prevail.

A careful inspection of the graph also reveals that all-*anti* conformation is viable for tetramer with extremely large stabilizing contribution of non-bonding interactions, however, this geometry is unattainable in case of PMPSi polymer chain that is of *transoid* conformation and leads to helical secondary structure.

The results for OMPSi<sub>4</sub> were compared with the energy plots obtained by the same procedure for tetrasilylenes with smaller alkyl- side groups (ODMSi<sub>4</sub>) and hydrogen atoms (OSi<sub>4</sub>), whose energy profiles are shown in Fig. 12. Generally, the energy barriers between conformers and the depth of local energy minima obtained for ODMSi<sub>4</sub> and OSi<sub>4</sub> are significantly lower than those calculated for OMPSi<sub>4</sub>. OSi<sub>4</sub> molecule can be characterised by extremely shallow energy barriers between stable conformers *gauche* and *anti* that can be associated to high flexibility of its chain. Experimental studies demonstrated directly that a mixture of *gauche* ( $\omega = 60^\circ$ ) and *anti* ( $\omega = 180^\circ$ ) conformers of OSi<sub>4</sub> is present in a nitrogen matrix [90, 91] indicating thus that  $\omega$ B97X-D functional performs best. In comparison with OSi<sub>4</sub>, ODMSi<sub>4</sub> molecule is more suitable for formation of a stable conformers that corresponds to its deeper minima on the energy profile with  $\omega = 50^\circ$  (*gauche*) and  $\omega = 160^\circ$  (*transoid*). This leads to conclusion that *gauche* conformation of ODMSi<sub>4</sub> can be expected as a kink defect in polymer-size PDMSi chains similarly as in PMPSi.

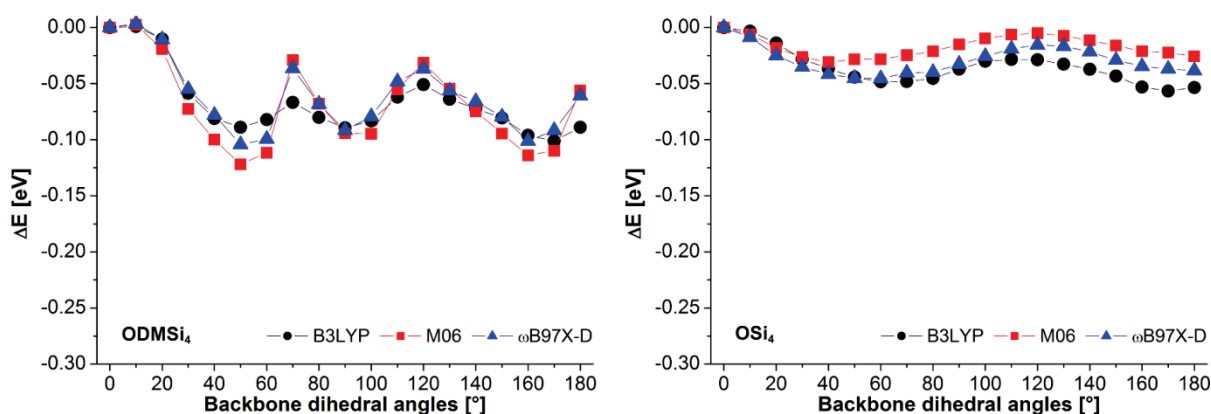


Fig. 12: Energy profile of ODMSi<sub>4</sub> and OSi<sub>4</sub> obtained by B3LYP, M06 and  $\omega$ B97X-D with 6-31G\* basis set

Poly[cyclohexyl(methyl)silylene] belongs to the groups of solution processable polysilylenes which invoked investigation of cyc-HMSi<sub>4</sub>. This tetrasilylene evinces surprisingly strong stabilization in *cisoid* and *gauche* conformation that is

assigned to Van der Waals interactions between cyclohexyl groups as this molecule represents non-aromatic case of the investigated set of tetrasilylenes.

It was found that long range interactions are very important when polysilylenes are described and they should not be ignored despite the fact that their conformational barriers are lower by order of magnitude than the barriers of carbonaceous analogues as molecules with carbon skeleton have much larger steric strain than their silicon counterparts, which was deduced from energy profile investigation of MPC<sub>4</sub>.

## 7.4 Conformational defect in oligosilylene ions – A model for polarons on polysilylene chain

*This chapter summarizes findings published in Paper V.*

Another step in OMPSi<sub>n</sub> electronic properties investigation was their evaluation in the form of positive and negative ions modelling thus polaron quasiparticles (P<sup>+</sup> and P<sup>-</sup>, respectively) with and without a defect – a kink. Calculations were done in three steps. First, an optimal geometry of neutral molecule was calculated (these geometries were taken from previously investigated OMPSi<sub>1-10</sub>). Second, an excessive charge (+1 in P<sup>+</sup> and -1 in P<sup>-</sup>) was set into calculation of single point energy with geometry from the first step; and third, the geometry of an ion (molecule with excessive charge either positive or negative) was optimized. An unrelaxed state, also called hot state, was obtained from the second step and the relaxed structure was obtained from the third step of calculation. Furthermore, vibrational frequencies were calculated for neutral and relaxed molecules. These values were used for calculation of polaron binding energy ( $E_p$ ) that consists of two terms; deformation energy ( $E_{def}$ , approx. 90 % of  $E_p$ ), which is the difference between the energy of hot and relaxed polaron and electron-photon energy ( $E_{el-ph}$ ) calculated from vibrational frequencies of neutral and polaron molecule and given in eq. 6 [12].

$$E_{el-ph} = -\frac{1}{2} \sum_{k=1}^{3D-6} \hbar \left( \omega_0^{(k)} - \omega_p^{(k)} \right), \quad (6)$$

where  $\hbar$  is reduced Planck constant,  $\omega_0^{(k)}$  and  $\omega_p^{(k)}$  is angular frequency of  $k$ -th vibrational mode of neutral and charged molecule, respectively,  $k$  is the number of vibrations and  $D$  is the number of atoms in the molecule.

$E_{def}$  evinced different behaviour for positive and negative polarons, i.e. for P<sup>+</sup> molecules  $E_{def}$  decreases with increasing oligomer size and on the contrary  $E_{def}$  of P<sup>-</sup> rather increases. Even though in P<sup>+</sup>, and especially in OMPSi<sub>2-4</sub>, the change in bond lengths is around 0.05 – 0.1 Å, P<sup>-</sup> of OMPSi<sub>n</sub> go through more substantial changes in bond angles up to 15° with respect to the geometry of the neutral



molecule. This probably caused the opposite trends in  $P^+$  and  $P^-$  dependencies of  $E_{def}$  on the oligomer size. The  $E_{def}$  decrease in  $P^+$  can be also attributed to  $\sigma$ -delocalization in longer  $OMPSi_n$  that facilitates the filling of the lack of electron density caused by removal of electron. On the other hand, a higher extent of  $\sigma$ -delocalization in  $P^-$  can cause the opposite effect and molecule must undergo more significant structural changes to cope with excessive electron density. It was further found that  $E_{el-ph}$  values are similar for all investigated  $P^+$  (0.01 eV) and  $P^-$  (0.13 eV) irrespective to both chain length and position of the kink.

Changes in spin density distribution along  $OMPSi_{10}$  molecule, which is depicted in Fig. 13, we also studied. As can be observed, this property is considerably influenced by the presence of a kink in the ion. Generally, the highest values of spin density are found in the centre of  $OMPSi_{10}$  chain, however, an introduced kink shifts the maxima to the part of a chain opposite to the location of the kink. Thus, the kink influences the polaron whose spin density is centralized to the longer undisturbed part of polymer backbone and a kink appears as a barrier limiting extension of the polaron.

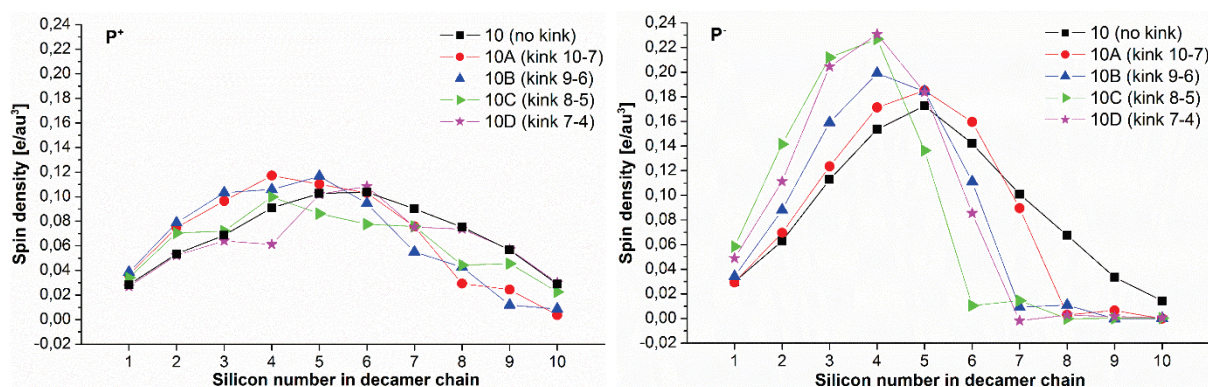


Fig. 13: Spin density distribution along  $OMPSi_{10}$  backbone in  $P^+$  and  $P^-$  structures

FMO of  $P^+$  and  $P^-$  are shown in Fig. 14. HOMO of  $P^+$  is distributed comparably as in neutral molecule (see also Fig. 7) and LUMO of  $P^+$  is distributed to central phenyl rings. On the other hand, HOMO of  $P^-$  oligomers is localized only on backbone part and the kink affects it as was described for neutral state in 7.1. LUMOs of  $P^-$  molecules are influenced the most by the presence of excessive electron density and are strictly distributed to two edge phenyl rings on one side of the oligomer (eventually the side of shorter segment). This implies that charge carriers (positive and negative) are delocalised in polysilylenes over relatively large segments (at least several mers) which is in compliance with relatively low  $E_p$ . The polaron binding energy is approx. two times smaller for  $P^+$  than  $P^-$  indicating thus that most plausible charge carrier is  $P^+$  which is in accordance with generally experienced hole type conductivity of polysilylenes. On the other hand, strong localization of LUMOs in both types of polarons may indicate strong

localization of eventual trapped states on phenyl groups at central parts of chains for  $P^+$  and chain ends for  $P^-$ .

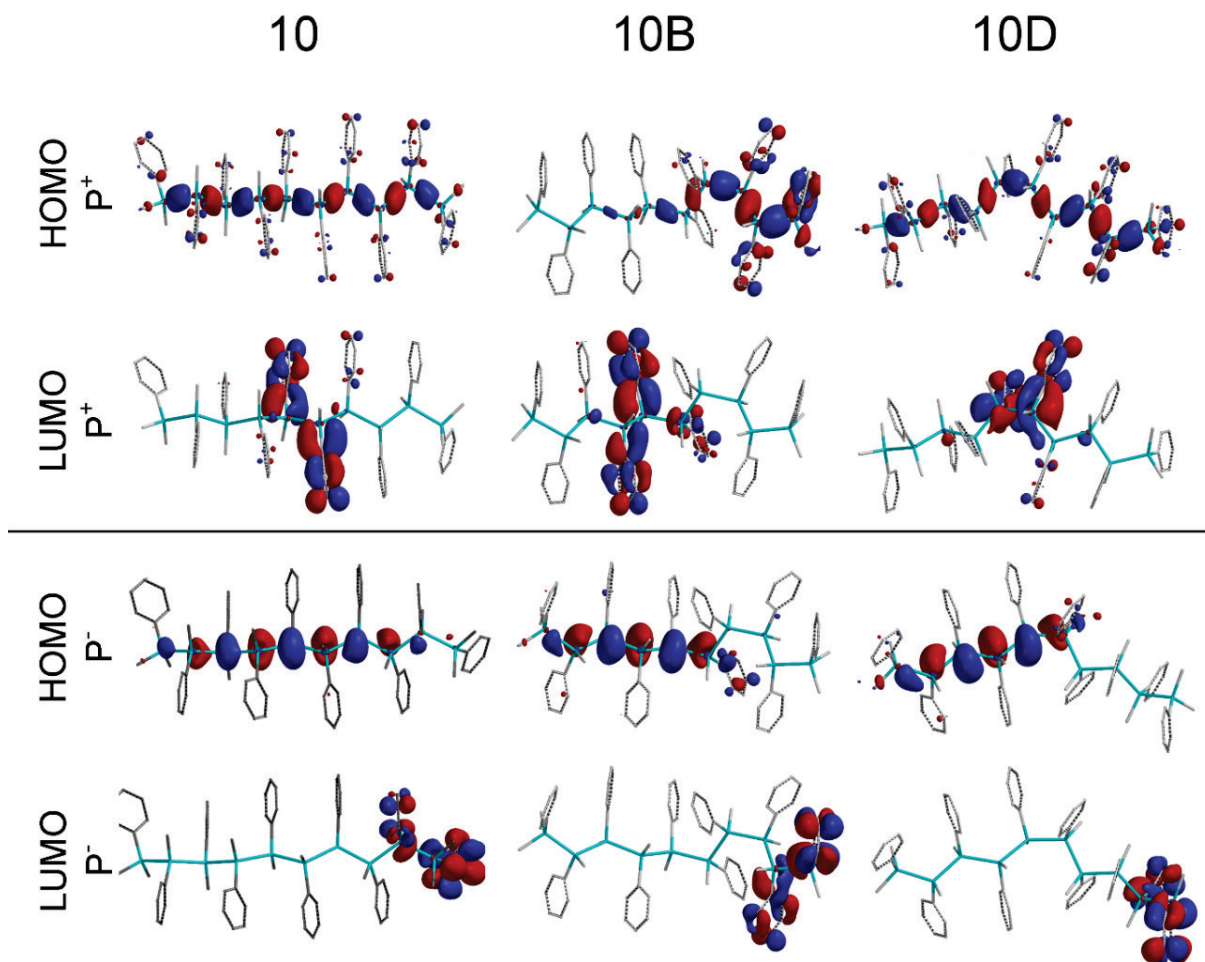


Fig. 14: FMO of OMPSi<sub>10</sub> (10, 10B and 10D) in the form of  $P^+$  and  $P^-$

## 8. CONCLUSIONS

Doctoral thesis has been submitted as a collection of five papers, three have been already published and two papers are at the stage of submitted manuscript. The series of complementary papers clarifies influence of the chain conformational defect – a kink (four Si atoms in approx. *gauche* conformation), and thus disruption of  $\sigma$ -conjugation on electronic properties of polysilylenes that were modelled on  $\text{OMPSi}_n$  and  $\text{ODMSi}_n$  in neutral as well as charged state (anions and cations as models for polaron).

$\sigma$ -conjugated polymers are considerably dependent on their geometrical arrangement. Electron delocalization is proportional to interactions of  $\sigma$ -orbital lobes and reaches maximum in all-*anti* arrangement. However, ideal conformation is disrupted mainly by two factors; the presence of bulky side groups, such as in PMPSi and also by conformational defects, such as kinks in backbones of semi-crystalline polymers (PMPSi, PDMSi) that serve as chain folding sites during crystallization or as bends in random coil formation in amorphous phase and in solution.

Following main points can be concluded from the contents of Doctoral thesis.

Conformational studies showed viable geometries of kink defect on polysilylene chains with various substituents (hydrogen, alkyl, aryl) and revealed the importance of non-bonding interactions in its stabilization. Phenyl-phenyl attractive interactions stabilize both conformations *gauche* and *transoid*. Repulsive forces between phenyls increase barriers between conformers. Conformation of non-aromatic polysilylenes is mainly governed by Van der Waals interactions due to relatively small steric strains in polysilylene molecules in contrast to their analogues with carbonaceous skeleton which is caused by longer Si-Si bond than C-C. Among tested functionals,  $\omega\text{B97X-D}$  functional was found to perform best for the studied group of molecules attaining best compliance with experimental data.

The position of a kink in Si backbone has been found one of the factors, which influence the value of energy gap between HOMO and LUMO and therefore  $\lambda_{max}$  in UV-Vis absorption spectrum. It has been discovered that the bandgap becomes wider as a kink position moves closer to the centre of Si backbone. Distribution of FMO is affected too. HOMO and LUMO are distributed symmetrically along Si backbone in case of molecules without a kink defect and molecules, where the kink is localized symmetrically in the central part of the backbone. Other kink positions cause redistribution of FMO to the longer chain segments, i.e. to the undisturbed parts of backbones. Moreover in  $\text{OMPSi}_n$  LUMO density is gathered on phenyl rings in the vicinity of the kink that is in contrast to LUMO delocalization on Si backbone in  $\text{OMPSi}_n$  without the kink. Therefore, the kink does influence the electronic properties. The effect of its position in the backbone is predominantly observable in shorter chains. Thus it is expected from extrapolation to polymer-size backbones that in PDMSi and PMPSi, the influence

of the kink position in the chain is reduced due to the presence of significantly longer undisturbed parts of backbones. On the other hand, more than one kink can be present on one chain dividing thus the long chain into segments. The all-*anti* and all-*transoid/deviant* conformation was discovered to be the most energetically favourable arrangement of ODMSi<sub>n</sub> and OMPSi<sub>n</sub>, respectively, regardless the presence of the kink defect. This structural defect was further found to be stabilized by phenyl-phenyl interactions and therefore it is expected as folding element in real PMPSi backbones. The trends that were observed in experimental (PMPSi) and calculated (OMPSi<sub>n</sub> in various conformations and with the kink) absorption spectra support these results as they imply possible helical arrangement of backbone and presence of the conformational defects.

The kink also causes significant changes in spin density and FMO distribution in positively and negatively charged OMPSi<sub>n</sub> that were used as models for polaron. Maximum of spin density is centralized to longer and by the kink undisturbed part of the Si backbones which means that the kink forms a structural barrier on the backbone that cannot be overcome by polaron. Similar conclusion can be observed on FMO distribution and it indicates that a kink defect contributes to trapping process of polaron and thus decreases a charge carrier mobility in PMPSi chains.

## 9. CLOSING REMARKS

### 9.1 Contributions to science and technology

The topic seemed to be covered and relatively quiet for a long time having a stable interpretational framework. However, the last findings in the field of thin films made from these polymers or conductive  $\pi$ -conjugated systems and other polymers revived interest on the importance of polymer chain ordering, stacking, H or J aggregate formation, chain alignment and dependence of the material properties on the development of the film thickness starting from sub-molecular cover degree through thin films from several to hundreds nanometres up to micrometric thickness. Solution processing of thin and thick polysilylene films is a key step in their application either in electronics and optoelectronics or as photo- and electro resist. Structural ordering (or disorder vice versa) influences their properties up to formerly unanticipated level and the present thesis contributes to interpretation of recent experimental findings attained at the Tomas Bata University in Zlín.

The study sheds light on the role of conformational disorder in development of electronic properties of various oligosilylenes and obtained knowledge has been successfully extended to their polymer homologues. New interpretational framework has been developed for this specific field of structure-property relationships in silicon chain polymers.

Among studied materials, the main attention has been paid to PMPSi which is the most experimentally investigated and theoretically studied most important member of the solution processable polysilylenes family suitable for electronic and other applications. The second studied polysilylene – PDMSi is insoluble, however, it finds applications in ceramics etc.

### 9.2 Ongoing research and future prospective

Ongoing and future research effort concerning polysilylenes in Zlín can be summarized as follows. **First**, PMPSi, PDMSi and their copolymer together with analogous oligomers are subjected to ongoing investigation of vibrational spectra, both Raman and infrared. **Second**, oligosilylene molecules with dopant are going to be studied. Fullerenes and cage-borane molecules have been selected as dopants and will be compared with experimental results obtained on PMPSi blends with these molecules by other members of the research group in cooperation with Academic institutions in Prague. **Third**, in the field of computational software, the main goal of the author is to deepen her knowledge of Gaussian software, especially in the area of emission and NMR spectra and become advanced user of full options offered by The National Grid Infrastructure – MetaCentrum.

## REFERENCES

- [1] ARJUNAN, Vijaya et al. Comprehensive quantum chemical and spectroscopic (FTIR, FT-Raman,  $^1\text{H}$ ,  $^{13}\text{C}$  NMR) investigations of (1,2-epoxyethyl)benzene and (1,2-epoxy-2-phenyl)propane. *Spectrochimica acta part A: Molecular and biomolecular spectroscopy*. 2015, vol. 135, pp. 120-136. DOI: 10.1016/j.saa.2014.07.001.
- [2] KRISHNAKUMAR, Vasudevannair et al. Molecular structure, vibrational spectra, HOMO, LUMO and NMR studies of 2-chloro-4-nitrotoluene and 4-chloro-2-nitrotoluene. *Spectrochimica acta part A: Molecular and biomolecular spectroscopy*. 2012, vol. 91, pp. 1-10. DOI: 10.1016/j.saa.2012.01.038.
- [3] BANI-YASEEN, Abdulilah D. and Abeer MO'ALA. Spectral, thermal, and molecular modeling studies on the encapsulation of selected sulfonamide drugs in  $\beta$ -cyclodextrin nano-cavity. *Spectrochimica acta part A: Molecular and biomolecular spectroscopy*. 2014, vol. 131, pp. 424-431. DOI: 10.1016/j.saa.2014.04.136.
- [4] XIA, Hong-Qiang et al. Theoretical studies of electronic and optical properties of the triphenylamine-based organic dyes with diketopyrrolopyrrole chromophore. *Dyes and pigments*. 2015, vol. 113, pp. 87-95. DOI: 10.1016/j.dyepig.2014.07.033.
- [5] SANDORFY, Camille. LCAO MO calculations on saturated hydrocarbons and their substituted derivatives. 1955, vol. 33, no. 8, pp. 1337-1351. DOI: 10.1139/v55-162.
- [6] BANDE, Annika and Josef MICHL. Conformational dependence of  $\sigma$ -electron delocalization in linear chains: Permethylated oligosilanes. *Chemistry. A European Journal*. 2009, vol. 15, no. 34, pp. 8504-8517. DOI: 10.1002/chem.200901521.
- [7] SCHEPERS, Thorsten and Josef MICHL. Optimized ladder C and ladder H models for sigma conjugation: Chain segmentation in polysilanes. *Journal of Physical Organic Chemistry*. 2002, vol. 15, no. 8, pp. 490-498. DOI: 10.1002/poc.527.
- [8] NESPUREK, Stanislav. Poly(organosilylene)s – perspective materials for optoelectronics. *Czechoslovak Journal of Physics*. 1999, vol. 49, no. 5, pp. 859-870. DOI: 10.1023/A:1021257611634.
- [9] NESPUREK, Stanislav. Thin polysilylene films. Their electronic and photoelectrical properties. *Material science and engineering C*. 1999, vol. 8-9, no. special issue, pp. 319-327. DOI: 10.1016/S0928-4931(99)00089-2.
- [10] KARATSU, Takashi. Photochemistry and photophysics of organomonosilane and oligosilanes: Updating their studies on conformation and intramolecular interactions. *Journal of Photochemistry and Photobiology C: Photochemistry Reviews*. 2008, vol. 9, no. 3, pp. 111-137. DOI: 10.1016/j.jphotochemrev.2008.06.001.

[11] SEMENOV, Vladimir V. Preparation, properties and applications of oligomeric and polymeric organosilanes. *Russian Chemical Reviews*. 2011, vol. 80, no. 4, pp. 313-339. DOI: 10.1070/RC2011v080n04ABEH004110.

[12] MARK, James E., Harry R. ALLCOCK and Robert WEST. *Inorganic polymers* 2<sup>nd</sup> ed. New York: Oxford University Press, Inc., 2005. ISBN: 978-0-19-513119-2.

[13] NESPUREK, Stanislav. From one-dimensional organosilicon structures to polymeric semiconductors: optical and electrical properties. *Journal of Non-Crystalline Solids*. 2002, vol. 299, part B, pp. 1033-1041. DOI: 10.1070/RC2011v080n04ABEH004110.

[14] PHIFER, Carol C. et al. Vacuum-ultraviolet spectroscopy of poly(methylphenylsilylene). *Journal of Chemical Physics*. 2004, vol. 120, no. 3, pp. 1613-1616. DOI: 10.1063/1.1633252.

[15] SKRYSHEVSKI, Yu et al. Triplet state spectroscopy of  $\sigma$ -conjugated poly[methyl(phenyl)silylene]. *Optical Materials*. 2007, vol. 30, no. 3, pp. 384-392. DOI: 10.1016/j.optmat.2006.11.062.

[16] HE, Lei, Baoxue CHEN and Mamoru ISO. Comparative study of photobleachable polysilane copolymers applied to optical waveguides. *Optical Materials*. 2011, vol. 33, no. 3, pp. 452-459. DOI: 10.1016/j.optmat.2010.10.016.

[17] NESPUREK, Stanislav, Geng WANG and Katsumi YOSHINO. Polysilanes – Advanced materials for optoelectronics. *Journal of Optoelectronics and Advanced Materials*. 2005, vol. 7, no. 1, pp. 223-230.

[18] NESPUREK, Stanislav et al. Origin of broad visible luminescence in poly[methyl(phenyl)silylene] thin films. *Journal of Luminescence*. 2002, vol. 11, no. 2, pp. 131-140. DOI: 10.1016/S0022-2313(02)00329-0.

[19] NOZAR, Juraj, Stanislav NESPUREK and Jakub SEBERA. Polaron binding energy in polymers: Poly[methyl(phenyl)silylene]. *Journal of molecular modeling*. 2012, vol. 18, no. 2, pp. 623-629. DOI: 10.1007/s00894-011-1056-x.

[20] VALERIAN, Hynek et al. The effect of polar additives on charge carrier transport in polysilylenes. *Journal of Applied Physics*. 1995, vol. 78, no. 10, pp. 6071-6078. DOI: 10.1063/1.360547.

[21] NESPUREK, Stanislav et al. Charge-transfer in some physical processes. *Journal of Physics: Conference Series*. 2010, vol. 253, no. 1, art. no. 012005. DOI: 10.1088/1742-6596/253/1/012005.

[22] NEMEC, Hynek et al. Charge carrier mobility in poly[methyl(phenyl)silylene] studied by time-resolved terahertz spectroscopy and molecular modelling. *Physical Chemistry and Chemical Physics*. 2011, vol. 13, no. 7, pp. 2850-2856. DOI: 10.1039/c0cp00774a.

[23] TACHIKAWA, Hiroto and Hiroshi KAWABATA. Electronic states of radical cations of all-*trans* oligo[methyl(phenyl)silane]. *Journal of Organometallic Chemistry*. 2007, vol. 692, no. 7, pp. 1511-1518. DOI: 10.1016/j.jorganchem.2006.11.053.

[24] TOMAN, Petr, Stanislav NESPUREK and Wojciech BARTKOWIAK. Modelling of charge carrier transport in conjugated polymers doped by polar additives. *Material Science – Poland*. 2009, vol. 27, no. 3, pp. 797-812.

[25] TOMAN, Petr et al. Oligo[methyl(phenyl)silane] ion–radical conformations calculated by the B3LYP method. *International Journal of Quantum Chemistry*. 2003, vol. 101, no. 6, pp. 746-752. DOI: 10.1002/qua.20332.

[26] NESPUREK, Stanislav et al. Poly[(diphenylsilanediy)ethynediyl]: Structure and optical and electroluminescent properties. *Journal of Applied Polymer Science*. 2007, vol. 105, no. 1, pp. 208-214. DOI: 10.1002/app.26084.

[27] TSUJI, Hayato, Josef MICHL and Kohei TAMAO. Recent experimental and theoretical aspects of the conformational dependence of UV absorption of short chain peralkylated oligosilanes. *Journal of Organometallic Chemistry*. 2003, vol. 685, no. 1-2, pp. 9-14. DOI: 10.1016/S0022-328X(03)00162-1.

[28] TSUJI, Hayato et al. Electronic transitions in conformationally controlled tetrasilanes with a wide range of SiSiSiSi dihedral angles. *Chemistry. A European Journal*. 2014, vol. 20, no. 30, pp. 9431-9441. DOI: 10.1002/chem.201403495.

[29] MACLEOD, Matthew K. and Josef MICHL. From ordinary to blue emission in peralkylated *n*-oligosilanes: The calculated structure of delocalized and localized singlet excitons. *Journal of Physical Chemistry A*. 2014, vol. 118, no. 45, pp. 10538-10553. DOI: 10.1021/jp504805y.

[30] TAREMAE, Hiroyuki and Josef MICHL. Geometry of the localized oo\* excited state of *n*-tetrasilane. *Chemical Physics Letters*. 1997, vol. 276, no. 1-2, pp. 127-132.

[31] MACLEOD, Matthew K. and Josef MICHL. Why do disilanes fail to fluoresce? *Collection of Czechoslovakia Chemical Communications*. 2011, vol. 76, no. 12, pp. 2085-2116. DOI: 10.1135/cccc2011179.

[32] MACLEOD, Matthew K., Lukas KOBR and Josef MICHL. Fifth stereoactive orbital on silicon: Relaxation of the lowest singlet excited state of octamethyltrisilane. *Journal of Physical Chemistry A*. 2012, vol. 116, no. 43, pp. 10507-10517. DOI: 10.1021/jp3068393.

[33] FUKUZAWA, Aiko, Hayato TSUJI and Kohei TAMAO. all-*anti*-Octasilane: Conformation control of silicon chains using the bicyclic trisilane as a building block. *Journal of American Chemical Society*. 2006, vol. 128, no. 21, pp. 6800-6801. DOI: 10.1021/ja0616231.

[34] WATANABE, Akira. Optical properties of polysilanes with various silicon skeletons. *Journal of Organometallic Chemistry*. 2003, vol. 685, no. 1-2, pp. 122-133. DOI: 10.1016/S0022-328X(03)00649-1.

[35] SATO, Takahiro et al. Molecular properties of helical polysilylenes in solution. *Polymer*. 2003, vol. 44, no. 19, pp. 5477-5495. DOI: 10.1016/S0032-3861(03)00574-3.

[36] KMINEK, Ivan et al. Poly(methyl-phenylsilylene) derivatives as photoconductors. *Collection of Czechoslovak Chemical Communications*. 1993, vol. 58, no. 10, pp. 2337-2348. DOI: 10.1135/cccc19932337.



[37] CIMROVA, Vera et al. Charge carrier photogeneration in poly(methylphenylsilylene) and its derivatives with  $\pi$ -conjugated side groups. *Synthetic Metals*. 1994, vol. 64, no. 2-3, pp. 271-275. DOI: 10.1016/0379-6779(94)90123-6.

[38] FUJIKI, Michiya et al. Optically active polysilanes. Ten years of progress and new polymer twist for nanoscience and nanotechnology. *Polymer Journal*. 2003, vol. 15, no. 4, pp. 297-344. DOI: 10.1295/polymj.35.297.

[39] MICHL, Josef and Robert WEST. Conformations of linear chains. Systematics and suggestions for nomenclature. *Accounts of Chemical Research*. 2000, vol. 33, no. 12, pp. 821-823. DOI: 10.1021/ar0001057.

[40] FUJIKI, Michiya. Switching handedness in optically active polysilanes. *Journal of Organometallic Chemistry*. 2003, vol. 685, no. 1-2, pp. 15-34. DOI: 10.1016/S0022-328X(03)00638-7.

[41] FOGARTY, Heather A., Carl-Henrik OTTOSSON and Josef MICHL. The five favoured backbone conformations of n-Si<sub>4</sub>Et<sub>10</sub>: *cisoid*, *gauche*, *ortho*, *deviant*, and *transoid*. *Journal of Molecular Structure*. 2000, vol. 506, no. special issue, pp. 243-255. DOI: 10.1016/S0166-1280(00)00416-4.

[42] FURUKAWA, Shoji and Hidekata OHTA. Structure and orientation of vacuum-evaporated poly(di-methyl silane) film. *Thin Solid Films*. 2003, vol. 438-439, pp. 48-55. DOI: 10.1016/S0040-6090(03)00755-7.

[43] LENHARD, Johannes. Disciplines, models and computers: The path to computational quantum chemistry. *Studies in history and philosophy of science*. 2014, in press, pp. 1-8. DOI: 10.1016/j.shpsa.2014.05.003

[44] SPESSARD, Gary O. and Gary L. MIESSLER. *Organometallic chemistry* 2nd ed. New York: Oxford University Press, 2010. ISBN: 978-0-19-533099-1.

[45] HEHRE, Warren J. *A guide to molecular mechanics and quantum chemical calculations*. Irvine: Wavefunction, Inc., 2003. ISBN: 1-890661-18-X.

[46] ATKINS, Peter and Ronald FRIEDMAN. *Molecular quantum mechanics* 4<sup>th</sup> ed. New York: Oxford University Press Inc., 2005. ISBN: 0-19-927498-3.

[47] LEVINE, Ira N. *Quantum chemistry* 5<sup>th</sup> ed. New Jersey: Prentice Hall, 2000. ISBN: 0-13-685512-1.

[48] LEVINE, Ira N. *Physical chemistry* 6<sup>th</sup> ed. New York: McGraw-Hill Companies, Inc., 2009. ISBN: 978-0-07-253862-5.

[49] PAULING, Linus and E. Bright WILSON. *Introduction to quantum mechanics*. New York: Dover Publications, Inc., 1985. ISBN: 978-0-486-64871-2.

[50] KOCH, Wolfram and Max HOLTHAUSEN. *A chemist's guide to density functional theory* 2<sup>nd</sup> ed. Wiley-VCH Verlag GmbH, 2001. ISBN: 3-527-30372-3.

[51] COOK, David B. *Handbook of computational quantum chemistry*. New York: Dover Publications 2005. ISBN: 0-486-44307-8.

[52] KOHN, Walter and Lu J. SHAM. Self-consistent equations including exchange and correlation effect. *Physical review*. 1965, vol. 140, no. 4A, pp. A1133-A1138. DOI: 10.1103/PhysRev.140.A1133.

[53] HOHENBERG, Pierre C. and Walter KOHN. Inhomogeneous electron gas. *Physical review*. 1964, vol. 136, no. 3B, pp. B864-B871.

[54] FIOLETTI, Carlo, Fernando NOGUEIRA and Miguel A. L. MARQUES. *A primer in density functional theory*. Germany, Springer-Verlag Berlin Heidelberg, 2003. ISBN: 3-540-03082-2.

[55] CUEVAS, Juan C. and Elke SCHEER. *Molecular electronics – An introduction to theory and experiment*. Singapore: World Scientific Publishing Co. Pte. Ltd., 2010. ISBN: 978-981-4282-58-1.

[56] BECKE, Axel D. Density-functional exchange-energy approximation with correct asymptotic behaviour. 1988, vol. 38, no. 6, pp. 3098-3100. DOI: 10.1103/PhysRevA.38.3098.

[57] LEE, Chengteq, Weitao YANG and Robert G. PARR. Development of the Colle-Salvetti correlation-energy formula into a functional of the electron density. *Physical Review B*. 1988, vol. 37, no. 2, pp. 785-789. DOI: 10.1103/PhysRevB.37.785.

[58] KOHN, Walter, Axel D. BECKE and Robert G. PARR. Density functional theory of electronic structure. *Journal of physical chemistry*. 1996, vol. 100, no. 31, pp. 12974-12980. DOI: 10.1021/jp960669l.

[59] STEPHENS, Philip J. et al. Ab initio calculation of vibrational absorption and circular dichroism spectra using density functional force fields. *Journal of physical chemistry*. 1994, vol. 98, no. 45, pp. 11623-11627. DOI: 10.1021/j100096a001.

[60] *Spartan '14 for Windows, Macintosh and Linux*. Irvine, CA: Wavefunction, Inc., 2014. ISBN: 978-1-890661-42-2.

[61] XAVIER, R. John and P. DINESH. Vibrational spectra, monomer, dimer, NBO, HOMO, LUMO and NMR analyses of trans-4-hydroxy-L-proline. *Spectrochimica Acta: Part A: Molecular and Biomolecular Spectroscopy*. 2014, vol. 128, pp. 54-68. DOI: 10.1016/j.saa.2014.02.047.

[62] RONG, Yuzhi et al. Study on structural and spectral properties of isobavachalcone and 4-hydroxyderricin by computational method. *Spectrochimica Acta: Part A: Molecular and Biomolecular Spectroscopy*. 2014, vol. 126, pp. 254-259. DOI: 10.1016/j.saa.2014.02.013.

[63] RENJITH, R. et al. Vibrational spectra, molecular structure, NBO, HOMO–LUMO and first order hyperpolarizability analysis of 1,4-bis(4-formylphenyl)anthraquinone by density functional theory. *Spectrochimica Acta: Part A: Molecular and Biomolecular Spectroscopy*. 2014, vol. 131, pp. 225-234. DOI: 10.1016/j.saa.2014.04.085.

[64] KART, Sevgi O. et al. Theoretical study of the structure–properties relationship in new class of 2,5-di(2-thienyl)pyrrole compounds. *Spectrochimica*

*Acta: Part A: Molecular and Biomolecular Spectroscopy*. 2015, vol. 137, pp. 1174-1183. DOI: 10.1016/j.saa.2014.08.143.

[65] SNIDER, A. Monroe Jr. X-ray analysis. In: KOLESKE, Joseph V. *Paint and coating testing manual*, 15<sup>th</sup> ed. of the Gardner-Sward Handbook. Bridgeport: ASTM International. 2012, pp. 920-938. ISBN: 978-0-8031-7017-9.

[66] CSD. *Cambridge Structural Database* [online]. [viewed 31-10-2014]. Available from: <http://www.ccdc.cam.ac.uk/pages/Home.aspx>

[67] YURDAKUL, Senay and Murat YURDAKUL. FT-IR, FT-Raman spectra, and DFT computations of the vibrational spectra and molecular geometry of chlorzoxazone. *Spectrochimica Acta: Part A: Molecular and Biomolecular Spectroscopy*. 2014, vol. 126, pp. 339-348. DOI: 10.1016/j.saa.2014.02.156.

[68] TEMEL, Ersin et al. DFT calculations, spectroscopy and antioxidant activity studies on (E)-2-nitro-4-[(phenylimino)methyl]phenol. *Spectrochimica Acta: Part A: Molecular and Biomolecular Spectroscopy*. 2015, vol. 136, pp. 534-546. DOI: 10.1016/j.saa.2014.09.067.

[69] ROCHA, Mariana et al. Ab-initio and DFT calculations on molecular structure, NBO, HOMO–LUMO study and a new vibrational analysis of 4-(Dimethylamino) Benzaldehyde. *Spectrochimica Acta: Part A: Molecular and Biomolecular Spectroscopy*. 2015, vol. 136, pp. 635-643. DOI: 10.1016/j.saa.2014.09.077.

[70] HIGSON, Seamus. *Analytical Chemistry*. New York: Oxford University Press, Inc., 2004. ISBN: 978-0-19-580289-0.

[71] GORDY, Walter and Robert L. COOK. *Microwave Molecular Spectra*. New York: John Wiley & Sons, Inc., 1984. ISBN: 0-471-08681-9.

[72] GIRICHEVA, Nina I. et al. The difference between gas-phase and crystal structures of ortho-nitromethylbenzenesulfonate. Conformation variety study of free molecules by electron diffraction and quantum chemistry. *Journal of Molecular Structure*. 2015, vol. 1085, pp. 191-197. DOI: 10.1016/j.molstruc.2014.12.082.

[73] McQUARRIE, Donald A., Peter A. ROCK and Ethan B. GALLOGLY *General chemistry* 4th ed. Mill Walley: University Science Books, 2011. ISBN: 987-1-891389-60-3.

[74] McMURRY, John E. *Organic chemistry* 6th ed. Brooks/Cole, a Thompsons Learning Company, 2004. Czech ed.: Brno, Vysoké učení technické v Brně VUTIUM. ISBN: 978-0-534-38999-4.

[75] LAMPMAN, Garz M. et al. *Spectroscopy* 4<sup>th</sup> ed. Belmont: Brooks/Cole Cengage Learning, 2010. ISBN: 978-0-538-73418-9.

[76] SKOOG, Douglas A., F. James HOLLER and Stanley R. CROUCH. *Principles of instrumental analysis* 6<sup>th</sup> ed. Belmont: Thompson Brooks/Cole, 2007. ISBN: 978-0-495-01201-6.

[77] PROMKATKAEW, Malinee et al. Absorption and emission properties of various substituted cinnamic acids and cinnamates, based on TDDFT

investigation. *International Journal of Quantum Chemistry*. 2013, vol. 113, no. 4, pp. 542-554. DOI: 10.1002/qua.24169.

[78] SAS, Babur E. et al. FT-IR, FT-Raman, NMR and UV–Vis spectra and DFT calculations of 5-bromo-2-ethoxyphenylboronic acid (monomer and dimer structures). *Spectrochimica Acta: Part A: Molecular and Biomolecular Spectroscopy*. 2015, vol. 137, pp. 1315-1333. DOI: 10.1016/j.saa.2014.08.049.

[79] SHAO Yihan et al. Advances in methods and algorithms in a modern quantum chemistry program package. *Physical Chemistry Chemical Physics*. 2006, vol. 8, no. 27, pp. 3172-3191. DOI: 10.1039/b517914a.

[80] RUNGE, Erich and Eberhard K. U. GROSS. Density functional theory for time dependent systems. *Physical Review Letters*. 1984, vol. 52, no. 2, pp. 997-1000. DOI: 10.1103/PhysRevLett.52.997.

[81] PAN Xiaoyin and Virah C. SAHNI. New perspectives on the fundamental theorem of density functional theory. *International Journal of Quantum Chemistry*. 2008, vol. 108, no. 15, pp. 2756-2762. DOI: 10.1002/qua.21826.

[82] BAUERNSCHMITT, Rudiger and Reinhart AHLRICHS. Treatment of electronic excitations within the adiabatic approximation of time dependent density functional theory. *Chemical Physics Letters*. 1996, vol. 256, no. 4-5, pp. 454-464. DOI: 10.1016/0009-2614(96)00440-X.

[83] PIQUERAS, Mari Carmen, Raul CRESPO and Josef MICHL. Interpretation of the electronic spectra of four disilanes. *Journal of Physical Chemistry A*. 2008, vol. 112, no. 50, pp. 13095-13101. DOI: 10.1021/jp804677v.

[84] CRESPO, Raul, Mari Carmen PIQUERAS and Josef MICHL. Electronic excitation in a *syn*-tetrasilane: 1,1,2,2,3,3, 4,4-octamethyltetrasilacyclopentane. *Theoretical Chemistry Accounts*. 2007, vol. 111, no. 1, pp. 81-87. DOI: 10.1007/s00214-007-0246-1.

[85] WALKER, Martin et al. Performance of M06, M06-2X, and M06-HF density functionals for conformationally flexible anionic clusters: M06 functionals perform better than B3LYP for a model system with dispersion and ionic hydrogen-bonding interactions. *Journal of Physical Chemistry A*. 2013, vol. 117, no. 47, pp. 12590-12600. DOI: 10.1021/jp408166m.

[86] CHAI, Jeng-Da and Martin HEAD-GORDON. Long-range corrected hybrid density functionals with damped atom–atom dispersion corrections. *Physical Chemistry Chemical Physics*. 2008, vol. 10, no. 44, pp. 6615-6620. DOI: 10.1039/b810189b.

[87] YANAI, Takeshi, David P. TEW and Nicholas C. HANDY. A new hybrid exchange–correlation functional using the Coulomb-attenuating method (CAM-B3LYP). *Chemical Physics Letters*. 2004, vol. 393, no. 1-3, pp. 51-57. DOI: 10.1016/j.cplett.2004.06.011.

[88] CIVALLERI, Bartolomeo et al. B3LYP augmented with an empirical dispersion term (B3LYP-D\*) as applied to molecular crystals. *CrystEngComm*. 2008, vol. 10, no. 4, pp. 405-410. DOI: 10.1039/b715018k.

[89] HUNTER, Christopher A. and Jeremy K. M. SANDERS. The nature of  $\pi$ - $\pi$  interaction. *Journal of American Chemical Society*. 1990, vol. 112, no. 14, pp. 5525-5534. DOI: 10.1021/ja00170a016.

[90] PIQUERAS, Mari Carmen et al. Conformational effects on the ultraviolet absorption spectrum of *n*-tetrasilane: Multistate complete active space second-order perturbation theory treatment. *Journal of Physical Chemistry A*. 2002, vol. 106, no. 42, pp. 9868-9873. DOI:10.1021/jp020460+.

[91] ALBINSSON, Bo et al. Matrix-isolation IR and UV spectra of  $\text{Si}_3\text{H}_8$  and  $\text{Si}_4\text{H}_{10}$ : Isomers and conformers of oligosilanes. *Journal of Physical Chemistry*. 1996, vol. 100, no. 21, pp. 8681-8691. DOI: 10.1021/jp9537318.

## LIST OF FIGURES

Fig. 1: Orbitals (A) and their intramolecular interaction (B) in polysilylene chain .....	2
Fig. 2: Energy diagram of bands in electronic structure of PMPSi .....	3
Fig. 3: Potential energy curves of neutral and polaron geometry .....	4
Fig. 4: One-dimensional potential energy curve for diatomic molecule.....	9
Fig. 5: Optimized helical structures of OMPSi <sub>10</sub> without (10) and with a kink (10A–D).....	16
Fig. 6: FMO energies of OMPSi <sub>n</sub> and ODMSi <sub>n</sub> structures .....	17
Fig. 7: HOMO and LUMO of OMPSi <sub>10</sub> – 10, 10B and 10D.....	18
Fig. 8: Absorption maximum (graph panel A) and oligomer energy (B3LYP/6-31G*) (graph panel B) reported vs. conformation of OMPSi <sub>10</sub> (empty symbols are non-constrained equilibrium geometries of OMPSi <sub>10</sub> ) .....	19
Fig. 9: Kink and designation of phenyl groups (A) and angle-distance dependence (B) in OMPSi <sub>10</sub> .....	20
Fig. 10: Energy profile of OMPSi <sub>10</sub> obtained by B3LYP, M06 and ωB97X-D with .....	21
Fig. 11: Energy profile of OMPSi <sub>4</sub> obtained by B3LYP, M06 and ωB97X-D with 6-31G* basis set .....	22
Fig. 12: Energy profile of ODMSi <sub>4</sub> and OSi <sub>4</sub> obtained by B3LYP, M06 and ωB97X-D with 6-31G* basis set.....	23
Fig. 13: Spin density distribution along OMPSi <sub>10</sub> backbone in P <sup>+</sup> and P <sup>-</sup> structures .....	25
Fig. 14: FMO of OMPSi <sub>10</sub> (10, 10B and 10D) in the form of P <sup>+</sup> and P <sup>-</sup> .....	26

# LIST OF ABBREVIATIONS AND SYMBOLS

## Abbreviations used in the text

Å	Angström
AO	atomic orbital
CT	charge transfer
cyc-HMSi <sub>4</sub>	tetra [cyclohexyl(methyl)silylene]
DFT	density functional theory
FMO	frontier molecular orbital
HF	Hartree-Fock
HOMO	highest occupied molecular orbital
LUMO	lowest unoccupied molecular orbital
MO	molecular orbital
MPC <sub>4</sub>	carbonaceous analogue of OMPSi <sub>4</sub>
n	number of repeating units
ODMSi <sub>n</sub>	oligo[(dimethyl)silylene]
OMPSi <sub>n</sub>	oligo[methyl(phenyl)silylene]
OSi <sub>4</sub>	tetra(silylene)
PDMSi	poly[(dimethyl)silylene]
PMPSi	poly[methyl(phenyl)silylene]
P <sup>-</sup>	negative polaron
P <sup>+</sup>	positive polaron
QC	quantum chemistry
Si	silicon
UV-Vis	ultraviolet-visible
XRD	X-ray diffraction

## Symbols used in the text

$A_f$	electron affinity	$E_c$	energy of conduction band
$\beta_{1,3}$	resonance integral (Si1; Si3)	$E_b$	vertical energy gap
$\beta_{1,4}$	resonance interga (Si1; Si4)	$E_p$	polaron binding energy
$\beta_{gem}$	germinal integral	$E_t^h$	energy of defect states
$\beta_{vic}$	vicinal integral	$E_v$	energy of valence band
$\Delta E$	energy difference	$I_c$	ionization potential
$E_b$	second energy gap	$\lambda_{max}$	absorption maximum
$E_{BP}$	energy of branching points	$\omega$	dihedral angle Si-Si-Si-Si

## Symbols used in equations

$E$	total energy of the state ( $\Psi$ )
$E_{HF}$	Hartree-Fock energy
$E^{el}$	energy of electrons
$E^{nuc}$	energy of nuclei
$F_{HK}[\rho_0]$	Hohenberg-Kohn functional
$\hat{f}$	Fock operator
$\hat{H}$	Hamiltonian operator
$\kappa$	force constant
$\Psi$	wavefunction
$M$	number of nuclei
$m_1$	mass of atom 1
$m_2$	mass of atom 2
$M_A$	mass of nucleus A
$\mu$	reduced mass
$N$	number of electrons
$\nabla^2$	Laplace operator
$\tilde{\nu}$	wavenumber
$r$	distance between nuclei
$\rho_0$	electron density
$T[\rho_0]$	functional of kinetic energy
$V_{ee}[\rho_0]$	functional of electron-electron repulsion
$V_{en}[\rho_0]$	functional of electron-nuclear interaction
$V_{HF}(i)$	repulsive potential of electron $i$ due to other electrons
$x_{AB}$	distance of nuclei A and B
$x_{iA}$	distance of nucleus A and electron $i$
$x_{ij}$	distance of electrons $i$ and $j$
$Z_A$	charge of nucleus A
$Z_B$	charge of nucleus B



# LIST OF PUBLICATIONS

## Journal articles for dissertation with author's contribution

- **Paper I:** HANULIKOVA, Barbora (60%) and Ivo KURITKA. Manifestation of conformational defect in electronic spectra of polysilanes – a theoretical study. *Macromolecular Symposia*. 2014, vol. 339, no. 1, pp. 100-111. DOI: 10.1002/masy.201300143.
- **Paper II:** HANULIKOVA, Barbora (50%), Ivo KURITKA and Pavel URBANEK. Effect of backbone conformation and its defects on electronic properties and assessment of the stabilizing role of  $\pi$ - $\pi$  interactions in aryl substituted polysilylenes studied by DFT on deca[methyl(phenyl)silylene]s. *Chemistry Central Journal*. 2016, vol. 10, no. 28. DOI: 10.1186/s13065-016-0173-0.
- **Paper III:** HANULIKOVA, Barbora (60%) and Ivo KURITKA. Contribution of non-bonding interactions to stabilization of aryl-substituted polysilylene chains conformational disorder examined by DFT on tetra[methyl(phenyl)silylene] model molecule. *Submitted to Journal of Molecular Modeling*.
- **Paper IV:** HANULIKOVA, Barbora (40%) and Ivo KURITKA. Stabilization of conformational defects of hydrogen, alkyl and aryl substituted polysilylene chains by non-bonding interactions: A DFT study on tetrasilylene model molecules. *Submitted to Theoretical Chemistry Accounts*.
- **Paper V:** HANULIKOVA, Barbora (60%) and Ivo KURITKA. Theoretical study of polaron binding energy in conformationally disrupted oligosilanes. *Journal of Molecular Modeling*. 2014, vol. 20, no. 10, pp. 2442-2450. DOI: 10.1007/s00894-014-2442-y.

## Other journal articles not joined for dissertation

- BABJAKOVA, Eva, Barbora HANULIKOVA (5%), Lenka DASTYCHOVA, Ivo KURITKA, Marek NECAS and Robert VICHA. Conformational dimorphism of isochroman-1ones in the solid state. *Journal of Molecular Structure*. 2014, vol. 1078, pp. 106-113. DOI: 10.1016/j.molstruc.2014.03.005.
- BABJAKOVA, Eva, Lenka DASTYCHOVA, Barbora HANULIKOVA (5%), Ivo KURITKA, Marek NECAS, Hana VASKOVA and Robert VICHA. Synthesis, molecular structure and vibrational spectra of 1,3-bis (1-adamantyl)-2-phenylpropan-1,3-diones. *Journal of Molecular Structure*. 2015, vol. 1085, pp. 207-214. DOI: 10.1016/j.molstruc.2014.12.074.

## CONFERENCE LIST

- 19<sup>th</sup> European Symposium on Polymer Spectroscopy  
Prague, 7.–11. 7. 2013
- European Symposium on Atomic Spectrometry ESAS 2014 & 15th Czech-Slovak Spectroscopic Conference  
Prague, 16.–21. 3. 2014

# CURRICULUM VITAE

Name: **Barbora Hanulíková**

Date of birth: 20<sup>th</sup> February 1986

Address: Fügnerovo nábřeží 5476, Zlín, 76001

Nationality: Czech

Contact: hanulikova@cps.utb.cz

---

Education: 2012 – present  
Tomas Bata University in Zlín, Faculty of Technology  
Doctoral degree studies in Chemistry and Materials  
Technology (Technology o Macromolecular compounds)

2010-2012  
Tomas Bata University in Zlín, Faculty of Technology  
Master's degree studies in Chemistry and Materials  
Technology (Polymer Engineering)

2007-2010  
Tomas Bata University in Zlín, Faculty of Technology  
Bachelor's degree studies in Chemistry and Materials  
Technology

Projects: 06/2013 – present  
Centre of Polymer Systems  
(CZ.1.05/2.1.00/03.0111 and LO1504)  
Researcher

2015 and 2016  
Internal Grant Agency of CPS TBU  
(IGA/CPS/2015/006 and IGA/CPS/2016/007)  
Member of research team

2013 and 2014  
Internal Grant Agency of FT TBU  
(IGA/FT/2013/025 and IGA/FT/2014/006)  
Member of research team

07 – 08/2013  
Innovation of education in polymer technology and  
application (CZ.1.07/2.2.00/15.0363)  
Innovated subject staff

## **APPENDIX**

Full texts of research papers involved in dissertation thesis

Research papers are provided in the order in which appeared in the text of Doctoral thesis.

Papers at the stage of submitted manuscript are included with a title page of journal submission file and the formatted text.

## **Research Paper I:**

**HANULIKOVA, Barbora** and Ivo KURITKA.

Manifestation of conformational defect in electronic spectra of polysilanes – a theoretical study

*Macromolecular Symposia*. 2014, vol. 339, no. 1, pp. 100-111.



## Manifestations of Conformational Defects in Electronic Spectra of Polysilanes – a Theoretical Study

Barbora Hanulikova,<sup>\*1,2</sup> Ivo Kuritka<sup>1,2</sup>

**Summary:** In this paper, density functional theory (DFT) and time dependent DFT (TDDFT) are applied on the calculation of electronic properties of alkyl- and aryl-substituted oligosilanes with conformational defect introduced into their silicon chain. Oligo[methyl(phenyl)silane]s and oligo(dimethylsilane)s up to 10 or 13 mer units, respectively, are treated as model structures by DFT and TDDFT with B3LYP/6–31 G\* base. Frontier molecular orbital (FMO) energies evince the dependence on the presence as well as on the position of the defect in oligomer backbones. Delocalization of FMO is strongly influenced by position of the defect which in some cases divides the molecule to the FMO-rich part and the part almost without FMO delocalization and therefore affects location of electrons. Behaviour of longer chains in analogous polysilanes is deduced from linear regression of plots of FMO energy over the inverse of the polymerization degree.

**Keywords:** calculations; density functional theory; kink; polysilanes; UV-vis spectroscopy

### Introduction

Poly[(alkyl)silylene]s and poly[alkyl(aryl)silylene]s (generally called polysilylenes, organosilanes, polysilanes) evince noteworthy properties and therefore they have been of increased researchers interest for almost three decades. The uniqueness of these compounds lies predominantly in their electronic and thus optical properties that originate in electron delocalization along the chain which is made of silicon (Si) atoms connected by single bonds.<sup>[1,2]</sup> The delocalization or  $\sigma$ -conjugation is explained by overlapping of the lobes of  $sp^3$  hybridized silicone  $\sigma$ -orbitals of the particular or adjacent Si atoms (also called vicinal and germinal orbitals) as was reported else-

where.<sup>[3,4,5]</sup> Hence, absorption spectra of polysilanes have become indispensable knowledge and still investigated topic in the area of polymers and have been described, for instance, by<sup>[3,6,7]</sup> or UV-vis spectra of polysilanes-containing composites by.<sup>[8]</sup> The longest wavelength absorption around 300–350 nm is assigned to  $\sigma \rightarrow \sigma^*$  transition on Si-Si bond and it is known that the position of this absorption peak shifts with different side groups attached to the main chain. This was studied as early as in late 1980s by West, who measured absorption spectra of poly[methyl(phenyl)silane], poly[cyclo-hexyl(methyl)silane], poly[n-dodecyl(methyl)silane] and obtained wavelength maximum on 340 nm, 325 nm and 310 nm, respectively.<sup>[9]</sup> The description of excitation transitions of poly[methyl(phenyl)silane] was provided in detail in ref.<sup>[2]</sup> where combinations of transition  $\sigma \rightarrow \sigma^*$  on Si backbone and  $\pi \rightarrow \pi^*$  of phenyl are shown. Transition from silicon backbone to phenyl substituent through charge transfer, designed as  $\sigma \rightarrow \pi^*$ ,

<sup>1</sup> Polymer Centre, Faculty of Technology, Tomas Bata University in Zlin, namesti T. G. Masaryka 275, Zlin 76272, Czech Republic  
E-mail: hanulikova@ft.utb.cz

<sup>2</sup> Centre of Polymer Systems, University Institute, Tomas Bata University in Zlin, Nad Ovcirnou 3685, Zlin 76001, Czech Republic

was also found in ref.<sup>[10,11]</sup> Piqueras et al. have computed recently that the first and the second transition could be assigned as  $\sigma \rightarrow \pi^*$  and  $\sigma \rightarrow \sigma^*$ , respectively but the latter is probably located on Si-C bond instead the Si-Si bond.<sup>[12]</sup> Generally, UV-vis spectra of organosilanes are dependent on temperature, electric and magnetic field or used solvent.<sup>[5]</sup>

Another substantial fact is the effect of secondary polymer structure on the electron excitation and related properties. That is why polysilane conformations were also object of abundant research, both experimental and theoretical. The structural arrangement of polysilanes is described by particular dihedral angle, which consists of four consecutive silicon atoms and which can adopt six local energy minima designed as *cisoid* (C, 40°), *gauche* (G, 60°), *ortho* (O, 90°), *deviant* (D, 150°), *transoid* (T, 165°) and *anti* (A, 180°) conformation. There are two more states of arrangement, *syn* (S, 0°) and *eclipsed* (E, 120°), however, they are not stable conformations and cannot be caught and held for some time by polysilane structure.<sup>[13,14]</sup> All of the angle values can be either positive (+) or negative (–) and in proper cases (e.g. rod-like crystalline polysilanes with *deviant* or *transoid* conformation along the chain) can create right- or left-handed helix, respectively.<sup>[15,16]</sup> The planar conformation for silicone backbone is called *all-anti* (in the earlier papers *all-trans*), which means that each successive dihedral angle is about 180°. This is the case of rigid, crystalline and insoluble poly(dimethylsilane), as was shown in ref.<sup>[17]</sup> Fuzakawa et al. used cyclic oligosilane structure, which was attached to linear octasilane chain and prepared *all-anti* conformer that can offer maximum of  $\sigma$ -conjugation.<sup>[18]</sup>

Furthermore, some of the polysilanes are polymorphous. For example, poly(methyl-n-propylsilane) is able to adopt *deviant*, *transoid* and *all-anti* conformation in dependence on the temperature and processing history.<sup>[19]</sup> The optimum conformation is also influenced by polaron or exciton formation.<sup>[20]</sup> These quasiparticles

are also involved in the changes of electron density distribution as well as vibrational and absorption spectra.<sup>[21]</sup>

However, the regularity of the chain can be disrupted when one of its parts is forced to change its conformation. One of these defects can be demonstrated as a kink which creates a bend on the otherwise regular chain. Some theoretical research on this topic with oligosilanes as quantum wires has already been done in past.<sup>[22]</sup> Nevertheless, deeper investigation which can indicate the direct influence of the particular kink on electronic properties (energy of frontier orbitals, absorption maximum or delocalization of molecular orbitals) of polysilanes is still missing and therefore is the aim of this research paper.

As proved in many references above, nowadays, it is more and more usual to support or directly lead the investigations of structural, electronic or other properties of various molecules on the theoretical level. The foundations of these computations, which were based on the Schrödinger equation, were developed into the form of the density functional theory (DFT) and later time-dependent density functional theory (TDDFT) by Hohenberg, Kohn and Sham in the original papers from 1960.<sup>[23,24,25]</sup> In the present investigations, DFT is among the most popular quantum chemical theories which are able to work with the large number of models and basis sets, which give them the required flexibility for calculation of both the ground and excited molecular state.<sup>[26,27]</sup> Quantum chemistry provides a palette of theoretical approaches which are able to give trustworthy results. One of them is DFT/B3LYP method. It brings a little of ambiguity to a precise solution of some theoretical terms used in description of DFT in comparison with Hartree-Fock models, such as an exchange-correlation functional.<sup>[28]</sup> On the other hand, it corresponds well to experimental data of conjugated systems, as it has been successfully demonstrated in<sup>[12,29]</sup> to name a few. Time dependent extension of DFT provides



results which are close to experimental values for excitation energies of many chemical compounds<sup>[30,31]</sup> and in combination with hybrid model B3LYP, DFT provides good computation-experimental agreement with the statistical deviation of excitation energies about 0.5 eV.<sup>[28]</sup>

In the present paper, DFT and TDDFT are used to predict electron properties of poly[(dimethyl)silylene] (PDMSi) and poly[methyl(phenyl)silylene] (PMPSi) by extrapolation of results obtained for analogous oligomers with the backbone length from one to ten (in case of (dimethyl)silylene oligomers to thirteen) silicone atoms.

## Molecules and Computational Methods

Alkyl- and aryl-substituted oligosilanes were investigated using Spartan '08<sup>[32]</sup> computational software. Oligo[methyl(phenyl)silane]<sub>s</sub> (OMPSi<sub>n</sub>) and oligo[(dimethyl)silane]<sub>s</sub> (ODMSi<sub>n</sub>), where *n* is 1–10 and 1–13, respectively, were used as model molecules. The terminal silicone atoms in each oligosilane chain were capped with methyl groups.

Each molecule of OMPSi<sub>n</sub> and ODMSi<sub>n</sub> was optimized by DFT with B3LYP hybrid model and 6–31G\* polarization basis set. Structures of approximately *transoid* (OMPSi<sub>n</sub>) and *all-anti* (ODMSi<sub>n</sub>) conformation were attained in the first step of calculation. Afterwards, a set of semi empirical PM3 calculations was done to obtain energy profiles of the oligosilane conformers (*n* ≥ 4) with different values of the dihedral angle representing the kink. From the plot of energy against this dihedral angle, the most suitable conformers, i.e. those containing the kink were chosen and set as initial guess to another structural optimization by DFT/B3LYP 6–31G\* to obtain the new energy minimum and at the same time to have more precise geometry of the required kink. Ideally, four silicon atoms forming the kink would have *syn* conformation, however, it is not

the energetically favourable position for systems with bulky substituents, and thus the energy minimum is not possible to obtain with this geometry. Therefore, the set of calculations was carried out with a different but realistic initial value of the kink angle to find the minimum as close to the *syn* value as possible. After optimization, this angle was virtually measured with the result of 50–60° for all oligosilanes and thus the kink with an approximate conformation of *gauche* was formed. All of these calculations were made in the ground state of oligomers and at the same time no constraints of bonds and angles were set in the calculations. In addition, neither temperature nor solvent effect was considered, thus all molecules were virtually treated *in vacuo*.

To properly evaluate electronic properties, excited state calculations were run with TDDFT B3LYP model and 6–31G\* basis set. In this case, the single point energy was calculated with the initial geometry which was obtained in previous steps.

As a result, absorption wavelengths, excitation energies, intensities, molecular orbital energies and others were attained and they are commented in the following text.

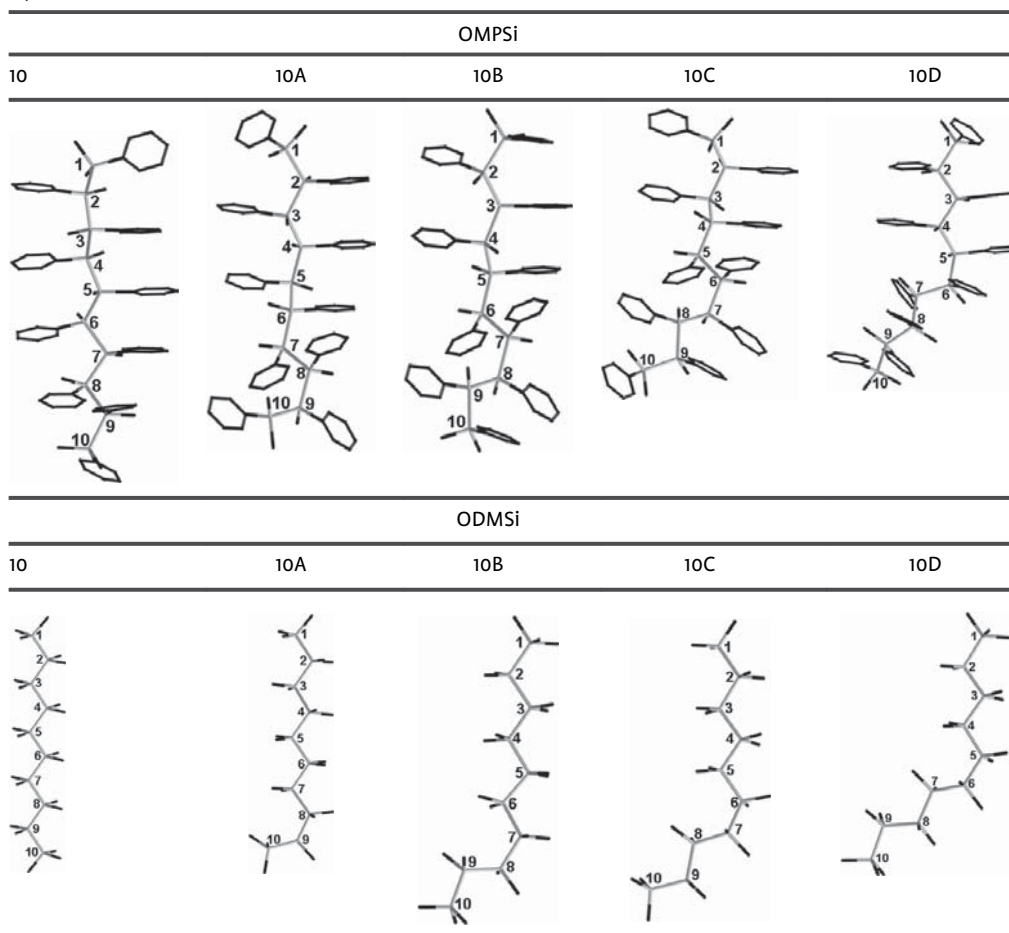
## Results and Discussion

### Geometry Optimization

*Gauche* conformation of the introduced kink was achieved during the optimization step in all studied molecules of OMPSi<sub>n</sub> and ODMSi<sub>n</sub>. Table 1 shows the optimized structures of decasilane oligomers and the position of the kink in the backbone to exemplify studied geometries. As can be seen, four kink positions can be obtained in decamer. The number of possible kink location is dependent on the length of the backbone, and from tetramer it increases by one per each two oligomers.

Oligosilane labels consist of a figure and a letter, where the first represents the number of silicon atoms in the backbone and the latter is the kink location. Carbon

**Table 1.**  
Optimized structures of decamer molecules with kink.



atoms are coloured in black and silicon atoms in light grey.

#### Delocalization and Absorption Spectra

The presence of the conformational defect represented by the kink causes significant

changes in molecular orbital (MO) energies in both alkyl- and aryl-substituted oligosilanes. Figure 1A depicts the highest and the lowest occupied molecular orbital (HOMO and LUMO, respectively) energies of ODMSi<sub>n</sub>. As can be clearly seen, LUMO

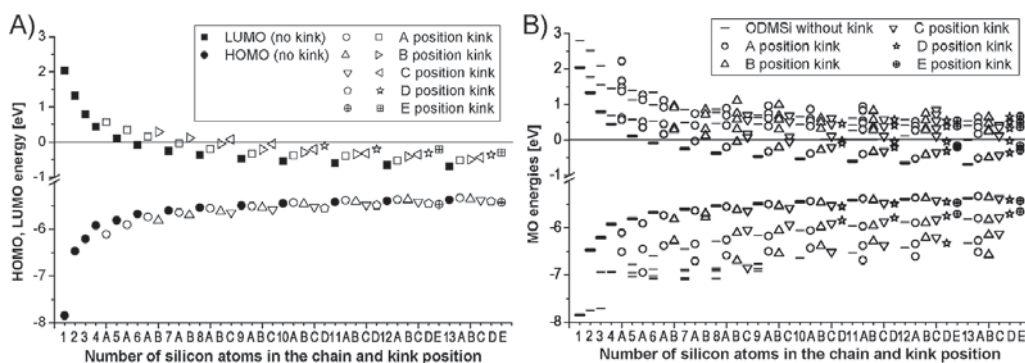


**Figure 1.**

- HOMO, LUMO energies of ODMSi oligomers depicted in detail (A) and MO energy levels involved in excitation process (B).

energy levels are reduced from positive to negative values with the increasing number of repeated units. However, the situation is more complex for ODMSi<sub>n</sub> with the kink. In case of kinked ODMSi<sub>1–5</sub>, LUMO energies have positive values. Therefore LUMO energies can be assumed as stable up from the ODMSi<sub>6–9</sub>, where LUMOs reach negative values in dependence on the particular position of the kink. Furthermore, a presence of the kink itself causes increase in the LUMO energies and this trend continues substantially as the conformational defect position alters along the chain. In detail, the further from the end of the chain the kink is located, the higher the LUMO energy. The similar difference between LUMO of the chain with no kink and LUMO of the last possible oligomer with the kink can be seen in all ODMSi<sub>n</sub> and its value is around 0.4 eV. On the other hand, HOMO energy levels of ODMSi<sub>n</sub> evince opposite behaviour as their energy decreases with the kink position and generally they are affected to the lesser extent. Apparently, these energies stabilise when heptamer chain length is reached and further they stay on the similar level. In this case the scatter of values in HOMO energies between ODMSi<sub>n</sub> of the same chain length is around 0.1 eV.

Part B of Figure 1 shows all MO energy levels of ODMSi<sub>n</sub>, which are involved in the excitation process. As can be observed, energies of the levels above LUMO (supra-levels) are in most ODMSi<sub>n</sub> unstable, which corresponds with their UV-vis spectra. This fact can be seen in graphical inset in Table 2 which represents calculated UV-vis spectra of ODMSi<sub>10</sub>. The absorption maximum at 280–250 nm is assigned to HOMO→LUMO transition. As the kink changes its position further from the chain end, the maximum absorption wavelength ( $\lambda_{\max}$ ) is shifted to lower values and therefore the band gap increases. Another fact is that with increasing values of LUMO energies in dependence on the kink position, the LUMO + 1 level evince complementary decrease approaching the frontier energy level.

Figures 2A, 2B and graphical inset in Table 3 show MO energies and UV-vis spectra of OMPSi<sub>n</sub>. When compared with ODMSi<sub>n</sub>, the main difference lies in the fact that all LUMO energies have stable negative values and HOMO energies are slightly more influenced than LUMO energy level by the kink presence and position.

Although the variations in energy values (LUMO around 0.1 eV, HOMO 0.15 eV) are not so evident as in ODMSi<sub>n</sub>, the clear shift is observable in absorption spectra in Table 3. The band gap is created between HOMO and supra-LUMO levels in OMPSi<sub>n</sub> (detailed assignments are also provided in Table 3) and combines  $\sigma \rightarrow \sigma^*$  transitions and  $\sigma \rightarrow \pi^*$ . HOMO→LUMO transition is realised in cases with LUMO delocalized along the backbone not only along aromatic substituents, as can be seen in Figure 4.

Computed values of both ODMSi<sub>n</sub> and OMPSi<sub>n</sub> excitation energies (E) are slightly overestimated (around 0.5 eV) in comparison with experimental results published in.<sup>[2,33,34]</sup>

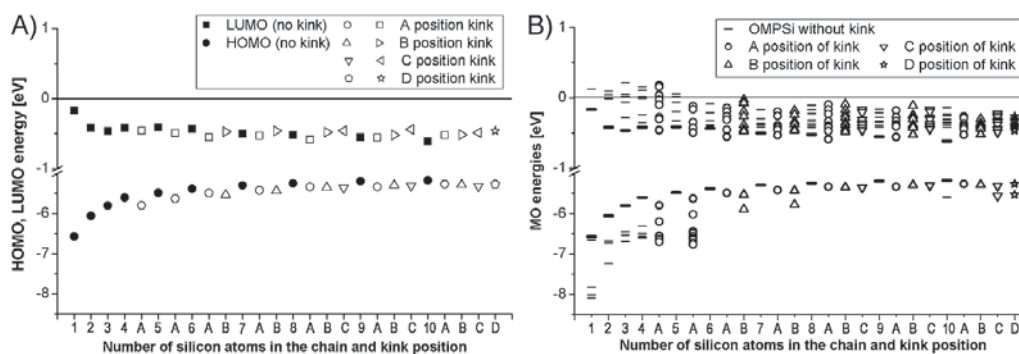
Delocalization of MO along the molecules of ODMSi<sub>n</sub> and OMPSi<sub>n</sub> is of essential importance. Figure 3 and Figure 4 display delocalization of HOMO, LUMO and other MO involved in UV-vis absorptions of ODMSi<sub>n</sub> and OMPSi<sub>n</sub>, respectively. The most important are HOMOs and LUMOs as they determine the absorption edge and maximum.

ODMSi<sub>10</sub> without the kink has both FMO (Frontier Molecular Orbitals) delocalized equally along the whole chain length. On the contrary, 10A, 10B and 10C oligomers seem to be divided into two parts by the introduced kink. Equal delocalization is kept only on the longer part of the chain and reaches the centre of the defect. At the same time, the rest of the molecule, representing the shorter part of the molecule, is almost completely without FMOs delocalization. This influence of *gauche* conformation occurs when the kink divides the structure into asymmetric parts. Therefore, in the case of 10D this effect disappears and FMOs are delocalized along the whole chain as in 10 because of perfect symmetry.

**Table 2.**  
Calculated UV-vis spectra and excitation process data of ODMSi<sub>10</sub>.

UV-vis spectra of ODMSi <sub>10</sub>					ODMSi 10							
	E [eV]	λ [nm]	M	I [a.u.]	MO	A	E [eV]	λ [nm]	M	I [a.u.]	MO	A
	4.3732	284	S	2.0023	H→L	0.985	5.1307	242	S	0	H-1→L	0.983
	5.1522	241	S	0.0002	H→L + 2	0.967	5.3956	230	S	0	H-1→L + 2	-0.357
					H→L + 3	0.908	5.4448	228	S	0	H→L + 1	0.980
							5.685	218	S	0.0021	H-2→L	0.977
ODMSi 10A						ODMSi 10B						
E [eV]	λ [nm]	M	I [a.u.]	MO	A	E [eV]	λ [nm]	M	I [a.u.]	MO	A	
4.4985	276	S	1.6962	H→L	0.985	4.6187	268	S	1.5149	H→L	0.982	
5.0854	244	S	0.0004	H→L + 1	0.946	5.0934	243	S	0.0105	H→L + 1	0.881	
										H→L + 2	0.373	
5.2453	236	S	0.0060	H-1→L	0.970	5.2139	238	S	0.0501	H-1→L	0.951	
5.2960	234	S	0.0011	H-1→L + 1	0.296	5.2984	234	S	0.0878	H→L + 1	-0.332	
				H→L + 2	0.759					H→L + 2	0.676	
				H→L + 3	0.487					H→L + 3	0.549	
5.5063	225	S	0.0048	H-2→L	0.403	5.4693	227	S	0.0673	H→L + 2	-0.580	
				H→L + 2	-0.457					H→L + 3	0.712	
				H→L + 3	0.690							
				H→L + 4	0.294							
5.5675	223	S	0.0013	H-2→L	0.828	5.6203	221	S	0.0279	H-2→L	0.957	
				H→L + 2	0.295							
				H→L + 3	-0.371							
ODMSi 10C						ODMSi 10D						
E [eV]	λ [nm]	M	I [a.u.]	MO	A	E [eV]	λ [nm]	M	I [a.u.]	MO	A	
4.7671	260	S	1.3360	H→L	0.965	4.9064	253	S	1.4185	H-1→L	-0.253	
										H→L + 1	0.946	
5.0506	245	S	0.1738	H→L + 1	0.908	4.9758	249	S	0.1583	H-1→L	0.977	
				H→L + 2	-0.305							
5.1904	239	S	0.2784	H-1→L	0.923	5.1751	240	S	0.4305	H-1→L	0.874	
				H→L + 2	0.238					H→L + 2	0.398	
5.2850	235	S	0.1265	H→L + 1	0.294	5.3250	233	S	0.0259	H-1→L	-0.368	
				H→L + 2	0.807					H-1→L + 3	-0.294	
				H→L + 3	-0.364					H→L + 1	-0.223	
										H→L + 2	0.841	
5.4329	228	S	0.0156	H-1→L + 1	-0.495	5.3279	233	S	0.0977	H-1→L + 1	0.796	
				H-1→L + 2	0.315					H-1→L + 2	0.342	
				H→L + 2	0.321					H→L + 3	-0.454	
				H→L + 3	0.633							
5.5279	224	S	0.2325	H-1→L + 1	0.788	5.4586	227	S	0.0575	H-1→L + 1	0.570	
				H→L + 3	0.480					H-1→L + 2	-0.383	
										H→L + 3	0.688	

E [eV] – excitation energy; λ [nm]– wavelength; M – multiplicity; I [a.u.] – intensity (oscillator strength); MO – molecular orbital; A –amplitude; S – singlet

**Figure 2.**

HOMO, LUMO energies of OMPSi oligomers depicted in detail (A) and MO energy levels involved in excitation process (B).

**Table 3.**

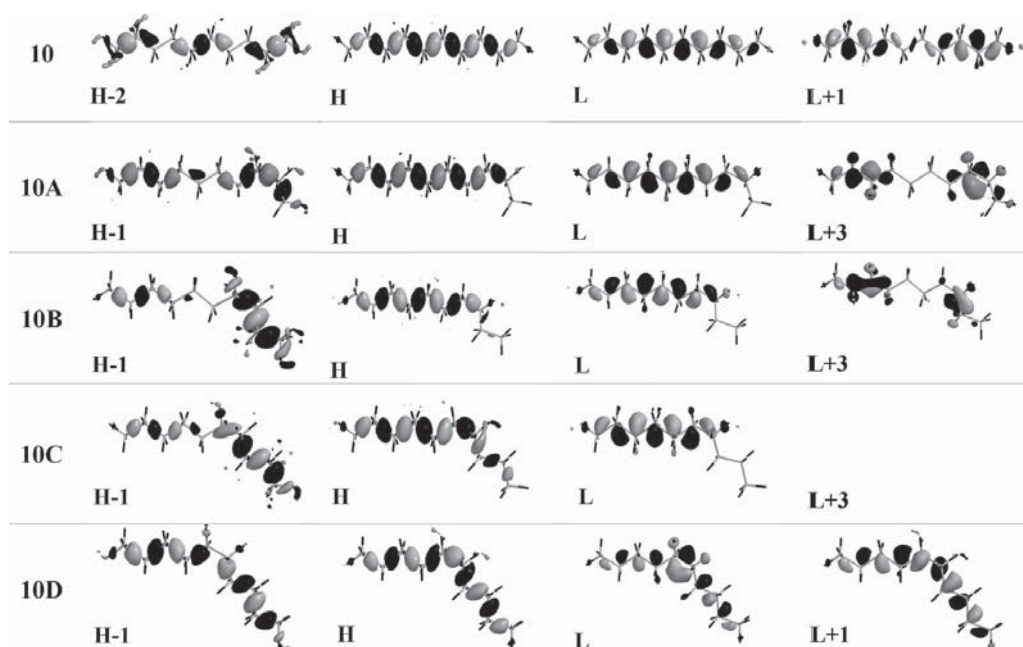
UV-vis spectra and excitation process data of OMPSi<sub>10</sub>. For explanation of symbols and abbreviations see the legend in Table 2.

UV-vis spectra of OMPSi <sub>10</sub>		OMPSi 10									
	10D	4.0063	309	S	1.3942	H→L	0.971				
	10C	4.2826	290	S	0.0676	H→L+1	0.937				
		4.3214	287	S	0.0438	H→L+2	0.845				
	10B	4.3360	286	S	0.0354	H→L+3	-0.270				
	10A	4.3677	284	S	0.0309	H→L+5	-0.235				
10	4.3803	283	S	0.0350	H→L+6	0.246					
						H→L+2	0.334				
						H→L+3	0.847				
						H→L+6	-0.302				
						H→L+3	-0.279				
						H→L+4	0.577				
						H→L+5	-0.348				
						H→L+6	-0.467				
						H→L+7	0.410				
						H→L+4	0.598				
						H→L+6	0.221				
						H→L+7	-0.600				
						OMPSi 10A		OMPSi 10B			
E [eV]	λ [nm]	M	I [a.u.]	MO	A	E [eV]	λ [nm]	M	I [a.u.]	MO	A
4.1950	296	S	1.1202	H→L	0.878	4.2548	291	S	0.8880	H→L	0.740
				H→L+1	-0.310					H→L+1	-0.408
										H→L+2	0.373
										H→L+4	-0.247
4.3301	286	S	0.0160	H→L	0.291	4.3190	287	S	0.0497	H→L	0.621
				H→L+1	0.875					H→L+1	0.595
				H→L+4	0.271					H→L+2	-0.263
										H→L+4	0.335
4.3613	284	S	0.0797	H→L	0.282	4.4057	281	S	0.0979	H→L+2	0.406
				H→L+2	0.819					H→L+3	-0.264
				H→L+3	-0.276					H→L+4	0.782
				H→L+4	0.230					H→L+5	0.241
				H→L+6	-0.240						
4.4173	281	S	0.0787	H→L+1	-0.261	4.4261	280	S	0.0638	H→L+2	0.438
				H→L+3	0.345					H→L+3	0.730
				H→L+4	0.864					H→L+5	-0.399

(Continued)

**Table 3.** (Continued)

OMPSi 10A						OMPSi 10B					
4.4663	278	S	0.0230	H→L+2 H→L+6	-0.239 -0.908	4.4628	278	S	0.1222	H→L+1 H→L+2 H→L+3 H→L+5	0.532 0.420 -0.517 -0.365
4.502	275	S	0.0690	H→L+2 H→L+3 H→L+4	0.299 0.789 -0.285	4.4916	276	S	0.0354	H→L+2 H→L+4 H→L+5	0.424 -0.332 0.724
OMPSi 10C						OMPSi 10D					
E [eV]	λ [nm]	M	I [a.u.]	MO	A	E [eV]	λ [nm]	M	I [a.u.]	MO	A
4.3319	286	S	0.4887	H→L	0.969	4.2649	291	S	0.8493	H→L	0.940
4.3769	283	S	0.1233	H→L+1 H→L+2 H→L+5	0.856 -0.303 -0.235	4.3408	286	S	0.2485	H→L+1 H→L+2 H→L+3 H→L+4	-0.527 0.496 0.529 0.334
4.4485	279	S	0.2987	H-1→L+1 H→L+1 H→L+2 H→L+5	0.257 0.388 0.772 0.290	4.3715	284	S	0.1900	H→L+1 H→L+2 H→L+3	0.801 0.407 0.344
4.4859	276	S	0.2510	H-1→L+5 H→L+2 H→L+5 H→L+6	-0.222 -0.388 0.776 -0.224	4.4296	280	S	0.0124	H→L+3 H→L+4 H→L+6	-0.561 0.676 -0.267
4.5331	274	S	0.1059	H-1→L+2 H→L+3 H→L+4 H→L+6	-0.281 0.594 0.471 -0.451	4.4571	278	S	0.0736	H-1→L+2 H→L+2 H→L+3 H→L+4 H→L+5 H→L+6	0.298 0.575 0.321 -0.339 0.331 -0.416
4.5449	273	S	0.0424	H-1→L+2 H-1→L+3 H→L+3 H→L+4 H→L+7	-0.250 -0.224 -0.478 0.591 -0.399	4.5029	275	S	0.0463	H-1→L+4 H→L+2 H→L+4 H→L+5 H→L+6	0.240 -0.311 0.318 0.737 0.256

**Figure 3.**Molecular orbitals of ODMSi<sub>10</sub> - positive MO grey, negative MO black.

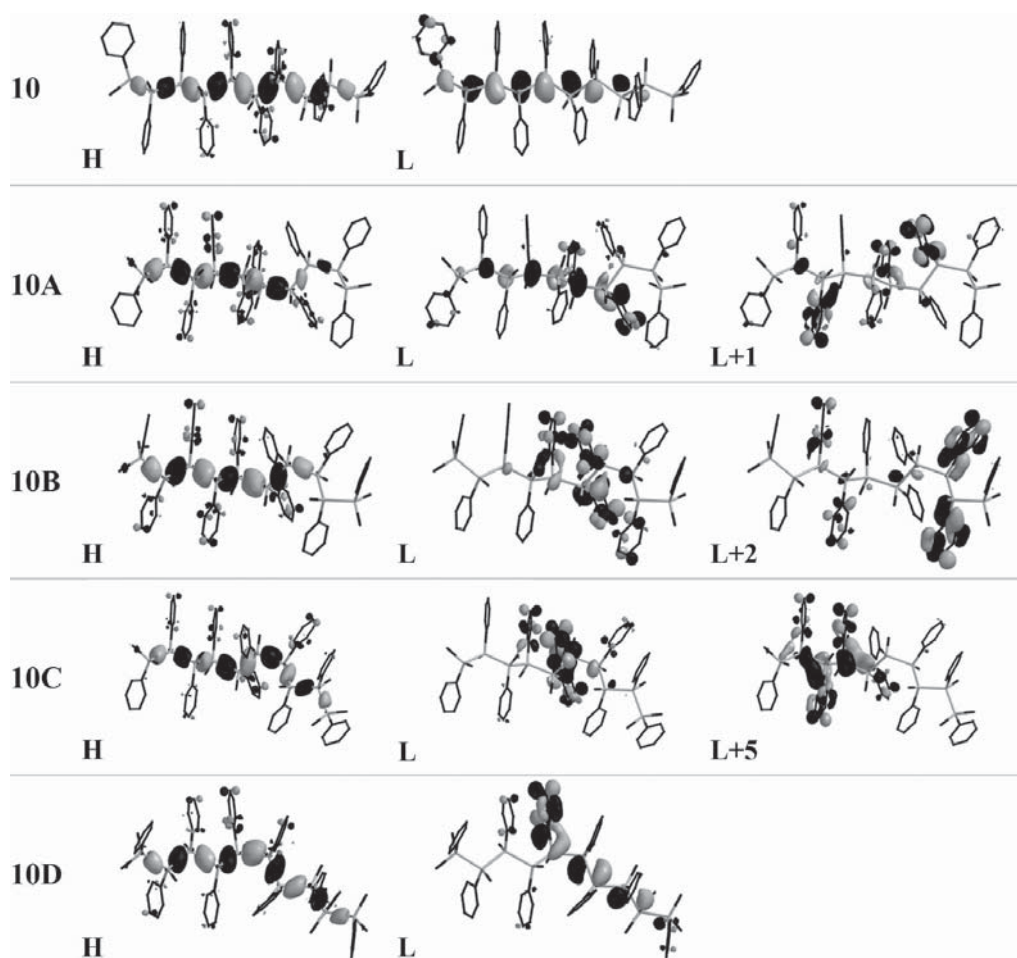


**Figure 4.**  
Molecular orbitals of  $\text{OMPSi}_{10}$ —positive MO grey, negative MO black.

In  $\text{OMPSi}_{10}$  the situation is partially different. Previous claims on orbital delocalization and density distribution are valid only for HOMOs. LUMOs are also delocalized to phenyl rings to some extent and in some cases (10B and 10C) they are located mostly on the rings which are attached exactly to the defect part of the structure. This indicates possible trap sites for eventual charge transfer state generation. In next, the symmetry of LUMOs involving  $\sigma$ - $\pi$  mixing with  $\pi$  orbitals of phenyl groups helically arranged along the chain is not that perfect as in purely  $\sigma$ -like LUMOs of  $\text{ODMSi}_n$  in case of the D-position of the kink. It can be seen in Figure 4 that a delocalisation of the  $\text{OMPSi}_{10}$  LUMO spreads from the chain over a phenyl group in suitable position extending thus the

conjugation length in one direction which is probably more energetically favourable than delocalisation over the other part of the chain which would be shorter.

#### Extrapolation to Polysilanes

The number of oligomers which served as model molecules was chosen according to the computational time convenience.  $\text{OMP-Si}_n$  were therefore investigated to decamers, while  $\text{ODMSi}_n$  to tridecamers. Obtained HOMO and LUMO energies were then plotted as a function of reciprocal number of Si atoms in the chain ( $1/N$ ) with linear regression. For the purpose of linearization, the first three values (monomer to trimer) of FMO energies were omitted as they cannot represent the defect structure involving four Si atoms at all. The

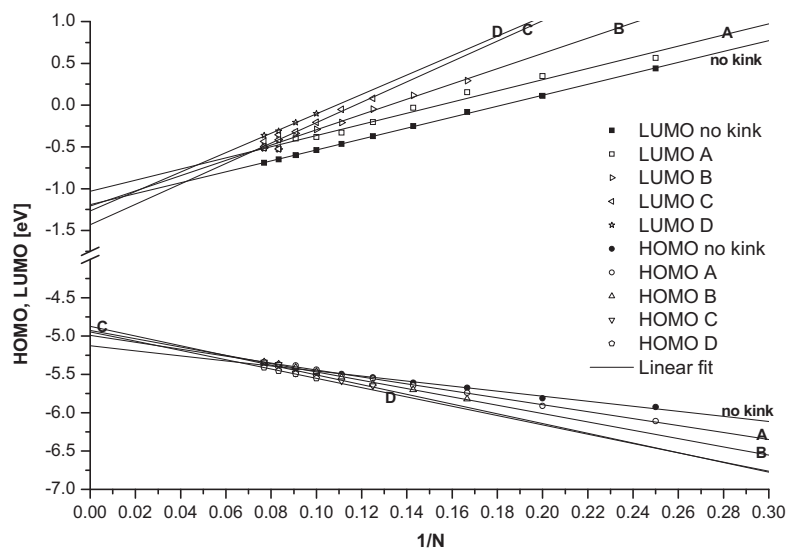


**Figure 5.**  
Linear regression of ODMSi<sub>n</sub> LUMO and HOMO energies vs. 1/N, N > 3.

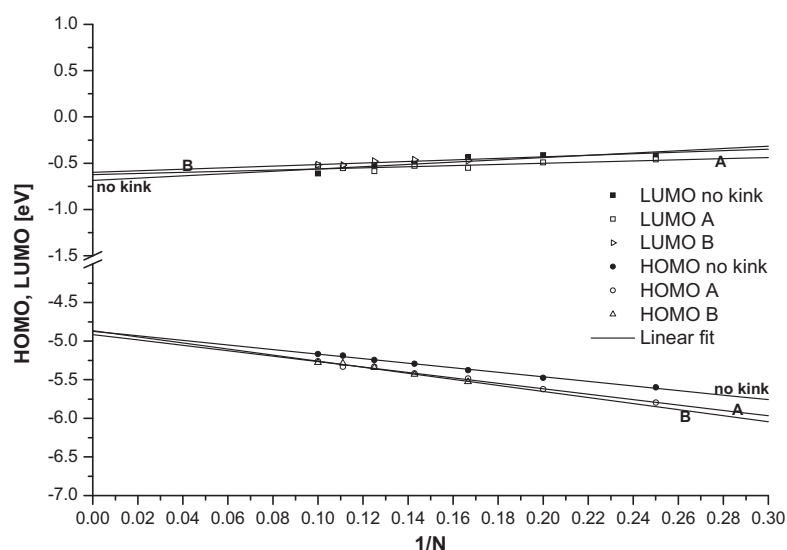


**Figure 6.**  
- Linear regression of OMPSi<sub>n</sub> LUMO and HOMO energies vs. 1/N, N > 3.

properties of higher polymeric chains can therefore be predicted. Figure 5 and Figure 6 illustrate linearized dependence of MO energies on the chain length for ODMSi<sub>n</sub> with the kink at A, B, C and D position and OMPSi<sub>n</sub> with the kink at A and B position, respectively. As can be seen, this fitting curve was chosen in vast majority of cases properly as the points are in agreement with linear function (predicted values

of FMO energies for polymer-size backbones, mean errors and coefficients of determination are listed in Table 4). The exception in these reliable linear trends is the dependence of LUMO energies of PMPSi on 1/N where coefficients of determination are only around 0.6.

FMO energy values for infinite defectless chain were predicted ( $-0.69 \pm 0.05$  eV and  $(-4.87 \pm 0.01)$  eV for PMPSi and



**Table 4.**  
Linear regression data

PDMSi	HOMO (poly)	R <sup>2</sup>	LUMO (poly)	R <sup>2</sup>
no kink	-5.13 ± 0.01	0.995	-1.19 ± 0.01	1.000
A	-4.99 ± 0.01	0.998	-1.03 ± 0.04	0.985
B	-4.94 ± 0.02	0.996	-1.16 ± 0.03	0.996
C	-4.97 ± 0.03	0.989	-1.28 ± 0.05	0.991
D	-4.95 ± 0.02	0.997	-1.27 ± 0.06	0.993
PMPSi	HOMO (poly)	R <sup>2</sup>	LUMO (poly)	R <sup>2</sup>
no kink	-4.87 ± 0.01	0.995	-0.69 ± 0.05	0.788
A	-4.91 ± 0.02	0.993	-0.62 ± 0.04	0.613
B	-4.87 ± 0.04	0.989	-0.60 ± 0.05	0.676

(-1.19 ± 0.01) eV and (-5.13 ± 0.01) eV for PDMSi. Introduction of the kink at the end of a semi-infinite chain causes observable decrease of LUMO energy from -0.69 eV to -0.6 eV for PMPSi and has no effect on its HOMO energy level. The opposite effect can be observed for PDMSi. In this case, the kink at the end of a semi-infinite chain slightly elevates HOMO level from -5.13 eV to -4.9 eV and there is almost no effect on LUMO energy. When deviations of HOMO and LUMO energies for infinite chain length are considered, it can be said that the fitting curves meet in one point, which is expectable due to the presumption that the kink, which is located in the backbone as was described above, does not significantly influence properties of very long molecules without any other defect. In addition, overall precision cannot be better than 0.5 eV which arises from the application of DFT.

Beside extrapolation, we claim that the other findings obtained for treated oligomers hold on for long chain polymers adequately as well.

## Conclusion

Delocalization of molecular orbitals is very asymmetric and localized to the longer segment when conformational defect, here presented by the kink of *gauche* conformation, is introduced into silicon backbones of both alkyl- and aryl-substituted oligosilanes. This causes the shift of absorption maxima to lower wavelengths as the

position of the kink is moved to the centre of the chain, in other words, the conjugated segments become shorter. If the linearity of polysilane chain is disrupted FMOs are located on longer segments as they allow greater extent of delocalization. A fully symmetric situation can occur for oligomers with even number of Si atoms which mean that no segment is energetically favourable as they are of the same length. For LUMO in OMPSi oligomers, this can be corrupted locally with the contribution of phenyl group which is in suitable position with respect to one of the two segments.

FMO energy also evinces clear dependence on the kink location. Generally, in both studied types of structures, HOMO energies decrease while LUMO energies increase as the *gauche* defect alters its position to the centre of the backbone. In case of PMPSi the kink is expected to be the potential trap site for charge transfer complex formation. However, optimal geometries of molecules in excited states have not been addressed in this study because the computational time is too high.

*Acknowledgement:* This work was supported by the Internal Grant Agency of Tomas Bata University in Zlin (grant No. IGA/FT/2013/025). This paper was written with support of Operational Program Research and Development for Innovations co-funded by the European Regional Development Fund (ERDF) and national budget of the Czech Republic, within the framework of project Centre of Polymer Systems (reg. number: CZ.1.05/2.1.00/03.0111) and with support of Operational Program Education for Competitiveness co-funded by

the European Social Fund (ESF) and national budget of the Czech Republic, within the framework of project Advanced Theoretical and Experimental Studies of Polymer Systems (reg. number: CZ.1.07/2.3.00/20.0104).

- [1] Y. V. Demchenko, J. Klimovic, S. Nespurek, *Macromol. Symp.* **2004**, 212, 461.
- [2] C. C. Phifer, W. J. Thomes, K. Simmnos-Potter, B. G. Potter, *J. Chem. Phys.* **2004**, 120, 1613.
- [3] S. Nespurek, G. Wang, K. Yoshino, *J. Optoelectron. Adv. M.* **2005**, 7, 223.
- [4] V. V. Semenov, *Russ. Chem. Rev.* **2011**, 80, 313.
- [5] J. E. Mark, H. R. Allcock, R. West, "Inorganic Polymers", Oxford University Press, New York **2005**, p. 200.
- [6] A. Watanabe, *J. Organomet. Chem.* **2003**, 685, 122.
- [7] H. Lei, C. Baoxue, I. Mamoru, *Opt. Mater.* **2011**, 33, 452.
- [8] R. Shankar, U. Sahoo, V. Shahi, *Macromolecules* **2011**, 44, 3240.
- [9] R. West, *J. Organomet. Chem.* **1986**, 300, 327.
- [10] S. Nespurek, J. Sworakowski, A. Kadashchuk, P. Toman, *J. Organomet. Chem.* **2003**, 685, 269.
- [11] S. Nespurek, A. Eckhardt, *Polym. Adv. Technol.* **2001**, 12, 427.
- [12] M. C. Piqueras, R. Crespo, J. Michl, *J. Phys. Chem. A* **2008**, 112, 13095.
- [13] J. Michl, R. West, *Accounts Chem. Res.* **2000**, 33, 821.
- [14] H. A. Fogarty, C.-H. Ottosson, J. Michl, *J. Mol. Struct. Theochem.* **2000**, 506, 243.
- [15] M. Fujiki, *J. Organomet. Chem.* **2003**, 685, 15.
- [16] T. Karatsu, *J. Photoch. Photobio. C* **2008**, 9, 111.
- [17] S. Furukawa, H. Ohta, *Thin Solid Films* **2003**, 438, 48.
- [18] A. Fuzakawa, H. Tsuji, K. Tamao, *J. Am. Chem. Soc.* **2006**, 128, 6800.
- [19] S. V. Bukalov, Y. V. Zubavichus, L. A. Leites, J. R. Koe, R. West, *Polymer* **2009**, 50, 4845.
- [20] P. Toman, *Synthetic Met.* **2000**, 109, 259.
- [21] J. Nozar, S. Nespurek, J. Sebera, *J. Mol. Model.* **2012**, 18, 623.
- [22] H. Taremae, N. Matsumoto, *Solid State Commun.* **1996**, 99, 917.
- [23] P. Hohenberg, W. Kohn, *Phys. Rev.* **1964**, 136, B864.
- [24] W. Kohn, L. J. Sham, *Phys. Rev.* **1965**, 140, A1133.
- [25] M. A. L. Marques, E. K. U. Gross, *Annu. Rev. Phys. Chem.* **2004**, 55, 427.
- [26] M. E. Casida, *J. Mol. Struct. Theochem.* **2009**, 914, 3.
- [27] K. Burke, J. Werschnik, E. K. U. Gross, *J. Chem. Phys.* **2005**, 123, 062206.
- [28] R. Bauernschmitt, R. Ahlrichs, *Chem. Phys. Lett.* **1996**, 256, 454.
- [29] R. Crespo, M. C. Piqueras, J. Michl, *Theor. Chem. Acc.* **2007**, 118, 81.
- [30] M. Promkatkaew, S. Suramitr, T. Karpkird, M. Ehara, S. Hannongbua, *Int. J. Quantum Chem.* **2013**, 113, 542.
- [31] A. Dreuw, M. Head-Gordon, *Chem. Rev.* **2005**, 105, 4009.
- [32] CA. Y. Spartan, '08 Wavefunction Inc, Irvine. L. F. Shao, Y. Molnar, J. Jung, S. T. Kussmann, C. Brown, A. T. B. Ochsenfeld, L. V. Gilbert, S. V. Slipchenko, D. P. Levchenko, R. A. O'Neill, R. C. DiStasio, Jr., T. Lochan, G. J. O. Wang, N. A. Beran, J. M. Besley, C. Y. Herbert, T. Lin, S. H. Van Voorhis, A. Chien, R. P. Sodt, V. A. Steele, P. E. Rassolov, P. P. Maslen, R. D. Korambath, B. Adamson, J. Austin, E. F. C. Baker, H. Byrd, R. J. Dachsel, A. Doerksen, B. D. Dreuw, A. D. Dunietz, T. R. Dutoi, S. R. Furlani, A. Gwaltney, S. Heyden, C.-P. Hirata, G. Hsu, R. Z. Kedziora, P. Khalliulin, A. M. Klunzinger, M. S. Lee, W. Z. Lee, I. Liang, N. Lotan, B. Nair, E. I. Peters, P. A. Proynov, Y. M. Pieniazek, J. Rhee, E. Ritchie, C. D. Rosta, A. C. Sherrill, J. E. Simmonett, H. L. Subotnik, I. I. Woodcock, W. Zhang, A. T. Bell, A. K. Chakraborty, D. M. Chipman, F. J. Keil, A. Warshel, W. J. Hehre, H. F. Schaefer, J. Kong, A. I. Krylov, P. M. W. Gill, M. Head-Gordon, *Phys. Chem. Chem. Phys.* **2006**, 8, 3172.
- [33] N. Matsomoto, *Jpn. J. Appl. Phys.* **1998**, 37, 5425.
- [34] Y. A. Skryshevskii, *J. Appl. Spectrosc.* **2003**, 70, 855.

## Research Paper II:

**HANULIKOVA, Barbora, Ivo KURITKA and Pavel URBANEK.**

Effect of backbone conformation and its defects on electronic properties and assessment of the stabilizing role of  $\pi$ - $\pi$  interactions in aryl substituted polysilylenes studied by DFT on deca[methyl(phenyl)silylene]s

*Chemistry Central Journal*. 2016, vol. 10, no. 28.



RESEARCH ARTICLE

Open Access



# Effect of backbone conformation and its defects on electronic properties and assessment of the stabilizing role of $\pi$ - $\pi$ interactions in aryl substituted polysilylenes studied by DFT on deca[methyl(phenyl)silylene]s

Barbora Hanulikova\*, Ivo Kuritka and Pavel Urbanek

## Abstract

**Background:** Recent efforts in the field of mesoscale effects on the structure and properties of thin polymer films call to revival interest in conformational structure and defects of a polymer backbone which has a crucial influence on electronic properties of the material. Oligo[methyl(phenyl)silylene]s (OMPSi) as exemplary molecules were studied theoretically by DFT in the form of optimal decamers and conformationally disrupted decamers (with a kink).

**Results:** We proved that *transoid* backbone conformation is true energy minimum and that a kink in the backbone causes significant hypsochromic shift of the absorption maximum ( $\lambda_{max}$ ), while backbone conformation altering from all-*eclipsed* to all-*anti* affects  $\lambda_{max}$  in the opposite way.  $\pi$ - $\pi$  stacking was investigated qualitatively through optimal geometry of OMPSi and mutual position of their phenyls along the backbone and also quantitatively by an evaluation of molecular energies obtained from single point calculations with functionals, which treat the dispersion effect in the varying range of interaction.

**Conclusions:** The kink was identified as a realistic element of the conformational structure that could be able to create a bend in a real aryl substituted polysilylene chain because it is stabilized by attractive  $\pi$ - $\pi$  interactions between phenyl side groups.

**Keywords:** Density functional calculations, Kink, Methyl(phenyl)silylene, Stacking interaction, UV/Vis spectroscopy

## Background

Silicon (Si) polymers with -Si-Si- backbones carry delocalized  $\sigma$ -electrons as their  $sp^3$  orbital lobes can overlap [1, 2]. From this point of view, polysilylenes substantially differ from single-bonded carbon analogues (e.g. polyethylene, polystyrene), especially in the area of optoelectronic properties [3]. Electron delocalization origins in Si atoms arrangement and therefore it is highly dependent on the polysilylene secondary structure [4]. Maximum of  $\sigma$ -conjugation is related with all-*anti* backbone

conformation, which can be found in dialkylsilylenes with small side groups, for instance poly(dimethylsilylene) (PDMSi) [5, 6]. On the other hand, poly[methyl(phenyl)silylene] (PMPSi) is arranged into helix due to presence of bulky phenyl (Ph) groups and with them related *deviant* or *transoid* backbone conformation [6-8]. Polysilylene chains are not single rod-like, they form random coil in solutions. Similarly in solid phase, the most of polysilylenes is semi-crystalline and contains regular as well as amorphous phase. Recent efforts in the field of mesoscale effects on structure and properties of thin polymer films made from both  $\pi$ - and  $\sigma$ -conjugated conductive polymers call to revival interest in conformational structure and defects of a polymer backbone which has crucial

\*Correspondence: hanulikova@cps.utb.cz  
Centre of Polymer Systems, Tomas Bata University in Zlin,  
trida Tomase Bati 5678, 76001 Zlin, Czech Republic

influence on electronic properties of the material. It has been already shown by different groups that polymer conformational order/disorder shows strong dependence on the thin film thickness in order of hundredths nm and results into non-trivial effects on optoelectronic properties in terms of segment conjugation length, luminescence, photovoltaic effect, exciton diffusion length [9–12] and fine bandgap electronic structure (density of deep states) [13, 14]. Obviously, the polymer structure itself and other typical polymer related properties [15–17] are influenced too. Hence, various bends of backbones are needed for the creation of regular or irregular arrangements. Such bend can be regarded as conformational defect because it disrupts regular  $\sigma$ -delocalization and therefore influences final polysilylene properties [18, 19]. This defect was defined as a *gauche*-kink in the backbone and described on oligo-DMSi<sub>n</sub> (ODMSi) and oligo-MPSi<sub>n</sub> (OMPSi) with  $n = 1$ –10 by density functional theory (DFT) in our previous work, where the kink influence on the electronic properties of oligosilylenes was confirmed [20]. The change has been clearly manifested in absorption spectra plots, where hypsochromic shift of the main absorption band had been detected. In addition, the shift is more strongly pronounced as the kink position altered closer the centre of a backbone. Another cause that is responsible for a rearrangement of the oligosilylene molecule can be identified as a charge carrier in its vicinity. From this reason, we have also investigated polaron quasiparticles of OMPSi<sub>n</sub> with the introduced kink [21]. In that research, a significant change has emerged in a dependence of the spin density on the conformation of a backbone and its shift to more regular part of a Si–Si chain, i.e. a shift from the kink.

The p orbitals are distributed on the Ph rings in PMPSi and it seems reasonable that  $\pi$ – $\pi$  interactions are employed during geometry arrangement and stabilization. This type of non-bonding interaction was described in detail by Hunter or Gung in 1990s, however the interaction has already been known since the first half of 20th century [22–24]. These interactions play an important role in stabilization of double helix of nucleic acids or other biologically active substances and they have been abundantly studied in these areas, e.g. Ref. [25–27]. The character of the interaction (i.e. whether the interaction is attractive or repulsive) depends on the mutual position of involved aromatic rings (on their distance and angle between planes). Several positions were described and defined; they are sandwich, parallel displaced (offset of rings), T-shape and edge-to-face arrangements. The first is representative of repulsive interactions as the p orbitals, which carry delocalized  $\pi$ -electrons, are oriented to each other. The rest evince attractive interaction, whose

intensity is dependent on the particular ring offset [28, 29]. Recent research, e.g. review [30], has suggested not to use only the term  $\pi$ -stacking for a description of all non-bonding interactions between aromatic groups as it could be related predominantly to a rarely observed face-to-face arrangement and regarded as insufficient for expression of other offset positions.

Contemporary theoretical research often uses DFT and time dependent-DFT (TD-DFT) that has been established by Kohn and Sham [31–33] and Runge and Gross [34, 35], respectively. B3LYP (Becke-3-Lee-Young-Parr) model has been confirmed as suitable for calculations on silicon compounds [32, 36]. Its use for geometry optimization is indisputable and in many cases, it is as well as sufficient for calculation of spectral or thermal properties [37, 38]. However, B3LYP functional is not able to clearly distinguish energy changes related with non-bonding interactions which are better covered in density functionals involving dispersion term in their definition [39]. For  $\pi$ – $\pi$  interaction energy evaluation are therefore usually used functionals such as M06 [40],  $\omega$ B97X-D [41] or B3LYP-D [42], which are also able to characterise low- and long-range electron–electron interactions at various levels.

The present paper is another from the series of a computationally-led investigation of oligosilylenes and the purpose of this work is a determination of a mutual influence of silicon backbone conformation and conformational defect on the excitation properties of OMPSi<sub>10</sub>. Several constrained structures are here investigated to obtain a detailed and comprehensive view on the conformation issues as well as to confirm *deviant* or *transoid* conformation to be the global energy minimum. Description of  $\pi$ – $\pi$  interactions of various conformations in the vicinity of the conformational defect is done through evaluation of phenyl angle-distance plot obtained from optimized geometries and molecular energy evaluation obtained from single point calculations with three different density functionals. We believe that results of this model study can be generalised and a useful lesson towards description of real polysilylene polymers can be learned from it.

## Experimental

PMPSi was obtained from Fluorochem Ltd. UK, GPC analysis revealed  $M_w = 27,600$  g/mol and  $M_n = 8500$  g/mol. Films for UV–Vis measurements were prepared by the spin coating method using spin coater Laurell WS-650-MZ-23NPP from the solution in toluene. Quartz glass was used as a substrate. The absorption spectrum was measured by Lambda 1050 UV/Vis/NIR spectrometer from Perkin Elmer.

## Computational methods

### Geometry optimization

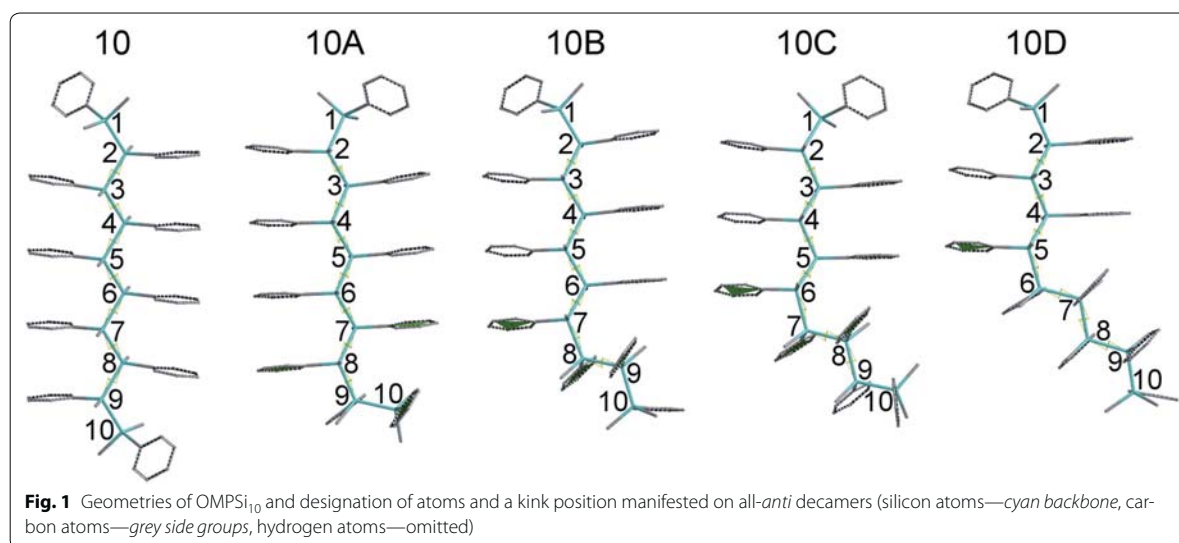
Structures of OMPSi with ten repeated units (OMPSi<sub>10</sub>) were modelled with Spartan '14 software (Wavefunction, Irvine, CA) [43]. Optimal geometry of decamer (later in this text designed as *10\_opt*) was calculated with DFT on the level of B3LYP hybrid model and 6-31G(d) polarization basis set [44]. The backbone end atoms were capped with methyl groups and calculation was set in vacuum with no constrained bonds or angles. OMPSi<sub>10</sub> with approximately *transoid* conformation was obtained as can be also found in our previous work [20]. This optimal structure was used for virtual preparation of other OMPSi<sub>10</sub> analogues with a kink, which represents a conformational defect. The optimization of kinked decamers was performed with the same DFT model as described above and resulted in four OMPSi<sub>10</sub> molecules. These structures differ in a position of the kink that adopted approximately *gauche* conformation. Geometry calculation of oligomers with a kink was described in detail in Ref. 11 these OMPSi<sub>10</sub> were designed with *A*, *B*, *C* and *D* according to position of the kink and suffixed with *opt* as it is optimal structure with no constrained angles.

More structurally specified molecules were modelled for the purpose of a description of an influence of the backbone conformation on the electronic structure of OMPSi<sub>10</sub> with and without the kink, as well as for an assignment of the  $\pi$ - $\pi$  interactions between phenyl groups. The dihedral angle of the kink was therefore constrained to 60° and all dihedral angles of a silicon backbone ( $\omega$ ) were set to 120°, 130°...180° and constrained

as well. Moreover, a kink position is clearly given in Fig. 1. Geometry optimization was performed with DFT B3LYP/6-31G(d) in vacuum. From this calculation, seven structures of each decamer (*10*, *10A*–*10D*) with a backbone gradually coiled into helix were obtained. These structures are suffixed with *120*...*180* in their designation.

### Non-bonding interactions

Single point energy calculations were performed for all *10A*...*10D* OMPSi<sub>10</sub> with M06 and  $\omega$ B97X-D functionals, which are directly available in Spartan 14' software. Although the absolute total energies obtained by these methods differ all three methods are known due to their low errors and variance of predicted values. Therefore, they can be used for prediction of trends and comparison of energy differences among series of conformers. The results calculated at higher levels of theory which includes non-bonding interactions were compared with molecular energy obtained with B3LYP which treats bonding interactions only. From the plots, which are given below, it was possible to determine the energy contribution to conformer stabilization caused by the weak phenyl–phenyl interactions because the Si backbone was constrained in all considered cases. The most energetically un-favourable conformation of the Si backbone with 120° dihedral angle was selected as the reference level. Hence, the contribution to the conformer stabilization due to  $\sigma$ -conjugation is predicted by B3LYP and the additional energy gain due to  $\pi$ -stacking is manifested as the difference between B3LYP and dispersion term including functionals.



### Absorption spectra

An investigation of electronic properties was done through examination of absorption spectra and excitation energies, including distribution of molecular orbitals and their percentage involvement into the process. These features and UV–Vis spectra were calculated with TD-DFT energy calculation in the excited state of OMPSi<sub>10</sub>. Functional, basis set and virtual environment of molecules were set as described in geometry optimization part. Optimal geometries in the excited state were not calculated due to excessive computer requirements.

## Results and discussion

### Backbone geometry and the kink

Optimal geometry of ODMSi<sub>10</sub> have already been determined in Ref. 11 and resulted in the helical backbone arrangement with dihedral angles corresponding to *transoid* conformation. An introduction of a kink has not influenced the rest of this arrangement in a significant extent. In the present work, more detailed conformational investigation have been done on several constrained OMPSi<sub>10</sub> molecules, whose bond lengths are provided in Additional file 1. Figure 2 shows an energy dependence on the backbone conformation, which was set from all-*eclipsed* (120°) to all-*anti* (180°) arrangement. Relative energy on the y-axis was calculated by subtraction of −154849.74 eV (the calculated total energy of 10\_120 decamer) from all other decamer energies. As can be seen, the energy minima are in all cases related with backbone dihedral angle 155° and 160° regardless the presence of the kink that is in agreement with optimal non-constrained OMPSi<sub>10</sub>. An approximately 5° difference can be attributed to 60°-locked kink dihedral angle in constrained structures.

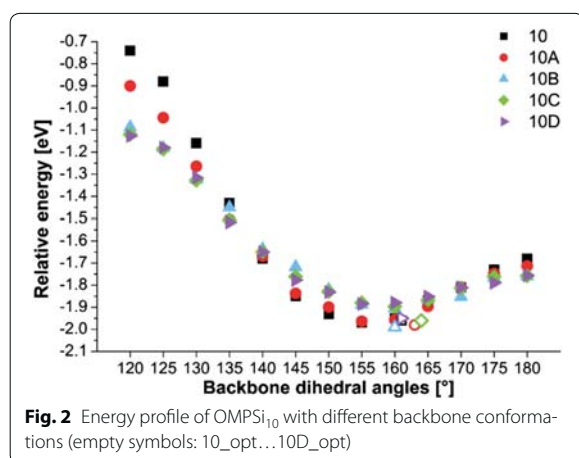


**Fig. 2** Energy profile of OMPSi<sub>10</sub> with different backbone conformations (empty symbols: 10\_opt...10D\_opt)

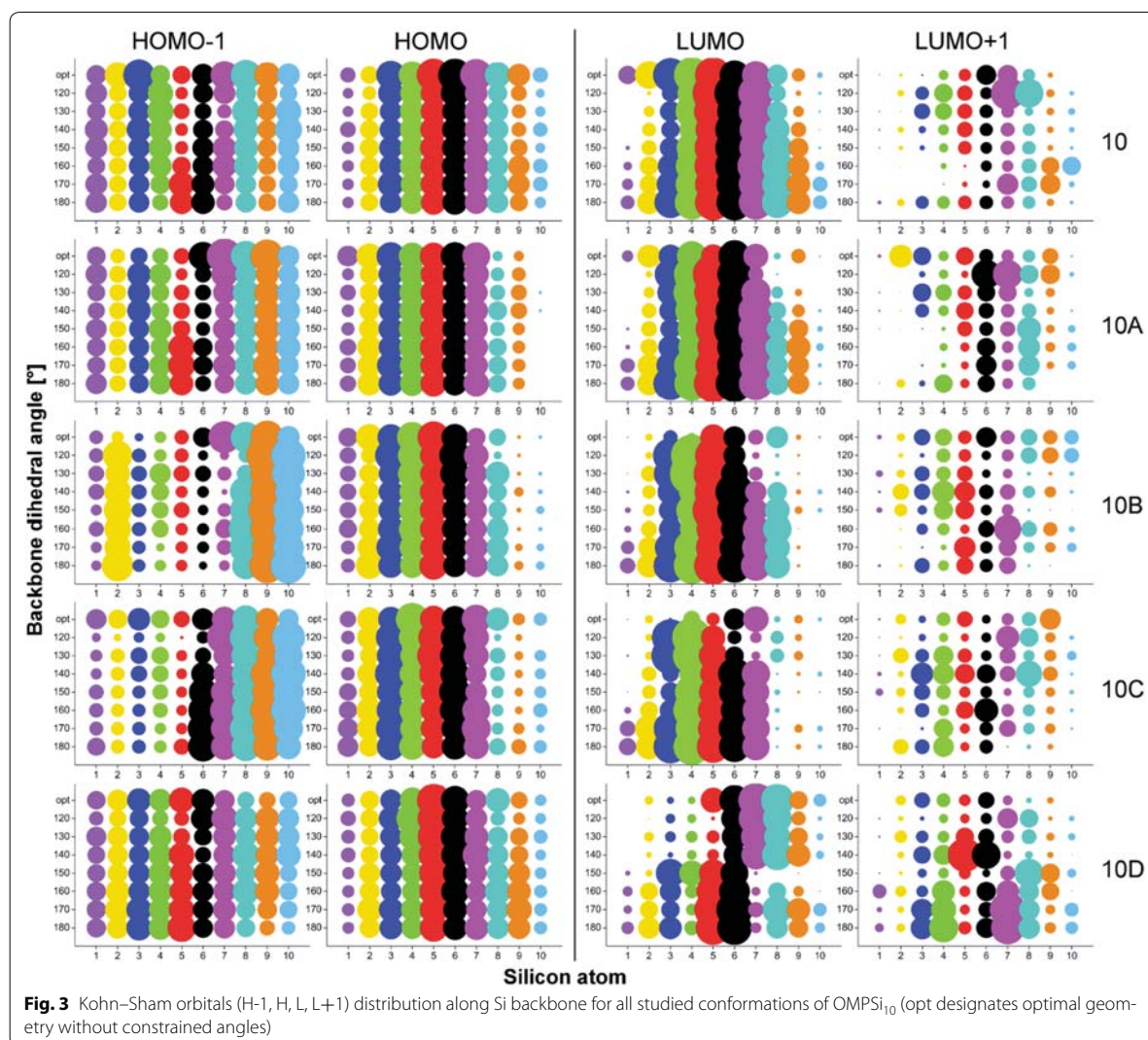
### Molecular orbitals

Four molecular orbitals (MO) were investigated, namely HOMO-1 (H-1), HOMO (H), LUMO (L) and LUMO+1 (L+1), because these are involved in the excitation processes at the absorption maximum (described below). MO distributions along silicon backbone and Ph groups were plotted in the form of bubble graphs (Figs. 3, 4). The size of the bubble expresses a value of MO coefficients ( $c_{\mu i}$  in LCAO equation [45]) that were obtained from calculation output. Specifically, coefficients, whose absolute value is above the 0.05 threshold value were taken into account and at the same time coefficients related with particular atom (e.g. Si1) were summed. Analogous approach was applied to MO distribution on Ph groups but, in addition, MO coefficients related with the phenyl ring (i.e. six carbon atoms, while no density was transferred to hydrogen in any case) were summed. The size of the bubbles was graphically adjusted by multiplication to make the bubbles comfortably comparable. Thus, occupied and unoccupied MO coefficients were multiplied by 150 and 50, respectively.

Figure 3 depicts MO distribution along Si backbones for all studied decamers. As can be found, the main difference is observable between symmetric (10 and 10D) and asymmetric structures (10A, 10B and 10C). The symmetry is here given by the position of the kink and the fact that in 10A, 10B and 10C is backbone divided into two unequally length parts—segments. HOMOs-1 are basically delocalized along whole Si backbone in 10 and D molecules. 10A OMPSi represents transition between symmetrical and asymmetrical structure as the kink is located in the very edge of a chain. HOMO-1 of 10A molecules is thus distributed almost symmetrically along the backbone, however a slight shift to a kink part is already observable. This shift of HOMO-1 towards the kink and its localization on the shorter segment is clearly visible in 10B and 10C decamers. Similarly as HOMOs-1, HOMOs of 10 and 10D decamers are distributed equally along Si–Si bonds and maximal values of  $c_{\mu i}$  can be found on central Si atoms. On the other hand, in 10A–10C, HOMO orbitals are shifted from the kink part and maxima are kept in the middle of chains on Si4–Si6. The effect of a kink introduction on HOMOs seems to be of lower intensity than in case of HOMO-1 but this is only a semblance perception of the graph because the delocalization length over the longer segment is just longer, naturally. An influence of different  $\omega$  is in both cases of HOMOs-1 and HOMOs distribution negligible.

Unoccupied MOs are more dependent on the overall backbone arrangement. As can be further seen in Fig. 3, LUMOs of all 10 structures are distributed along chain with higher values of coefficients in the central parts. This central gathering is particularly observable in 10\_120. 10As, 10Bs and 10Cs carry LUMOs in longer parts of Si

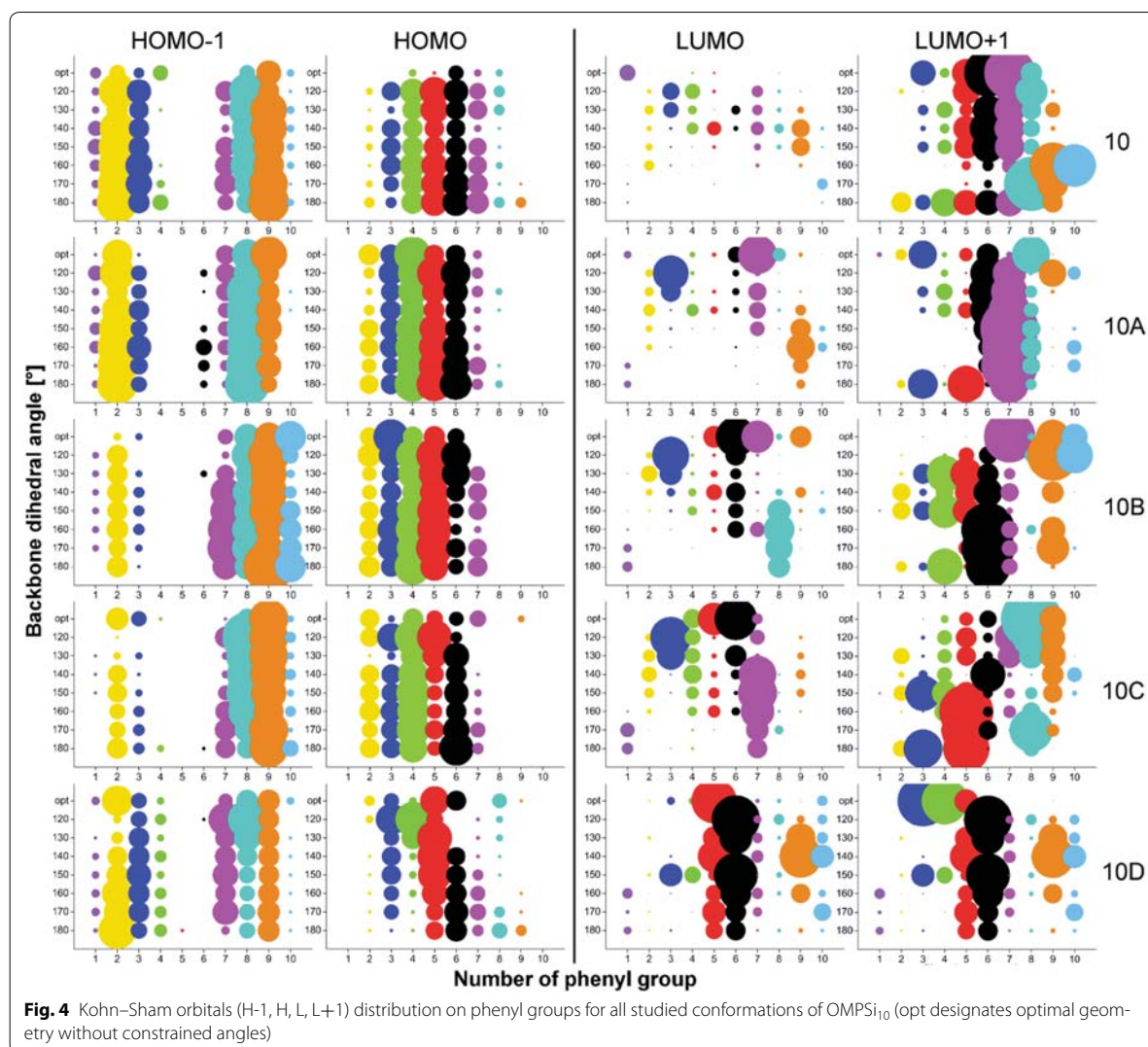




chain and this shift from kink part is especially observable in conformers with  $\omega = 120^\circ$ . *10Ds* are the most influenced structures by  $\omega$  value. Since the kink is located in the middle, the preference for LUMO delocalization is determined by the values of backbone dihedral angles. *10D\_120-150* have LUMO orbitals located rather on one half of backbone and in *10D\_160-180*, the delocalization is again symmetrical almost along the whole chain. LUMO+1 orbitals are delocalized on Ph parts (described below) and they are presented on Si backbone in much less extent. There is no simple trend that could easily sum the kink and conformation influence up. Increasing  $\omega$  causes variable shifts including opposite trends in dependence on the kink position. Images of all these

Kohn-Sham orbitals that graphically express the bubble graphs are given in Additional file 2: Figures S1–S4.

Figure 4 reflects MO distribution on Ph rings attached along backbone. Rings are numbered according to the position of Si atom to which the ring is attached (e.g. a bubble on a position (1; 120) corresponds to sum of MO coefficients from six carbons that form the Ph ring attached to Si1 in conformer 120°). As can be observed, MO on Ph rings are much more localized in comparison with MO along Si backbone. HOMOs-1 are distributed on the edge phenyls while the phenyl groups attached to central Si5 and Si6 atoms remain practically not involved into the orbital delocalization. In no-kink structures of *10* delocalization is symmetrical and this characteristic splitting



is also kept in other molecules but with a lesser extent of symmetry. HOMOs-1 of *10A–10C* are preferentially localized on Ph groups adjacent to the kink and to the shorter segment of the decamer. In the case of *10D* molecules, the symmetry is again restored, although to a lesser extent than in *10* oligomers. On the other hand, HOMOs seem to appear rather on the central Ph rings and on the longer segment up to Si1 (cases *A, B, C*). The more is the kink close to the centre of the decamer, the more these HOMOs are squeezed to that longer segment and kink-attached Ph groups are more involved in HOMO, which is an opposite effect than manifested for HOMOs-1. The population density of HOMOs on the two segments of symmetric *10D* cases depends on  $\omega$ . The optimized structure has the

HOMO distributed more on the silicon chain than any other structure under investigation. The tested geometries have bigger population density located on phenyl groups. With increasing angle from 120° to 180°, the density becomes less symmetric and shifts from left to right (from lower number positions to higher number positions) having thus always quite densely populated Ph5 and Ph6. It must be stressed out that Ph rings adjacent to Si atoms forming the kink are involved in the MO delocalization. In both cases of HOMOs-1 and HOMOs, the overall distribution of occupied MOs is influenced by the presence of the kink and conformation of the backbone however it does not mean that Ph rings adjacent to the kink Si atoms are excluded from the delocalization.

It can be stated that LUMOs are present on Ph rings rarely. There are only a few Ph groups that carry LUMO in the considerable extent. Seemingly, the Ph group attributable portion of LUMOs in optimal conformations of OMPSi<sub>10</sub> is located on that Ph group from the kink part in all kinked structures which is attached to the Si atom closer to the longer segment or in other cases the LUMO density is located on the two Ph groups attached to those two Si from the kink with lower position numbers, which means that these MOs are shifted from Ph7 to Ph5. 10D OMPSi<sub>10</sub> carry LUMOs particularly on Ph5 and Ph6 irrespective of the dihedral angle of the backbone with exception of some population density located to the Ph9 for angles 130° and 140°. On the contrary, LUMO+1 delocalization is strongly related with Ph rings when compared with Si backbone orbitals. 180° conformations are the most symmetrical cases, which are affected by the kink presence. Generally, LUMOs+1 are significantly distributed on one or two Ph rings according to a kink position and backbone conformation. The  $\omega$  has the largest effect on the distribution of LUMOs+1 among tested parameters as it evidently prevail over the importance of the kink position. This influence scatters the manifestation of kink-caused trends and makes the results less readable than in all previous cases. Images of Kohn–Sham orbitals distributed along phenyl rings are appended in the Additional file 2.

#### Excitation properties

TD-DFT approach was used to calculate UV–Vis spectra and related excitation properties. Figure 5 depicts a palette of absorption spectra corresponding to every

considered OMPSi<sub>10</sub> conformer. There are also line spectral bands that are helpful for determination and comparison of transition intensities. Graphical information are supplemented by Table 1, where the data describing excitation at the highest wavelength ( $\lambda_{\max}$ ) are given. Comprehensive characterization of all calculated transitions is given in Additional file 3: Table S1.

As can be deduced, the maximum wavelength absorption is, in the vast majority, at the same time the most intensive one. The main character of this transition is  $\sigma \rightarrow \sigma^*$  occurring between Si orbitals  $H \rightarrow L$ , in some cases  $H-1 \rightarrow L$  or  $H \rightarrow L+1$  and exceptionally  $H \rightarrow L+4$  and  $L+6$ . Further, in 120°, 130°, 170° and 180° analogues, second absorption band is clearly seen. The transition is from H or H-1 to higher unoccupied MO, which are located on phenyl rings. This indicates  $\sigma \rightarrow \pi^*$  transition from Si atoms to Ph groups. This transition is in literature often assigned as  $\pi-\pi^*$  [46], however we propose in accordance with our theoretical results that this band better corresponds to  $\sigma \rightarrow \pi^*$  transition.  $\pi-\pi^*$  transition is probably of higher energy and it is located close to 200 nm. The band below 200 nm is partially observable in experimental spectrum of PMPSi in Fig. 6.

Calculated wavelengths are compared with experimentally measured UV–Vis spectra of PMPSi which is shown in Fig. 6. The spectrum contains peaks in the UV part of the spectrum since no sign of the absorption is manifested in Vis area. There are two absorption bands in UV range which can be also identified in calculated spectra, rather of coiled decamers with a non-centrally placed kink. This indicates that the real PMPSi backbone is not planar and straighten but it is rather in

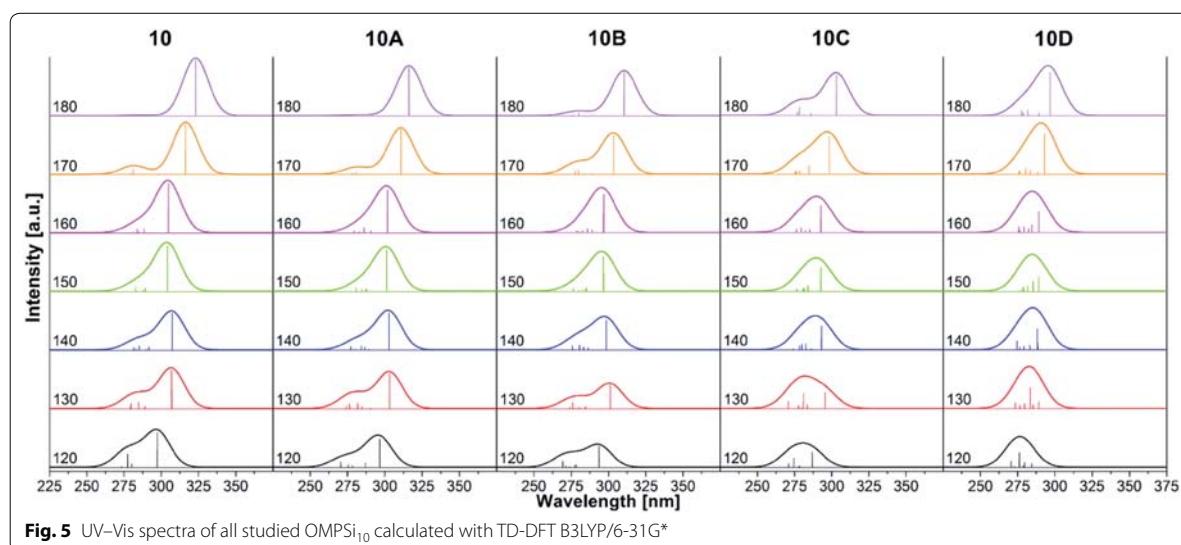


**Table 1 Summary of excitation process at  $\lambda_{max}$  for all OMPSi<sub>10</sub>**

	$\omega$ [°]	120	130	140	150	160	170	180
10	E [eV]	4.1699	4.0404	4.0366	4.0773	4.0690	3.9203	3.8389
	$\lambda$ [nm]	297.33	306.86	307.15	304.08	304.70	316.26	322.96
	F	0.9208	1.0192	0.9681	1.2094	1.3080	1.3262	1.4727
	TT	H $\rightarrow$ L	H $\rightarrow$ L	H $\rightarrow$ L	H $\rightarrow$ L	H $\rightarrow$ L	H $\rightarrow$ L	H $\rightarrow$ L
	Amp.	0.9708	0.9683	0.9671	0.9615	0.9746	0.9783	0.9809
	P [%]	94	94	94	92	95	96	96
10A	E [eV]	4.1817	4.0899	4.0966	4.1151	4.1085	3.9892	3.9221
	$\lambda$ [nm]	296.49	303.15	302.65	301.29	301.77	310.80	316.20
	F	0.7367	0.9185	0.9709	1.0888	1.1393	1.1801	1.2672
	TT	H $\rightarrow$ L	H $\rightarrow$ L	H $\rightarrow$ L	H $\rightarrow$ L	H $\rightarrow$ L	H $\rightarrow$ L	H $\rightarrow$ L
	Amp.	0.9698	0.9672	0.9624	0.9545	0.9467	0.9755	0.9801
	P [%]	94	94	93	91	90	90	96
10B	E [eV]	4.2219	4.1181	4.1520	4.1795	4.1771	4.0856	3.9927
	$\lambda$ [nm]	293.67	301.07	298.42	296.65	296.82	303.47	310.53
	F	0.5475	0.6299	0.7831	0.9174	1.0123	1.0427	1.1435
	TT	H $\rightarrow$ L	H $\rightarrow$ L	H $\rightarrow$ L	H $\rightarrow$ L	H $\rightarrow$ L	H $\rightarrow$ L	H $\rightarrow$ L
	Amp.	0.9630	0.9762	0.9411	0.9509	0.9270	0.9634	0.9756
	P [%]	93	95	89	90	86	93	95
10C	E [eV]	4.3223	4.1951	4.2310	4.2375	4.2371	4.1556	4.0906
	$\lambda$ [nm]	286.85	295.54	293.04	292.59	292.61	298.35	303.09
	F	0.3999	0.4321	0.6311	0.6312	0.7266	0.9813	1.0675
	TT	H $\rightarrow$ L	H $\rightarrow$ L	H $\rightarrow$ L	H $\rightarrow$ L	H $\rightarrow$ L	H $\rightarrow$ L	H $\rightarrow$ L
	Amp.	0.9155	0.9194	0.8261	0.9330	0.9385	0.9607	0.9684
	P [%]	84	85	68	87	88	92	94
10D	E [eV]	4.3609	4.2885	4.2973	4.2880	4.2879	4.2313	4.1795
	$\lambda$ [nm]	284.30	289.11	288.52	289.14	289.15	293.02	296.67
	F	0.1020	0.1895	0.1880	0.3833	0.5503	1.0527	1.1367
	TT	H-1 $\rightarrow$ L	H $\rightarrow$ L	H $\rightarrow$ L	H $\rightarrow$ L	H $\rightarrow$ L	H $\rightarrow$ L	H $\rightarrow$ L
	Amp.	0.2525	0.8842	-0.3215	0.9266	0.9117	0.9305	0.9439
	P [%]	85	78	10	86	83	87	89

$\omega$  dihedral angle,  $E$  excitation energy,  $\lambda$  wavelength of excitation,  $f$  strength,  $TT$  type of transition,  $Amp$  amplitude,  $P$  percentage of allowed transition

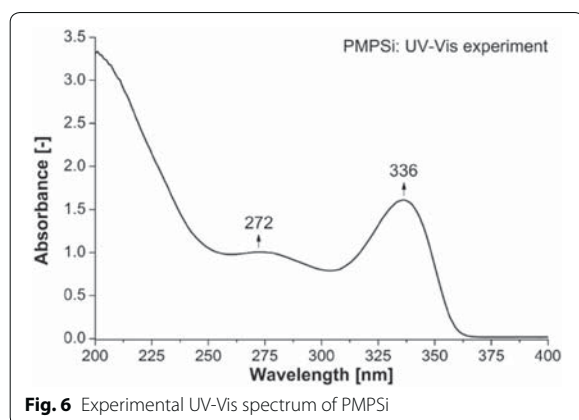


**Fig. 6** Experimental UV-Vis spectrum of PMPSi

helical arrangement. This is in agreement with our optimal geometries with lowest potential energy. On the other hand, two bands are observable in *180\_B* and *180\_C* OMPSi<sub>10</sub> too. In these cases, the kink probably serves as a “helical mimic” structural element which delivers twisted-like conformation to the oligomer that causes similar spectral behaviour, which has been described for helical backbones. The difference between experiment and theory is, of course, observable predominantly due to comparison of experimental spectrum of polymer and theoretical spectrum of isolated decamer and therefore calculated spectral bands are energetically overestimated about several tenths of eV which is in accord with expectable eventual solvation effect of toluene. However, this drawback would not destroy the main trends referring to conformation and electronic behaviour of polysilylene and addition of solvent force field terms to calculations can neither significantly improve our virtual experiment nor clarify the role of phenyl–phenyl group interaction.

It is important to note that no states in the bandgap are formed by the investigated conformational defects, which means that no peaks are present in the Vis area of the absorption spectrum. This is in accordance with state-of-the-art interpretation of origin of such features which are normally manifested in luminescence spectra only [11].

Figure 7 provides another view on a dependence of  $\lambda_{max}$  on the backbone conformation. It is unambiguous that  $\lambda_{max}$  shifts to longer UV wavelengths as  $\omega$  is higher and thus as backbone conformation reaches planar all-*anti* arrangement. All structures with  $\omega = 150^\circ$ ,  $160^\circ$  evince decrease of  $\lambda_{max}$  or in case of *10D* a stabilization of  $\lambda_{max}$  value. These conformers are also the most energetically stable as was discussed above (see again Fig. 2). Following change in  $\omega$  causes another and substantial growth of  $\lambda_{max}$  that reaches maximum for  $\omega = 180^\circ$ . There is also obvious that presence and position of the kink

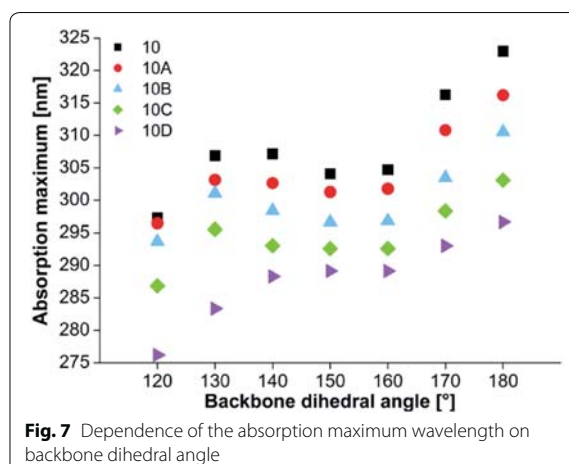


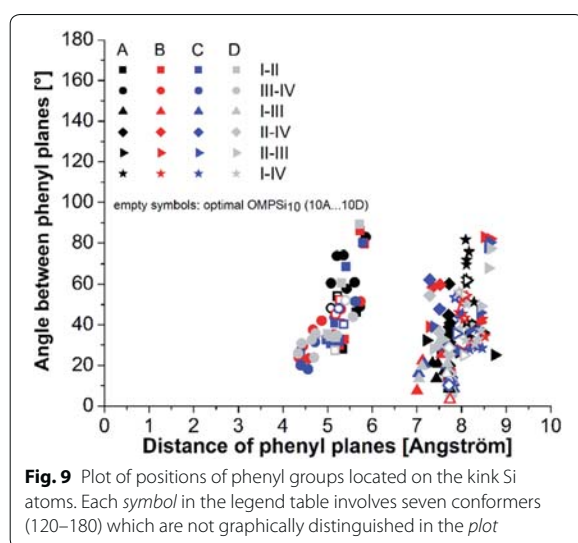
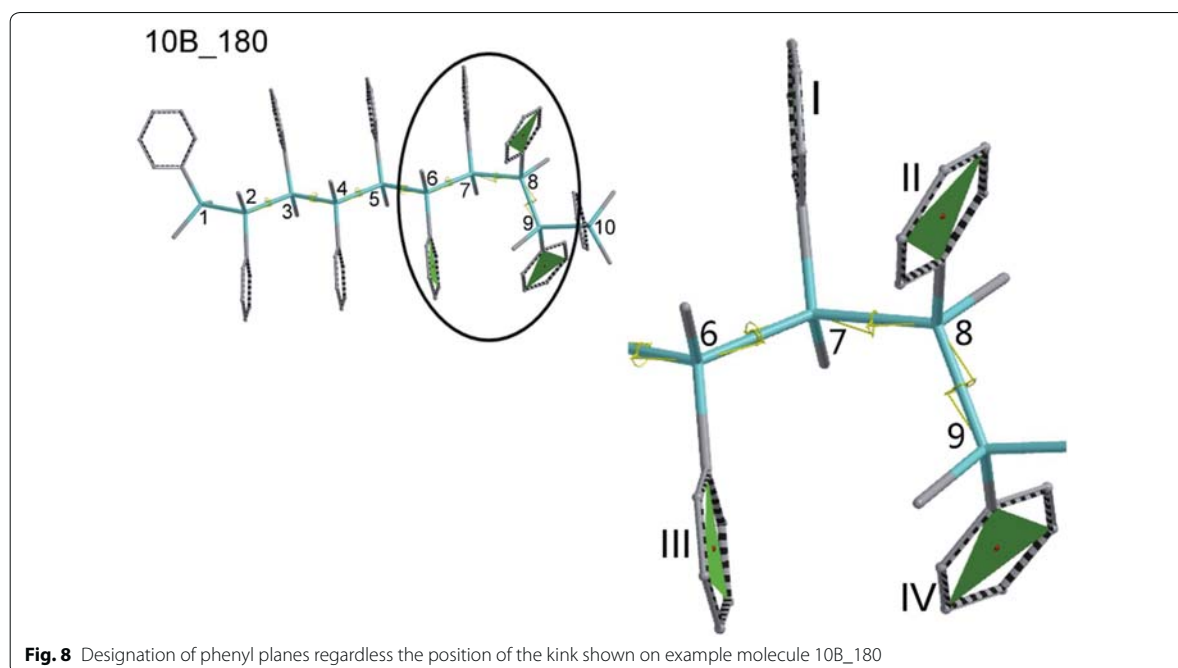
**Fig. 7** Dependence of the absorption maximum wavelength on backbone dihedral angle

significantly influences a value of  $\lambda_{max}$ . As can be seen, *10* and *10A* decamers are the most similar and change in  $\lambda_{max}$  for *10A* is not so large. On the other hand, difference between *10* and *10C* molecules is in some conformations around 10 nm and between *10* and *10D* even 25 nm. This proves that conformational defect has essential effect on excitation wavelength that is a crucial factor of UV-Vis absorbing substances.

#### $\pi$ – $\pi$ interactions between phenyl side groups

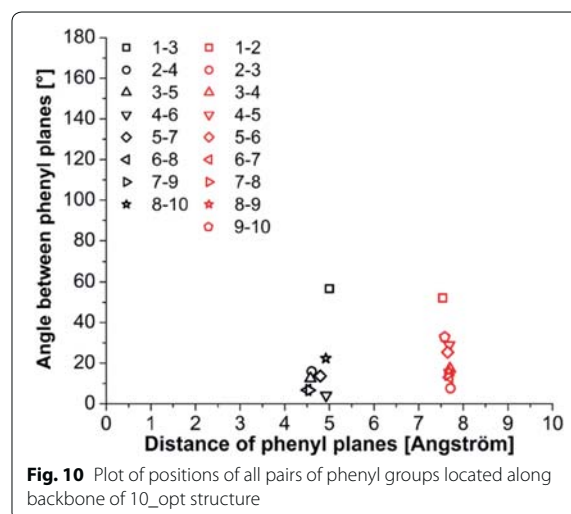
Studied OMPSi<sub>10</sub> structures are example of the system, which can interact through p orbitals occupied by  $\pi$ -electrons. Figure 8 contains a structure of *10B\_180* molecule with a detailed image of a kink part and a designation of phenyl planes, which are attached right on four Si atoms which form the kink. Numbers of planes are valid for all structures regardless the position of the kink. The kink has set exact arrangement of *gauche* in all cases and since the backbone is also geometrically defined Ph groups could have therefore adopted various optimal positions.

A qualitative evaluation of  $\pi$ – $\pi$  interactions is done through definition of mutual positions of the phenyl groups obtained solely from geometry optimization procedure. A plane on each involved Ph have been determined with three points (three phenyl C atoms) and a central point was defined as a point in the middle of a line, which links two opposite phenyl C atoms. Thus, Fig. 9 depicts an angle-distance dependence of these Ph groups. An angle was measured between two Ph planes and a distance was measured between two plane central points. In total, six pairs of phenyl groups have been investigated for each *A–D* and *120–180* decamer. As can be seen from the plot, there are two distinct clouds of points clearly separated by an approximately 1 Å wide



gap virtually centred at 6.5 Å. According to Ref. 15, attractive  $\pi$ - $\pi$  interactions can be found between planes I-II and planes III-IV, whose mutual positions are in the graph area of 4–6 Å and 10–90°. This indicates that a kinked arrangement of the chain could be stabilized by these interactions and therefore this type of bending is possible to consider as a folding contribution element in

the real polymer backbones. These constructive interactions may also contribute to the localization of MOs on Ph rings attached to Si atoms forming the kinks. Another cluster of points is located in the area of 7–9 Å and 0–90° and it can be stated that the vast majority of plane pair I–III, II–IV, II–III and I–IV is in a further distance than that which is suitable for any kind of  $\pi$ - $\pi$  stacking interactions. Further, Fig. 10 is similar representation of  $\pi$ - $\pi$



interactions for  $10_{opt}$  structure, which were here investigated along the whole chain. For this purpose, phenyl rings were numbered from 1 to 10. As can be seen, there are also two groups of points. The first cluster (at approx. 4–5 Å) belongs to measurements of angle-distance dependence of Ph pair which are next to each other (on the same side of a chain) along the backbone. Ph groups are designed in this graph with numbers corresponding

to a Si atom they are attached on. These interactions can be regarded as attractive and thus the helical arrangement of a backbone is favourable. The latter cluster (at approx. 7–8 Å), which involves interactions of adjacent Ph (in zig-zag way), is again beyond the marginal distance suitable for  $\pi$ -stacking.

Figure 11 depicts the energy profile that is related with a phenyl rings rearrangement on model molecules with

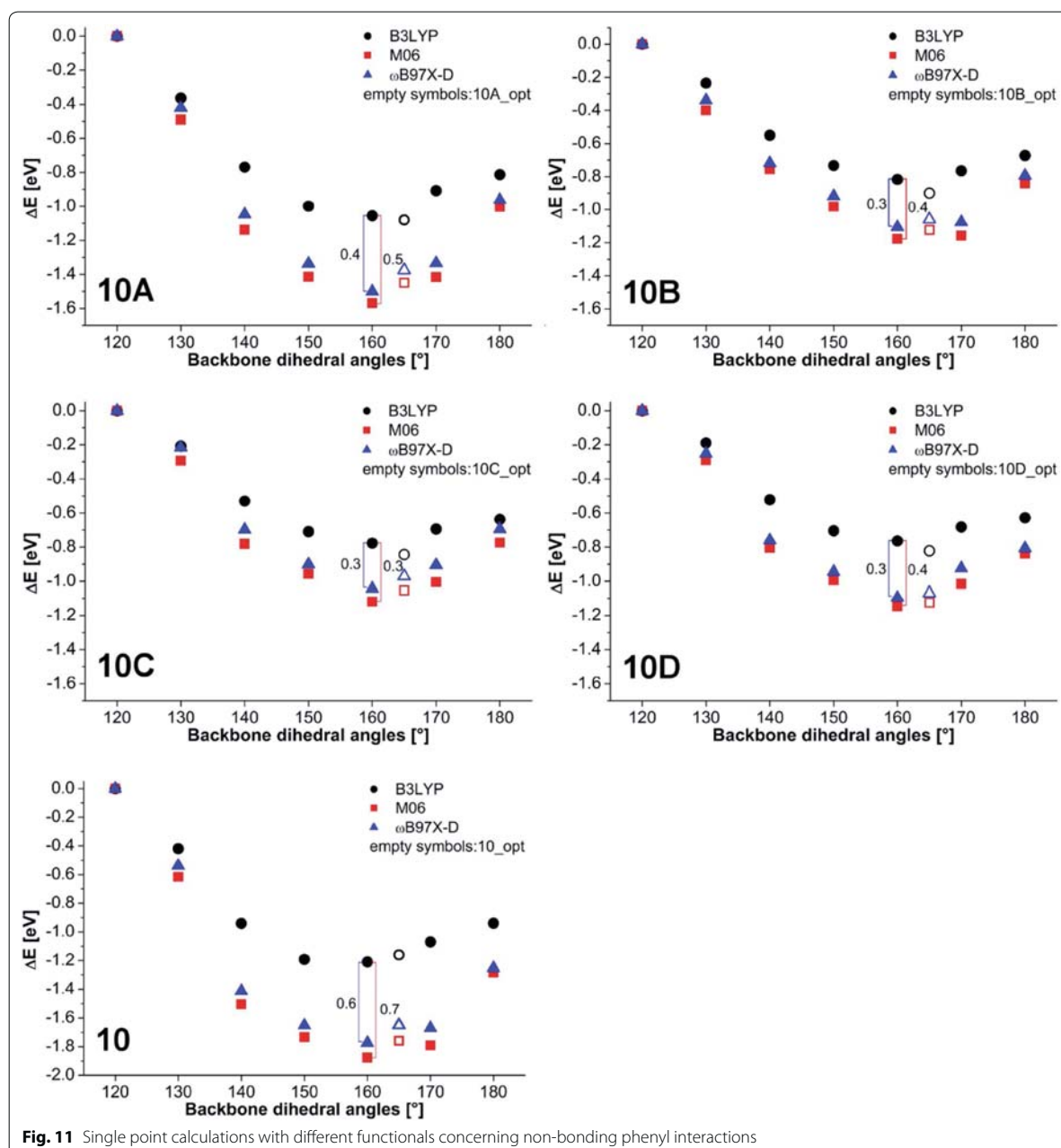


**Fig. 11** Single point calculations with different functionals concerning non-bonding phenyl interactions

different backbone geometry (kink position and dihedral angle). The plots were obtained from single point calculations and comparison of B3LYP and dispersion containing functionals M06 and  $\omega$ B97X-D. Raw energy data are displayed in Additional file 4: Table S2, however y-axis in Fig. 11 expresses the energy difference ( $\Delta E$ ) in eV between OMPSi with the kink in the same position (i.e. 10A, 10B, 10C, 10D) and at the same time the zero value corresponds to conformers with  $\omega = 120^\circ$ . Calculated B3LYP energies reflect the situation where long distance phenyl interactions are not involved. These curves describe only energy dependence on the dihedral angle and they can be interpreted as the contribution of  $\sigma$ -conjugation to the chain stability which increases as the geometry approaches closer to the ideal value for  $\omega$  which is approximately  $165^\circ$ . Therefore the B3LYP energies can be considered as reference values. On the other hand, M06 and  $\omega$ B97X-D energies do involve low-range and long-range electron–electron interactions, respectively. Since backbone dihedral angles were constrained in all cases, these energies are directly related to phenyl rings energy contribution to their mutual interactions. Molecules which are conformationally more convenient for  $\pi$ - $\pi$  stacking thus have lower energy. The kink-less geometry (10) shows the highest stabilization contribution 0.6 eV which is consistent with its most relaxed geometry and ideal-likeness of molecule conformation. According to our results,  $\pi$ - $\pi$  interactions are employed gradually with an increasing  $\omega$  and they reach maximum in OMPSi which have  $\omega$  constrained to  $160^\circ$  and  $170^\circ$  and then their strength again decreases. The additional contribution of these interactions is marked in graphs by vertical line segments with indicated difference in eV. These conformations are tightly close to optimal geometries obtained without any backbone constrain (also displayed in Fig. 11) and therefore it is highly probable that kink stabilization by non-bonding interactions can be expected in PMPSi chains. In other words, the kink formation disturbs slightly the stabilization effect of  $\pi$ -interactions, however it does not vanish totally and still keeps a reasonable contribution. The maximal difference between B3LYP and M06 and B3LYP and  $\omega$ B97X-D for molecules A–D is 0.4 eV and 0.3 eV in average, respectively.

## Conclusions

OMPSi<sub>10</sub> served as model systems for the DFT study of overall backbone conformation with conformational defect (a kink), its influence on electronic properties and an investigation of the kink stability provided by  $\pi$ - $\pi$  stacking interactions. Helical backbones with Si–Si–Si angles equal to  $150^\circ$  and  $160^\circ$  have been determined as the most stable backbone arrangements. Conformations have been treated from  $120^\circ$  to  $180^\circ$  and together

with the kink they significantly affect the distribution of Kohn–Sham orbitals along both Si backbone and Ph side groups. HOMO-1 orbitals are distributed along the backbone, while LUMO+1 orbitals are strictly kept on Ph groups. Further, HOMO and LUMO densities can be found delocalized over the whole molecule.

The main calculated absorption transition is assigned as  $\sigma$ - $\sigma^*$  and located at around 310 nm, in experimental UV–Vis spectrum at 336 nm. Second transition around 275 nm is probably of  $\sigma$ - $\pi^*$  character despite traditional assignment to  $\pi$ - $\pi^*$ . We presume that  $\pi$ - $\pi^*$  corresponds energetically to lower wavelengths below 200 nm. However, optimal geometries of excited states have not been successfully calculated due to too demanding computer requirements and at the same time these calculations could be a topic of the next research leading to specification of excitation transitions.

The analysis of angle–distance dependence between Ph planes determined from optimized geometries has revealed that even the molecule with a kink is stabilized by positive interactive mode of  $\pi$ - $\pi$  stacking between pairs of Ph groups. Conformations with backbone dihedral angle of  $160^\circ$  are the most convenient for phenyl interactions, which was concluded from energy investigation with B3LYP, M06 and  $\omega$ B97X-D models. There can be distinguished two principally different contributions to the PMPSi backbone geometry. First, it is the previously well-known  $\sigma$ -conjugation effect that has been estimated in order of approximately 1.2 eV. Next, the long range  $\pi$ - $\pi$  interaction contribution was found to be about 0.6 eV for linear chain and about 0.3–0.4 eV for kink defect containing chains. Since  $160^\circ$  conformation is close to the optimal geometry of OMPSi without constrained parts, it can be stated that the kink type of conformational defect is viable in real PMPSi chains.

## Additional files

**Additional file 1.** Contains raw data of bond lengths of all OMPSi<sub>10</sub> structures as obtained from Spartan 14<sup>†</sup> output. The following additional data are available with the online version of this paper.

**Additional file 2.** Contains four sets of figures of Kohn–Sham orbitals for all studied deca[methyl(phenyl)silylene]s in various backbone conformations and with an introduced kink in the chain. Backbone dihedral angles altered from  $120^\circ$  to  $180^\circ$  and the kink position altered from the edge of chain (A) to the centre part of chain (D).

**Additional file 3: Table S1.** Contains a table with information on excitation process of all studied deca[methyl(phenyl)silylene]s in various backbone conformations and with an introduced kink in the chain. Backbone dihedral angles altered from  $120^\circ$  to  $180^\circ$  and the kink position altered from the edge of chain (A) to the centre part of chain (D).

**Additional file 4: Table S2.** Molecular energies calculated for all studied deca[methyl(phenyl)silylene]s obtained with B3LYP, M06 and  $\omega$ B97X-D functionals.



**Authors' contributions**

BH proposed the research subject, carried out the computational studies, arranged the results and wrote the paper. IK assisted with results and discussion part and revised the final manuscript. PU carried out experimental measurement of UV-Vis spectrum. All authors read and approved the final manuscript.

**Acknowledgements**

This work was supported by the Ministry of Education, Youth and Sports of the Czech Republic—Program NPU I (LO1504). This work was supported by Internal Grant Agency of Tomas Bata University in Zlin (reg. number IGA/CPS/2015/006).

**Competing interests**

The authors declare that they have no competing interests.

Received: 23 November 2015 Accepted: 25 April 2016

Published online: 05 May 2016

**References**

- Mark JE, Allcock HR, West R (2003) *Inorganic polymers*. Oxford University Press, New York
- Karatsu T (2008) Photochemistry and photophysics of organomonosilane and oligosilanes: updating their studies on conformation and intramolecular interactions. *J Photochem Photobiol, C* 9:111–137
- Nespurek S (2002) From one-dimensional organosilicon structures to polymeric semiconductors: optical and electrical properties. *J Non-Cryst Sol* 299–302:1033–1041
- Fujiki M, Koe JR, Terao K, Sato T, Teramoto A, Watanabe J (2003) Optically active polysilanes. Ten years of progress and new polymer twist for nanoscience and nanotechnology. *Polym J* 35:297–344
- Fukawa S, Ohta H (2003) Structure and orientation of vacuum-evaporated poly(di-methyl silane) film. *Thin Sol Films* 438–439:48–55
- Fujiki MJ (2003) Switching handedness in optically active polysilanes. *Organomet Film* 685:15–34
- Michl J, West R (2000) Conformations of linear chains. Systematics and suggestions for nomenclature. *Acc Chem Res* 33:821–823
- Fogarty H-A, Ottoson C-H, Michl J (2000) The five favored backbone conformations of n-Si4Et10: cisoid, gauche, ortho, deviant, and transoid. *J Mol Struct-Theochem* 506:243–255
- Nguyen TQ, Martini I, Liu J, Schwartz BJ (2000) Controlling interchain interactions in conjugated polymers: the effects of chain morphology on exciton-exciton annihilation and aggregation in MEH-PPV films. *J Phys Chem B* 104:237–255
- Mirzov O, Scheblykin IG (2006) Photoluminescence spectra of a conjugated polymer: from films and solutions to single molecule. *Phys Chem Chem Phys* 8:5569–5576
- Urbanek P, Kuritka I (2015) Thickness dependent structural ordering, degradation and metastability in polysilane thin films: a photoluminescence study on representative  $\sigma$ -conjugated polymers. *J Lumin* 168:261–268
- Urbanek P, Kuritka I, Danis S, Tousek J (2014) Thickness threshold of structural ordering in thin MEH-PPV films. *Polymer* 55:4050–4056
- Gmucova K, Nadazdy V, Schauer F, Kaiser M, Majkova E (2015) Electrochemical Spectroscopic Methods for the Fine Band Gap Electronic Structure Mapping in Organic Semiconductors. *J Phys Chem C* 119:15926–15934
- Nadazdy V, Schauer F, Gmucova K (2014) Energy resolved electrochemical impedance spectroscopy for electronic structure mapping in organic semiconductors. *Appl Phys Lett C* 119:15926–15934
- Overney RM, Buenviaje C, Luginbuhl R, Dinelli F (2000) Glass and structural transitions measured at polymer surfaces on the nanoscale. *J Therm Anal Cal* 59:205–225
- Benight SJ, Knorr DB Jr, Johnson LE, Sullivan PA, Lao D, Sun J, Kocherlakota LS, Elangovan A, Robinson BH, Overney RM, Dalton LR (2012) Nano-engineering lattice dimensionality for a soft matter organic functional material. *Adv Mater* 24:3263–3268
- Despotopoulou MM, Frank CW, Miller RD, Rabolt JF (1995) Role of the restricted geometry on the morphology of ultrathin poly(di-n-hexylsilane) films. *Macromolecules* 28:6687–6688
- Tsuji H, Michl J, Tamao K (2003) Recent experimental and theoretical aspects of the conformational dependence of UV absorption of short chain peralkylated oligosilanes. *J Organomet Chem* 685:9–14
- Teramae H, Matsumoto N (1996) Theoretical study on gauche-kink in polysilane polymer. *Sol State Com* 99:917–919
- Hanulíková B, Kuritka I (2014) Manifestations of conformational defects in electronic spectra of polysilanes—a theoretical study. *Macromol Symp* 339:100–111
- Hanulíková B, Kuritka I (2014) Theoretical study of polaron binding energy in conformationally disrupted oligosilanes. *J Mol Model* 20:2442–2450
- Hunter CA, Sanders JKM (1990) The nature of  $\pi$ - $\pi$  interactions. *J Am Chem Soc* 112:5525–5534
- Chung SJ, Kim DH (1997) Intramolecular edge-to-face aromatic-aromatic ring interactions in 3-(3-aryl-2-isopropylpropanoyl)-4-phenylmethyl-1,3-oxazolidin-2-ones prepared from Evans' chiral auxiliary. *Bull Kor Chem* 18:1324–1327
- Hunter CA, Singh J, Thornton JM (1991)  $\pi$ - $\pi$  interactions: the geometry and energetics of phenylalanine-phenylalanine interactions in proteins. *J Mol Biol* 218:837–846
- Meyer EA, Castellano RK, Diederich F (2003) Interactions with aromatic rings in chemical and biological recognition. *Angew Chem Int Ed* 42:1210–1250
- Mignon P, Loverix S, De Proft F, Geerlings P (2004) Influence of stacking on hydrogen bonding: quantum chemical study on pyridine-benzene model complexes. *J Phys Chem* 108:6038–6044
- Akher FB, Ebrahimi A (2015)  $\pi$ -stacking effects on the hydrogen bonding capacity of methyl 2-naphthoate. *J Mol Graph Model* 61:115–122
- Hunter CA, Lawson KR, Perkins J, Urch CJ (2001) Aromatic interactions. *J Chem Soc, Perkin Trans* 2:651–669
- Waters ML (2002) Aromatic interactions in model systems. *Curr Opin Chem Biol* 6:736–741
- Martinez CR, Iverson BL (2012) Rethinking the term "pi-stacking". *Chem Sci* 3:2191–2201
- Kohn W, Sham WL (1965) Self-consistent equations including exchange and correlation effect. *Phys Rev* 140:A1133–A1138
- Biswas AK, Lo R, Ganguly B (2013) First principles studies toward the design of silylene superbases: a density functional theory study. *J Phys Chem A* 117:3109–3117
- Hohenberg P, Kohn W (1964) Inhomogeneous electron gas. *Phys Rev* 136:B864–B871
- Runge E, Gross EKH (1964) Density-functional theory for time-dependent systems. *Phys Rev Lett* 52:997–1000
- Pan X-Y, Sahn V (2008) New perspectives on the fundamental theorem of density functional theory. *Int J Quantum Chem* 108:2756–2762
- Pichaandi KR, Mague JT, Fink MJ (2015) Synthesis, photochemical decomposition and DFT studies of 2,2,3,3-tetramethyl-1,1-bis(dimethylphenylsilyl)silacyclopropane. *J Organomet Chem* 791:163–168
- Y-q Ding, Q-a Qiao, Wang P, Chen G-w, Han J-j, Xu Q, Feng S-y (2010) A DFT study of electronic structures of thiophene-based organosilicon compounds. *Chem Phys* 367:167–174
- Boo BH, Im S, Lee S (2009) Ab initio and DFT studies of the thermal rearrangement of trimethylsilyl(methyl)silylene: remarkable rearrangements of silicon intermediates. *J Comput Chem* 31:154–163
- Zhao Y, Truhlar DG (2006) A new local density functional for main-group thermochemistry, transition metal bonding, thermochemical kinetics, and noncovalent interactions. *J Chem Phys* 125:194101
- Walker M, Harvey AJA, Sen A, Dessent CEH (2013) Performance of M06, M06-2X, and M06-HF density functionals for conformationally flexible anionic clusters: M06 functionals perform better than B3LYP for a model system with dispersion and ionic hydrogen-bonding interactions. *J Phys Chem A* 117:12590–12600
- Chai J-D, Head-Gordon M (2008) Long-range corrected hybrid density functionals with damped atom-atom dispersion corrections. *Phys Chem Chem Phys* 10:6615–6620
- Civalleri B, Zicovich-Wilson CM, Valenzano L, Ugliengo P (2008) B3LYP augmented with an empirical dispersion term (B3LYP-D\*) as applied to molecular crystals. *Cryst Eng Comm* 10:405–410

43. Shao Y, Molnar LF, Jung Y, Kusmann J, Ochsenfeld C, Brown ST, Gilbert ATB, Slipchenko LV, Levchenko SV, O'Neill DP, DiStasio RA Jr, Lochan RC, Wang T, Beran GJO, Besley NA, Herbert JM, Lin CY, Van Voorhis T, Chien SH, Sodt A, Steele RP, Rassolov VA, Maslen PE, Korambath PP, Adamson RD, Austin B, Baker J, Byrd EFC, Dachsel H, Doerksen RJ, Dreuw A, Dunietz BD, Dutoi AD, Furlani TR, Gwaltney SR, Heyden A, Hirata S, Hsu C-P, Kedziora G, Khalliulin RZ, Klunzinger P, Lee AM, Lee MS, Liang W, Lotan I, Nair N, Peters B, Proynov EI, Pieniazek PA, Rhee YM, Ritchie J, Rosta E, Sherrill CD, Simonett AC, Subotnik JE, Woodcock HL III, Zhang W, Bell AT, Chakraborty AK, Chipman DM, Keil FJ, Warshel A, Hehre WJ, Schaefer HF III, Kong J, Krylov AI, Gilla PMW, Head-Gordon M (2006) Advances in methods and algorithms in a modern quantum chemistry program package. *Phys Chem Chem Phys* 8:3172–3191
44. Frisch MJ, Pople JA, Binkley JS (1984) Self-consistent molecular orbital methods 25. Supplementary functions for Gaussian basis sets. *J Chem Phys* 80:3265–3269
45. Hehre WJ (2003) Guide to molecular mechanics and quantum chemical calculations. Wavefunction Inc., Irvine
46. Nespurek S, Wang G, Yoshino K (2005) Polysilanes - Advanced materials for optoelectronics. *J Optoelectron Adv M* 7:223–230

Submit your manuscript to a SpringerOpen<sup>®</sup> journal and benefit from:

- Convenient online submission
- Rigorous peer review
- Immediate publication on acceptance
- Open access: articles freely available online
- High visibility within the field
- Retaining the copyright to your article

---

Submit your next manuscript at ► [springeropen.com](http://springeropen.com)

---

## **Research Paper III:**

**HANULIKOVA, Barbora** and Ivo KURITKA.

Contribution of non-bonding interactions to stabilization of aryl-substituted polysilylene chains conformational disorder examined by DFT on tetra[methyl(phenyl)silylene] model molecule

*Submitted to Journal of Molecular Modeling.*



## Journal of Molecular Modeling

### Contribution of non-bonding interactions to stabilization of aryl-substituted polysilylene chains conformational disorder examined by DFT on tetra[methyl(phenyl)silylene] model molecule --Manuscript Draft--

<b>Manuscript Number:</b>	
<b>Full Title:</b>	Contribution of non-bonding interactions to stabilization of aryl-substituted polysilylene chains conformational disorder examined by DFT on tetra[methyl(phenyl)silylene] model molecule
<b>Article Type:</b>	Original paper
<b>Keywords:</b>	Conformation; DFT; kink; poly[methyl(phenyl)silylene]; non-bonding interaction
<b>Corresponding Author:</b>	Barbora Hanulikova Tomas Bata University in Zlín CZECH REPUBLIC
<b>Corresponding Author Secondary Information:</b>	
<b>Corresponding Author's Institution:</b>	Tomas Bata University in Zlín
<b>Corresponding Author's Secondary Institution:</b>	
<b>First Author:</b>	Barbora Hanulikova
<b>First Author Secondary Information:</b>	
<b>Order of Authors:</b>	Barbora Hanulikova Ivo Kuritka
<b>Order of Authors Secondary Information:</b>	
<b>Funding Information:</b>	
<b>Abstract:</b>	Density functional theory calculations are used for a study of non-bonding interactions in tetra[methyl(phenyl)silylene] (MPSi4) conformers, whose Si-Si-Si-Si dihedral angle was set to exact values 0°, 10°...360° because this tetramer can serve as a model for conformational defect - a kink that disrupts optimal $\sigma$ -electron delocalization in polysilylene backbones but that also serves as a chain folding element. In this range of dihedral angles, three local and dispersion stabilized minima were calculated. Gauche conformation that corresponds to the kink structure was found as the most suitable arrangement for phenyl-phenyl interactions employment. Three various functionals accounting non-bonding interactions and dispersion to different levels were used to assess the contribution of interaction between aromatic side groups to the molecular energy of each studied conformer. This virtual experiment was corroborated with a classical interpretation framework obtaining consistent results. This confirms that the kink disruptions are viable in poly[methyl(phenyl)silylene] chains and moreover they have energetically favourable arrangement.



# Contribution of non-bonding interactions to stabilization of aryl-substituted polysilylene chains conformational disorder examined by DFT on tetra[methyl(phenyl)silylene] model molecule

Barbora Hanulikova\*, Ivo Kuritka

Centre of Polymer Systems, Tomas Bata University in Zlín, trida Tomase Bati 5678, 76001, Zlin, Czech Republic

\*Corresponding author - email address: hanulikova@cps.utb.cz  
- tel.: +420576038128

## Abstract

Density functional theory calculations are used for a study of non-bonding interactions in tetra[methyl(phenyl)silylene] (MPSi<sub>4</sub>) conformers, whose Si-Si-Si-Si dihedral angle was set to exact values 0°, 10°...360° because this tetramer can serve as a model for conformational defect – a kink that disrupts optimal  $\sigma$ -electron delocalization in polysilylene backbones but that also serves as a chain folding element. In this range of dihedral angles, tree local and dispersion stabilized minima were calculated. Gauche conformation that corresponds to the kink structure was found as the most suitable arrangement for phenyl-phenyl interactions employment. Three various functionals accounting non-bonding interactions and dispersion to different levels were used to assess the contribution of interaction between aromatic side groups to the molecular energy of each studied conformer. This virtual experiment was corroborated with a classical interpretation framework obtaining consistent results. This confirms that the kink disruptions are viable in poly[methyl(phenyl)silylene] chains and moreover they have energetically favourable arrangement.

**Keywords:** Conformation, DFT, kink, poly[methyl(phenyl)silylene], non-bonding interaction

# 1. Introduction

Polymer materials are generally composed of long chains usually of amorphous or semi-crystalline structure. In order to adopt a regular arrangement, chains must be flexible and therefore able to create the bends. In case of polysilylenes, such bend can be regarded as four silicon (Si) atoms arranged in approximately gauche conformation also called a kink [1, 2]. These kinks are interruptions of a regular backbone arrangement (helical, zig-zag) and they can be considered as local conformational defects. This is especially important for conjugated systems and therefore polysilylenes, whose  $\sigma$ -electron delocalization is disrupted by the kink that results in the changes in electronic properties of material [3, 4, 5, 6, 7]. Poly[methyl(phenyl)silylene] (PMPSi) is a representative, which evince  $\sigma$ -conjugation and strong electron-structural dependence typical for linear silicone backbone polymers. The presence of aryl substituent group (aromatic  $\pi$ -conjugated system on the side group) imparts even more specific properties to the polymer. It has been shown experimentally as well as theoretically [8, 9, 10, 11] that Si backbone conformation and presence of a kink defect and its position influence oligo[methyl(phenyl)silylene] (MPSi<sub>n</sub>, where n is the number of mers) and thus PMPSi absorption behaviour and distribution of molecular orbitals and spin density in charged analogues [12, 13]. On the other hand, total energy of molecule is not significantly increased by a kink presence as has been calculated during our previous work [14] and therefore we believe that the defect is self-stabilized via non-bonding interactions and specifically in case of MPSi<sub>n</sub>/PMPSi via phenyl-phenyl interactions. On that account, the kink is viable as a chain folding element. As has already been discovered, the interactions between phenyl groups are employed the most in MPSi<sub>10</sub> (decamers), whose backbones adopt approximately transoid-deviant conformation that leads to helical arrangement of the polymer backbone in case of long chains which is most energetically favourable. However, a study of a kink conformation, which would be the most suitable for its self-stabilization by phenyl interactions, has not been discussed anywhere in the literature yet and from this reason, it is the goal of this paper.

The kink is regarded as four Si atoms ideally in syn conformation, whose dihedral angle ( $\omega$ ) corresponds to  $0^\circ$ . Several studies of linear tetrasilylenes with small substituents, such as hydrogen, methyl or halogen, were described in ref. [2, 15, 16]. These tetrasilylenes were found in the almost whole range of  $\omega$  as enantiomeric pairs with one exception of conformation  $180^\circ$  (anti) with local minima representing angles  $\omega = \pm 40^\circ$  (cisoid),  $\omega = \pm 60^\circ$  (gauche),  $\omega = \pm 90^\circ$  (ortho),  $\omega = \pm 150^\circ$  (deviant) and  $\omega = \pm 165^\circ$  (transoid). Conformation syn is thus unfavourable even for polysilylenes with small side groups. In case of MPSi<sub>4</sub> is expected that the adoption of kinked arrangement is significantly influenced by phenyl groups and their steric limitations and also by the fact that this tetramer is not necessary of enantiomeric type. Therefore this investigation of conformation is the object of the present paper.



The work is based on the DFT computational investigation of molecular arrangement and energy of MPSi<sub>4</sub>. Density functionals were chosen with the respect of involvement of the dispersion term [17, 18]. The classical B3LYP functional is considered among computational chemist as a good workhorse however as it suffers on underestimation of long range (non-bonding) interactions. This can be improved by employment of meta-hybrid GGA DFT functionals, among them M06 which has 27% of HF exchange and has a very good response under dispersion forces [19]. The non-Coulomb part of exchange functionals typically dies off too rapidly and becomes very inaccurate at large distances. Empirical dispersion can be implemented to handle such cases, e.g. the  $\omega$ B97X-D [20]. The 6-31G\* basis set was used overall the study, as it is sufficient for involved elements (H, C, Si). The above described selection of functionals allows a virtual experiment based on comparison of three calculated conformational energy profiles with different extent of employment of long range interactions. Hence, it is expected that the increasing contribution of non-bonding interactions will be manifested as increasing either positive or negative energy difference for each studied conformer.

## 2. Computational Methods

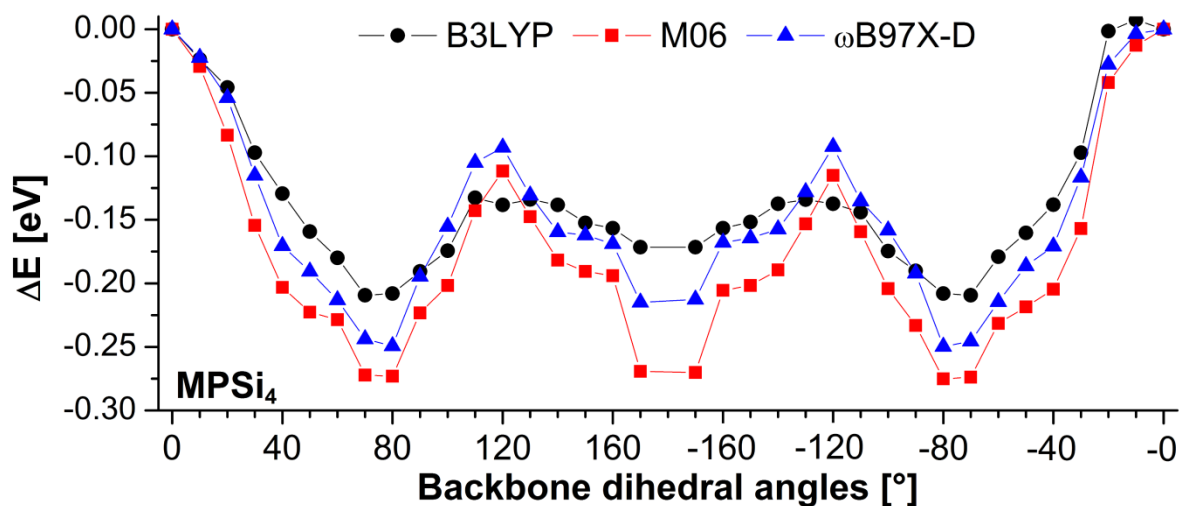
Studied MPSi<sub>4</sub> was modelled in several conformations. Dihedral angle  $\omega$  was constrained by step of 10° to following values 0°, 10°...180° and further from -170° to -0° (which means that 360° corresponds to -0°). The edge atoms were capped with methyl groups and conformers were treated as isolated in a vacuum environment. In total, 37 structures of MPSi<sub>4</sub> were subjected, first, to geometry optimization on the level of B3LYP/6-31G\* and then to single point energy calculation with M06 and  $\omega$ B97X-D functionals (using identical 6-31G\* basis set) involving dispersion terms to describe energy contribution of weak interactions between phenyl rings in the dependence on  $\omega$ .

All calculations were performed with Spartan 14 software [21].

## 3. Results and discussion

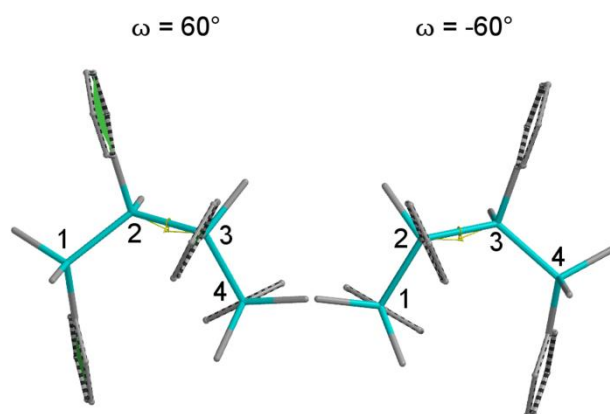
Virtually prepared methyl and phenyl substituted tetrasilylenes were subjected to geometry optimization in several conformations of Si backbone corresponding to various values of  $\omega$  and they were designed throughout the text as follows, for example MPSi<sub>4</sub>\_120, which stands for conformer with  $\omega=120^\circ$ .

Fig. 1 shows energy profile of MPSi<sub>4</sub> corresponding to conformational energy dependence of MPSi<sub>4</sub> in the  $\omega$  range from 0° to 360, i.e. from 0° to -0°. Conformation with  $\omega = 0^\circ$  has the highest energy, therefore, it has been set as the reference level for all obtained energy profiles which are then plotted as energy differences  $\Delta E$ , while raw calculated data with molecular energies are given in Online Resource 1. This enabled to clearly see differences between results obtained with particular density functionals that were used for calculation.



**Fig. 1** Molecular energies of  $MPSi_4$  calculated with B3LYP, M06 and  $\omega$ B97X-D functionals and 6-31G\* basis set

Curves of potential energy dependence are symmetrical according to the value  $\omega = 180^\circ$ . It means that conformations with opposite sign of  $\omega$  are energetically on the same level. Such molecules are diastereomers as they are reversed mirror images of each other as can be found in Fig. 2 for  $MPSi_4_{60}$  and  $MPSi_4_{-60}$ . Further, three minima of potential energy can be observed at  $\omega = 70-80^\circ$ ,  $170-190^\circ$  and  $-(70-80^\circ)$ . According to B3LYP,  $MPSi_4_{70}$ ,  $-70$  and  $MPSi_4_{80}$ ,  $-80$  are the most energetically favourable arrangements of a backbone while  $MPSi_4_{180}$  represents a local minimum only. In these molecules, the difference between B3LYP and M06 and  $\omega$ B97X-D is the largest, in numbers 0.07 and 0.05 eV for  $MPSi_4_{70}$ ,  $-70$  and  $OMPSi_4_{80}$ ,  $-80$ , and 0.10 and 0.05 eV for  $MPSi_4_{180}$ , respectively. Most significant stabilization by phenyl interaction is also observed for  $\omega = 180^\circ$ , where the difference between results obtained by used functionals is the most obvious. On the other hand, this local minimum is quite shallow when B3LYP is used, which indicates that stability of arrangements close to all-*anti* is probably assured primarily by phenyl interactions and cannot be accounted on  $\sigma$ -delocalization only. However, the  $MPSi_4_{180}$  molecule is irrelevant for a description of the kink stability as it represents the all-*anti* and thus stretched backbone. Moreover, the all-*anti* conformation is unattainable as stable (energetically viable) for linear PMPSi. Thus, it has no direct implications towards the purpose of the work.



**Fig. 2** Example of diastereomers of  $MPSi_4_{60}$  and  $MPSi_4_{-60}$

From another point of view, local energy maxima are related to  $MPSi_4_{120}$ ,  $-120$  which can be described as conformational barriers. The energy difference obtained by M06 and  $\omega$ B97X-D is higher than B3LYP energy. It seems that, besides attractive interactions between aromatic rings, phenyl-phenyl interactions contribute to destabilization of these unfavourable conformers due to repulsive effect. The most energetically inconvenient arrangements and therefore the most improbable is the pair (of identical conformations)  $MPSi_4_0$ ,  $-0$ , which represents maximally bent chain, an ideal kink i.e. a defect theoretically causing largest conformational disorder. To summarize, these results show that approximately *gauche* conformation of a kink is the most favourable arrangement of  $MPSi_4$  and therefore is suitable for occurrence in PMPSi chains as folding element.

As was described above, the main evaluation of dispersion contribution to geometry stabilization of  $MPSi_4$  was done through calculation of molecular energy with dispersion describing functionals M06 and  $\omega$ B97X-D. This paragraph deals with the issue of phenyl interactions employment from the viewpoint of geometry arrangement that refers to classical interpretation framework [22, 23]. Fig. 3a depicts four structures of  $MPSi_4$  with  $\omega = 0, 60, 120$  and  $170^\circ$ , which were graphically aligned by Si atoms no. 1, 2 and 3. There can be found two views on the molecules, which show response, (and corresponding rotation) of phenyl rings on the changes in the backbone conformation. Phenyl rings attached to atoms Si3 and Si4 were marked with red and blue plane labels, respectively. They alter positions in the direction of green arrows from  $MPSi_4_0$  subsequently to  $MPSi_4_{170}$ . Further, Fig. 3b contains insets of the same  $MPSi_4$  structures which are in this case displayed separately to see the differences in mutual positions of particular phenyl groups. The graph plot in Fig. 3b represents angles between phenyl groups related to their distance. The angle was measured as an angle between planes, which were constructed by connection of three points (aromatic carbon atoms) and the distance was measured as a distance between central points of phenyl ring planes. Generally, the distance suitable for employment of  $\pi$ -stacking attractive interactions between two benzenes is, according to ref. [22, 24], around 6–8 Å in maximum

and under the condition that angle between planes is close to  $0^\circ$ . The attractive interactions between phenyl groups are employed when their aromatic rings are positioned to T-shape or they are in convenient offset, i.e. an angle and distance between two rings is proper for interaction employment.

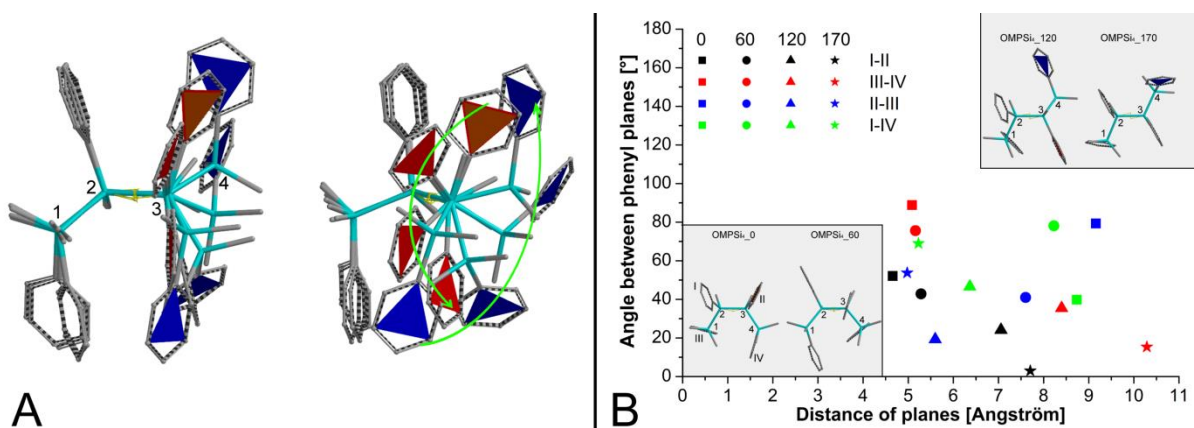


**Fig. 3** Aligned structures of  $MPSi_4_0$ , 60, 120, 170 with highlighted planes of phenyl groups at  $Si_3$  – red, at  $Si_4$  – blue (A) and angle-distance dependence of phenyl group pairs and their structures displaying mutual positions of phenyl groups (B).

As can be deduced from both structures and plot in this figure, the most convenient arrangement of the backbone should be the case of  $MPSi_4_60$ . Its phenyl groups attained convenient mutual position corresponding to angle  $45^\circ$  and  $80^\circ$  between planes I-II and III-IV, respectively. As the backbone of four Si atom alters its structure from kinked *syn* to stretched *anti*, a convenient arrangement of phenyl rings is adopted by plane II-III and I-IV and a good stability of this molecule is expected, however this structure does not form a kink anymore. Therefore,  $MPSi_4_60$  seems to be favourably disposed to kink stabilization.  $MPSi_4_70$  and  $MPSi_4_80$  then follow the properties of  $MPSi_4_60$  and based on the virtual measurement of phenyl plane angles and distances for  $MPSi_4$  with  $\omega = 0-170^\circ$ , which are given in Online Resource 2, they have even better arrangement. Positions of the phenyl groups I-III and II-IV are in all cases in larger distance than  $7 \text{ \AA}$  and therefore these pairs are not involved to the kink stabilization by non-bonding interactions.

## Conclusion

An investigation of a stabilizing effect of non-bonding interaction on a kink in poly[methyl(phenyl)silylene] backbone was performed with DFT and three types of functionals – B3LYP, M06 and  $\omega$ B97X-D. Model tetramer-size molecules of  $MPSi_4$  with exactly arranged Si-Si-Si-Si dihedral angles were used for calculation. The three of various functionals accounting non-bonding interactions and dispersion to different levels were used to assess the contribution of interaction between aromatic side groups to the conformational energy. It was discovered that  $MPSi_4$  in gauche conformation is the

arrangement, which is the most favourable energetically and also supported by employment of non-bonding interactions between phenyl rings. This virtual experiment was corroborated with a classical interpretation framework obtaining consistent results.

This finding that gauche conformation is viable in other words the only representative of a shortest possible kink is in agreement with our previous DFT research of the electronic properties of oligosilylenes with a kink in the backbones.

## Acknowledgement

This work was supported by the Ministry of Education, Youth and Sports of the Czech Republic – Program NPU I (LO1504).

## References

- [1] Teramae H, Matsumoto N (1996) Theoretical study on gauche-kink polysilane polymer.. *Solid State Commun.* doi:10.1016/0038-1098(96)00333-X
- [2] Michl J, West R (2000) Conformations of linear chains. Systematics and suggestions for nomenclature. *Account Chem Res.* doi:10.1021/ar0001057
- [3] Imhof R, Antic D, David DE et al (1997) Conformational effects in photoelectron spectra of tetrasilanes, *J Phys Chem. A.* doi:10.1021/jp970693e
- [4] Imhof R, Teramae H, Michl J (1997) Conformational effects in UV absorption spectra of tetrasilanes. *Chem Phys Lett.* doi:10.1016/S0009-2614(97)00405-3
- [5] Tsuji H, Toshimitsu A, Tamao K et al (2001) UV, MCD, and LD spectra of a conformationally constrained ortho-tetrasilane: Support for the avoided crossing model of conformational effects on excited states. *J Phys Chem A.* doi:10.1021/jp010792z
- [6] Crespo R, Piqueras MC, Michl J (2007) Electronic excitation in a syn-tetrasilane: 1,1,2,2,3,3,4,4-octamethyltetrasilacyclopentane. *Theor Chem Acc.* doi:10.1007/s00214-007-0246-1
- [7] Piqueras MC, Crespo R, Michl J (2008) Interpretation of the electronic spectra of four disilanes. *J Phys Chem A.* doi:10.1021/jp804677v
- [8] Tsuji H, Fogarty HA, Ehara M et al (2014) Electronic transitions in conformationally controlled tetrasilanes with a wide range of SiSiSiSi dihedral angles. *Chem Eur J.* doi:10.1002/chem.201403495
- [9] Fogarty HA, Imhof R, Michl J (2004) Magnetic circular dichroism of peralkylated tetrasilane conformers. *PNAS.* doi:10.1073/pnas.0403209101
- [10] Karatsu T (2008) Photochemistry and photophysics of organomonosilane and oligosilanes: Updating their studies on conformation and intramolecular interactions. *J Photoch Photobio C.* doi:10.1016/j.jphotochemrev.2008.06.001
- [11] Tsuji H, Michl J, Tamao K (2003) Recent experimental and theoretical aspects of the conformational dependence of UV absorption of short chain

peralkylated oligosilanes. *J Organomet Chem.* doi:10.1016/S0022-328X(03)00162-1

[12] Hanulikova B, Kuritka I (2014) Manifestations of conformational defect in electronic spectra of polysilanes – A Theoretical Study. *Macromol Symp.* doi:10.1002/masy.201300143

[13] Hanulikova B, Kuritka I (2014) Theoretical study of polaron binding energy in conformationally disrupted oligosilanes. *J Mol Model.* doi:10.1007/s00894-014-2442-y

[14] Hanulikova B, Kuritka I, Urbanek P (2016) Effect of backbone conformation and its defects on electronic properties and assessment of the stabilizing role of  $\pi$ - $\pi$  interactions in aryl substituted polysilylenes studied by DFT on deca[methyl(phenyl)silylene]s. *Chem Cent J.* doi:10.1186/s13065-016-0173-0

[15] Fujiki M (2003) Switching handedness in optically active polysilanes. *J Organomet Chem.* doi:10.1186/s13065-016-0173-0

[16] Fogarty HA, Ottosson C-H, Michl J (2000) The five favored backbone conformations of n-Si<sub>4</sub>Et<sub>10</sub>: cisoid, gauche, ortho, deviant, and transoid. *J Mol Struct-Theochem.* doi:10.1016/S0166-1280(00)00416-4

[17] Civalleri B, Zicovich-Wilson CM, Valenzano L et al (2008) B3LYP augmented with an empirical dispersion term (B3LYP-D\*) as applied to molecular crystals. *CrystEngComm.* doi:10.1039/b715018k

[18] Chai J-D, Head-Gordon M (2008) Long-range corrected hybrid density functionals with damped atom–atom dispersion corrections. *Phys Chem Chem Phys.* doi:10.1039/b810189b

[19] Walker M, Harvey AJA, Sen A et al (2013) Performance of M06, M06-2X, and M06-HF density functionals for conformationally flexible anionic clusters: M06 functionals perform better than B3LYP for a model system with dispersion and ionic hydrogen-bonding interactions. *J Phys Chem A.* doi:10.1021/jp408166m

[20] Chai J-D, Head-Gordon (2008) Systematic optimization of long-range corrected hybrid density functionals. *J Chem Phys.* doi:10.1063/1.2834918

[21] Shao Y, Molnar LF, Jung Y et al (2006) Advances in methods and algorithms in a modern quantum chemistry program package. *Phys Chem Chem Phys.* doi:10.1039/b517914a

[22] Hunter CA, Sanders JKM (1990) The nature of  $\pi$ - $\pi$  interactions. *J Am Chem Soc.* doi: 10.1021/ja00170a016

[23] Hunter CA, Singh J, Thornton JM (1991)  $\pi$ - $\pi$  interactions: The geometry and energetics of phenylalanine-phenylalanine interactions in proteins. *J Mol Biol.* doi:10.1016/0022-2836(91)90271-7

[24] Hunter CA, Lawson KR, Perkins J et al (2001) Aromatic interactions, *J Chem Soc Perkin Trans 2.* doi:10.1039/b008495f

## Online Resource 1

Molecular energy data of studied  $\text{MPSi}_4$  calculated by DFT with B3LYP, M06 and  $\omega$ B97X-D functionals and 6-31G\* basis set. Energies are dependent on the Si-Si-Si-Si dihedral angle  $\omega$  that was in calculation constrained by step of  $10^\circ$  from  $0^\circ$  through  $180^\circ$  to  $-0^\circ$ .

**Table A1** Molecular energy of  $\text{MPSi}_4$  obtained with different functionals

$\omega$	B3LYP	M06	$\omega$ B97X-D	$\omega$	B3LYP	M06	$\omega$ B97X-D
0	-63243.7477	-63215.1785	-63231.9518	-170	-63243.9192	-63215.4486	-63232.1644
10	-63243.7714	-63215.2093	-63231.9754	-160	-63243.9043	-63215.3840	-63232.1197
20	-63243.7936	-63215.2654	-63232.0077	-150	-63243.8995	-63215.3802	-63232.1162
30	-63243.8449	-63215.3360	-63232.0675	-140	-63243.8851	-63215.3679	-63232.1091
40	-63243.8771	-63215.3856	-63232.1240	-130	-63243.8818	-63215.3317	-63232.0799
50	-63243.9069	-63215.4072	-63232.1420	-120	-63243.8851	-63215.2936	-63232.0443
60	-63243.9276	-63215.4075	-63232.1635	-110	-63243.8918	-63215.3379	-63232.0871
70	-63243.9571	-63215.4525	-63232.1977	-100	-63243.9223	-63215.3827	-63232.1100
80	-63243.9558	-63215.4535	-63232.2014	-90	-63243.9378	-63215.4117	-63232.1439
90	-63243.9383	-63215.4049	-63232.1451	-80	-63243.9558	-63215.4536	-63232.2016
100	-63243.9221	-63215.3826	-63232.1100	-70	-63243.9571	-63215.4523	-63232.1974
110	-63243.8803	-63215.3268	-63232.0544	-60	-63243.9268	-63215.4101	-63232.1663
120	-63243.8860	-63215.2933	-63232.0451	-50	-63243.9080	-63215.3970	-63232.1381
130	-63243.8817	-63215.3306	-63232.0789	-40	-63243.8858	-63215.3831	-63232.1226
140	-63243.8859	-63215.3686	-63232.1092	-30	-63243.8449	-63215.3354	-63232.0683
150	-63243.9001	-63215.3794	-63232.1144	-20	-63243.7493	-63215.2205	-63231.9795
160	-63243.9043	-63215.3833	-63232.1193	-10	-63243.7404	-63215.1913	-63231.9554
170	-63243.9192	-63215.4479	-63232.1636	-0	-63243.7477	-63215.1786	-63231.9518

## Online Resource 2

The list of angles [°] and distances [Å] that were measured between pairs of phenyl planes of each conformer with Si-Si-Si-Si dihedral angle  $\omega$  in the range from 0° to 170°. The angle was measured as an angle between planes, which were constructed by connection of three points (aromatic carbons atoms) and the distance was measured as a distance between central points of phenyl ring planes. Planes are depicted in Fig. 3 in the article with illustration of their designation I, II, III and IV.

**Table A2** Angles and distances that were measured between pairs of phenyl groups

$\omega$	I-II [Å]	I-II [°]	III-IV [Å]	III-IV [°]	I-III [Å]	I-III [°]
0	4.655	52.08	5.086	88.82	7.409	56.82
10	4.697	51.91	5.106	88.32	7.742	13.88
20	4.799	51.73	5.181	89.65	7.727	14.26
30	4.924	51.47	5.176	86.41	7.735	14.24
40	4.986	48.63	5.155	80.31	7.701	15.01
50	5.143	45.71	5.162	80.30	7.676	14.31
60	5.285	42.86	5.161	75.59	7.728	12.93
70	5.693	48.29	5.962	54.35	7.748	14.24
80	5.899	39.80	6.238	49.87	7.721	4.80
90	6.145	37.67	6.827	45.67	7.719	5.35
100	6.465	28.69	7.716	48.09	7.706	4.54
110	6.763	21.71	8.190	43.10	7.687	24.50
120	7.055	24.14	8.399	35.46	7.690	28.94
130	7.319	33.56	8.717	13.73	7.677	24.17
140	7.485	36.29	9.077	11.83	7.690	37.42
150	7.634	26.36	9.196	8.55	7.633	27.98
160	7.703	16.17	9.454	14.93	7.615	35.83
170	7.705	2.97	10.288	15.34	7.571	54.60
$\omega$	II-IV [Å]	II-IV [°]	II-III [Å]	II-III [°]	I-IV [Å]	I-IV [°]
0	7.751	12.44	9.159	79.26	8.736	39.82
10	7.474	54.36	8.699	38.27	9.090	80.68
20	7.523	50.77	8.601	40.91	8.949	82.34
30	7.618	47.11	8.409	39.78	8.798	83.89
40	7.671	43.60	8.321	36.72	8.590	88.79
50	7.726	43.00	8.154	37.47	8.412	88.20
60	7.730	35.70	7.601	41.01	8.228	76.09
70	7.731	14.86	6.625	39.52	8.023	62.91
80	7.744	13.74	6.349	36.17	7.800	53.35
90	7.769	11.76	6.089	33.95	7.632	49.43
100	7.746	24.39	5.834	24.65	7.212	52.44
110	7.731	25.47	5.893	23.98	6.794	47.04
120	7.742	22.77	5.599	19.26	6.366	46.59
130	7.705	4.07	5.447	14.00	5.892	30.49
140	7.704	2.81	5.321	9.30	5.273	37.70
150	7.711	2.47	5.112	6.47	4.927	27.66
160	7.719	8.87	4.975	21.21	4.677	25.04
170	7.549	2.95	4.977	53.75	5.229	68.95



## **Research Paper IV:**

**HANULIKOVA, Barbora** and Ivo KURITKA.

Stabilization of conformational defects of hydrogen, alkyl and aryl substituted polysilylene chains by non-bonding interactions: A DFT study on tetrasilylene model molecules

*Submitted to Theoretical Chemistry Accounts.*



## Theoretical Chemistry Accounts

### Stabilization of conformational defects of hydrogen, alkyl and aryl substituted polysilylene chains by non-bonding interactions: A DFT study on tetrasilylene model molecules

--Manuscript Draft--

<b>Manuscript Number:</b>	
<b>Full Title:</b>	Stabilization of conformational defects of hydrogen, alkyl and aryl substituted polysilylene chains by non-bonding interactions: A DFT study on tetrasilylene model molecules
<b>Article Type:</b>	Regular Article
<b>Keywords:</b>	Alkyl; aryl; conformation; DFT; kink; tetrasilylenes; non-bonding interaction
<b>Corresponding Author:</b>	Barbora Hanulikova Tomas Bata University in Zlin CZECH REPUBLIC
<b>Corresponding Author Secondary Information:</b>	
<b>Corresponding Author's Institution:</b>	Tomas Bata University in Zlin
<b>Corresponding Author's Secondary Institution:</b>	
<b>First Author:</b>	Barbora Hanulikova
<b>First Author Secondary Information:</b>	
<b>Order of Authors:</b>	Barbora Hanulikova Ivo Kuritka
<b>Order of Authors Secondary Information:</b>	
<b>Funding Information:</b>	
<b>Abstract:</b>	Density functional theory calculations with B3LYP, M06 and $\omega$ B97X-D functionals with 6-31G* basis set are used for a study of non-bonding interactions in tetra[methyl(phenyl)silylene] (MPSi4), tetra[(dimethyl)silylene], tetra[silylene] (Si4) and further with molecules of tetra[cyclohexyl(methyl)silylene] and carbon chain analogue of MPSi4. Tetramer can serve as a model for conformational defect - a kink that is worth to understand especially in case of polysilylenes with $\sigma$ -conjugated backbones and therefore with direct relation between chain conformation and polymer properties. The kink disruptions are viable in poly[methyl(phenyl)silylene], poly[(dimethyl)silylene] as well as in poly[cyclohexyl(methyl)silylene] chains because the energy profiles of their oligomer analogues go through minimum in gauche conformation and moreover in this conformation are stabilized by non-bonding interactions (either $\pi$ - $\pi$ or Van der Waals). Si4 is more flexible and keeping of a kinked conformation is less probable due to lower energy barriers in its energy profile. The choice of dimethyl, cyclohexyl and namely methyl-phenyl substituents for building of model molecules rely on experimental importance of the respective polymers.
<b>Suggested Reviewers:</b>	Petr Toman, RNDr., Ph.D. toman@imc.cas.cz  Juraj Nozar, Mgr. nozar@imc.cas.cz  Sebera Jakub, Mgr., Ph.D. sebera@fzu.cz  Sonia Coriani, Dr. coriani@units.it  Stanislav Nespurek, prof. RNDr., DrSc.



# Stabilization of conformational defects of hydrogen, alkyl and aryl substituted polysilylene chains by non-bonding interactions: A DFT study on tetrasilylene model molecules

Barbora Hanulikova\*, Ivo Kuritka

Centre of Polymer Systems, Tomas Bata University in Zlín, trida Tomase Bati 5678, 76001, Zlin, Czech Republic

\*Corresponding author - email address: hanulikova@cps.utb.cz  
- tel.: +420576038128

## Abstract

Density functional theory calculations with B3LYP, M06 and  $\omega$ B97X-D functionals with 6-31G\* basis set are used for a study of non-bonding interactions in tetra[methyl(phenyl)silylene] (MPSi<sub>4</sub>), tetra[(dimethyl)silylene], tetra(silylene) (Si<sub>4</sub>) and further with molecules of tetra[cyclohexyl(methyl)silylene] and carbon chain analogue of MPSi<sub>4</sub>. Tetramer can serve as a model for conformational defect – a kink that is worth to understand especially in case of polysilylenes with  $\sigma$ -conjugated backbones and therefore with direct relation between chain conformation and polymer properties. The kink disruptions are viable in poly[methyl(phenyl)silylene], poly[(dimethyl)silylene] as well as in poly[cyclohexyl(methyl)silylene] chains because the energy profiles of their oligomer analogues go through minimum in gauche conformation and moreover in this conformation are stabilized by non-bonding interactions (either  $\pi$ - $\pi$  or Van der Waals). Si<sub>4</sub> is more flexible and keeping of a kinked conformation is less probable due to lower energy barriers in its energy profile. The choice of dimethyl, cyclohexyl and namely methyl-phenyl substituents for building of model molecules rely on experimental importance of the respective polymers.

**Keywords:** Alkyl, aryl, conformation, DFT, kink, tetrasilylenes, non-bonding interaction

# 1. Introduction

Among polymers, linear polysilanes called polysilylenes (and other linear polymers with backbone made from heavier atoms of the fourth main group from periodical table of elements) have special position due to  $\sigma$ -conjugation along their main chain which does not require alternating scheme of single and double bonds as in  $\pi$ -conjugated carbonaceous polymers. Some of the polysilylenes have aromatic substituents in positions of polymer side groups which imparts even more complicated electronic properties due to mixing of  $\sigma$ - and  $\pi$ -delocalized systems. A great effort has been developed to synthesize, characterize and explain all observed phenomena including hard theoretical works [1, 2, 3]. Exhaustive studies on oligomeric model molecules in order to approach long chain polymer properties by extrapolation have been performed too [4, 5]. The topic seemed to be covered and relatively quiet for a long time having a stable interpretational framework. However, the last findings in the field of thin films made from these polymers [6, 7] or conductive  $\pi$ -conjugated systems [8, 9] and even general polymers [10, 11, 12, 13] revived interest on the importance of polymer chain ordering, stacking, H or J aggregate formation, chain alignment and dependence of the material properties on the development of the film thickness starting from sub-molecular cover degree through thin films from several to hundreds nanometres up to micrometric thickness. Among other factors, conformational disorder play crucial role in development of various structural features and properties emerging with increasing thickness of polymer films.

As has been cited above, poly and oligosilylene conformational studies have been successfully performed in the past [14, 15] however, with respect to the need of proper interpretation of conformational defects in the polysilylene material structure the newly developed calculation methods are expected to be useful in identification of contribution of long range interactions especially. Polysilylene chains are not purely rod-like in shape. It has been already shown, that they are able to adopt geometry with bends between conjugated linear segments. The smallest conformational unit of a bend structure can be regarded as four consecutive silicon (Si) atoms arranged in approximately gauche conformation also called a kink [16, 17]. Such kinks are interruptions of a regular backbone arrangement (helical, zig-zag) and they can be considered as local conformational defects that disrupt  $\sigma$ -electron delocalization resulting in the changes in electronic properties of material [18, 19, 20, 21]. Although a whole family of defects can occur in polysilylene solid phase, the kink is the simplest one but omnipresent hence extremely important and worth of attention.

It has already been shown experimentally as well as theoretically [22] on model oligo[methyl(phenyl)silylene] molecules and thus poly[methyl(phenyl)silylene] (PMPSi) that Si backbone conformation and presence of a kink defect and its position influence energy levels and spatial distribution of molecular orbitals and spin density in charged (cations and anions) analogues [23, 2x] modelling polarons in real solid state polymers. In

spite the dramatic effect of the kink on the structure of electronic levels, the total energy of neutral molecule is not significantly increased by virtual introduction of a kink as has been demonstrated in our previous work [25]. In a preliminary study on tetra[methyl(phenyl)silylene] (MPSi4), we have shown that the defect is self-stabilized via strong phenyl-phenyl non-bonding interactions which can be generalized for PMPSi in that sense that the kink is viable as chain folding element.

In order to clarify specific structure-property relationships we present a re-examination study in this field. The kink is considered as four consecutive Si atoms ideally in syn conformation, whose dihedral angle ( $\omega$ ) corresponds to  $0^\circ$ . Tetrasilanes are the smallest and most tractable model molecular units. Several studies of linear tetrasilylenes with small substituents, such as hydrogen, methyl or halogen, were described in ref. [26, 27]. These tetrasilylenes were found in the almost whole range of  $\omega$  as enantiomeric pairs with one exception of conformation  $180^\circ$  (anti) with local minima representing angles  $\omega = \pm 40^\circ$  (cisoid),  $\omega = \pm 60^\circ$  (gauche),  $\omega = \pm 90^\circ$  (ortho),  $\omega = \pm 150^\circ$  (deviant) and  $\omega = \pm 165^\circ$  (transoid). Conformation syn is thus unfavourable even for polysilylenes with small side groups. Therefore, hydrogen, methyl, cyclohexyl and phenyl groups were chosen as side groups to build a suitable set of models including tetra(silylene) (Si4), tetra[(dimethyl)silylene] (DMSi4), tetra[cyclohexyl(methyl)silylene] (cyc-HMSi4) and MPSi4. The choice of model side groups is also practically relevant as poly[(dimethyl)silylene], poly[cyclohexyl(methyl)silylene] and namely PMPSi are the most reported polysilane materials in experimental literature [28]. It is expected that the adoption of kinked arrangement is significantly influenced by different steric limitations of chosen groups, attractive or repulsive interactions of phenyl groups or other non-bonding interactions of used groups. It is important to note, that these groups also affect the main chain, namely aromatic substituents. The data for the case of MPSi4 is adopted from preliminary study [29]. The molecule of MPSi4 carries chiral centres however, the symmetry of its conformational profile has been proven, as the reasonable model molecule is a diastereomer. Aside this, a molecule with carbon atoms inserted instead of Si was also studied although the calculations were limited only to 1,2,3,4,5,6-hexamethyl-2,3,4,5-tetraphenylhexane (MPC4) with methyl and phenyl groups in the same arrangement as MPSi4 and considering the others is known and trivial. A five membered (Si4, DMSi4, cyc-HMSi4, MPSi4 and MPC4) set of models was completed in this way.

The aim of this paper is to investigate the above described set of models with DFT computational analysis of molecular arrangement and energy. Density functionals were chosen with the respect of involvement of the dispersion term and at the same time each of them in a different extent [30, 31]. The B3LYP functional is considered among computational chemist as a good workhorse although it suffers on underestimation of long range (non-bonding) interactions and treat them poorly. This can be improved by the utilization of M06 functional which has 27 % of HF exchange and has a very good response under dispersion

forces [32]. The non-Coulomb part of exchange functionals typically dies off too rapidly and becomes very inaccurate at large distances. Empirical dispersion can be implemented to deal successfully such calculations, e.g. the  $\omega$ B97X-D [33]. The 6-31G\* basis set was used overall the study, as it is appropriate for involved elements (H, C, Si). The above described selection of functionals allows a virtual experiment based on comparison of three calculated conformational energy profiles with different extent of long range interactions involvement. Hence, it is expected that the increasing contribution of non-bonding interactions will be manifested as increasing either positive or negative energy difference for each conformer enabling thus conformational analysis and comparison between tested model molecules with different chemical structure.

## 2. Computational Methods

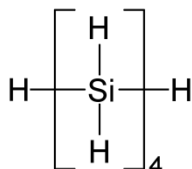
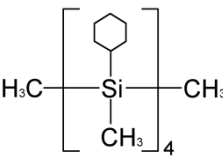
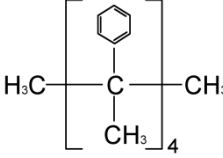
All calculations were performed with Spartan 14 software [34]. Studied MPSi<sub>4</sub>, DMSi<sub>4</sub>, Si<sub>4</sub> and cyc-HMSi<sub>4</sub>. MPC<sub>4</sub> were modelled in several conformations. Dihedral angle  $\omega$  was constrained by step of 10° to following values 0°, 10°...180° for DMSi<sub>4</sub>, Si<sub>4</sub> and for MPSi<sub>4</sub>. For cyc-HMSi<sub>4</sub> and MPC<sub>4</sub> was step value 20° and the range was set also from 0° to 180°. The edge atoms of all types of molecules with exception of Si<sub>4</sub> were capped with methyl groups. Further, molecules were treated as isolated in a vacuum environment. In total, 19 structures of DMSi<sub>4</sub>, Si<sub>4</sub>, MPSi<sub>4</sub> and 9 structures of cyc-HMSi<sub>4</sub> and MPC<sub>4</sub> were subjected, first, to geometry optimization by B3LYP/6-31G\* and then to single point energy calculation with M06 and  $\omega$ B97X-D functionals using identical 6-31G\* basis set involving dispersion terms to describe energy contribution of weak interactions in the dependence on  $\omega$ .

### Chemical formulas of used model molecules

In order to make understanding of the reader to the text easier, formulas of all investigated molecules are shown in Fig. 1 together with their various names that can be found throughout the cited literature.

Name	Abbreviation	Formula
<b>tetra[methyl(phenyl)silylene]</b> 1,1,2,3,4,4-hexamethyl-1,2,3,4-tetraphenyl-tetrasilane	<b>MPSi<sub>4</sub></b> OMPSi <sub>n</sub>	
<b>tetra[(dimethyl)silylene]</b> permethylated tetrasilane decamethyltetrasilane 1,1,1,2,2,3,3,4,4,4-decamethyltetrasilane	<b>DMSi<sub>4</sub></b> ODMSi <sub>n</sub>	



<b>tetra(silylene)</b> <i>n</i> -tetrasilane	<b>Si<sub>4</sub></b>	
<b>tetra[cyclohexyl(methyl)silylene]</b> 1,2,3,4-tetracyclohexyl-1,1,2,3,4,4-hexamethyl-tetrasilane	<b>cyc-HMSi<sub>4</sub></b>	
<b>1,2,3,4,5,6-hexamethyl-2,3,4,5-tetraphenylhexane</b>	<b>MPC<sub>4</sub></b>	

**Fig. 1** Nomenclature and formulas of studied molecules (names and abbreviations in bold are used in this paper)

### 3. Results and discussion

Virtually prepared tetrasilylenes and their various analogues were subjected to geometry optimization in several conformations of Si backbone corresponding to various constrained values of  $\omega$ . Designation of molecules is through the whole paper consistent and is composed from the type of tetramer and the value of  $\omega$ , for example MPSi<sub>4</sub>\_120.

Fig. 2 carries plots of the molecular energy dependence calculated for DMSi<sub>4</sub> and Si<sub>4</sub>. Each graph was constructed from differences of molecular energies  $\Delta E$  and the energy of tetramer with  $\omega = 0^\circ$  was chosen as the reference value for subtraction as it belongs to DMSi<sub>4</sub> and Si<sub>4</sub> with highest energy. The plot contains energy values corresponding to  $\omega$  value 0–180°. Raw energy data are for all studied molecules are given in Table A1–A3 in Online Resource 1. Calculations for  $\omega$  greater than 180° were not performed as the molecules and therefor their energy profiles are symmetric. In case of DMSi<sub>4</sub>, results clearly show that adoption of the most stable conformation in the  $\omega$  range 80–170° is only the issue of steric effects because differences between energies obtained by B3LYP, M06 and  $\omega$ B97X-D functionals for *eclipsed* conformation are nearly negligible. It means that *ortho* and *transoid* conformations and eventual transition between them are fully governed by geometrical (steric) factors. The transition between *transoid* (160–170°) and *antitransoid* (-(160–170°) or 190–200°) – actually *anti* conformation – has a very small energy barrier calculated by B3LYP but higher obtained for other functionals testifying thus for increased role of long range interactions. On the other hand, results for  $\omega$  range 30–80° are extremely sensitive on the applied functional. The *cisoid-gauche* conformation has significant stabilization contribution due to long range interactions and the barrier between *cisoid-gauche* and *ortho* conformations is increased (destabilized) by repulsive interactions which discriminates *anti* conformation.

Obtained results are in accord with previous studies [35] and references therein confirm agreement with experimental data too.

Slightly more complicated situation can be seen for  $\text{Si}_4$  although the plots in graph look simpler than in the case above. Hydrogen atoms form only minimal energy barriers in comparison with  $\text{DMSi}_4$  resulting in stable arrangements *gauche* and *transoid* with extremely shallow minima on the energy profile in case of B3LYP. Functionals accounting better dispersion predict even smaller barriers than B3LYP pointing towards relatively highest flexibility of  $\text{Si}_4$  among tested molecules which is in accord with basic mechanistic expectations as hydrogen is the smallest substituent. The carbonaceous analogue of  $\text{Si}_4$  is the notoriously known *n*-butane ( $\text{C}_4$ ) which has stable conformations *gauche* and *anti*.  $\text{C}_4$  has much higher energy barrier (*eclipsed*) between these two conformations, i.e. approx. 0.17 eV while our estimation of the same barrier for  $\text{Si}_4$  is about 0.03 eV only which could be assigned to the  $\sigma$ -conjugation effect as well to longer bonding distance between second and third backbone atoms resulting into less spatially demanding geometry. Moreover, both M06 and  $\omega\text{B97X-D}$  predict *anti* conformation for large dihedral angles ( $\omega = 180^\circ$ ). In the range of smaller  $\omega$  the M06 predict *cisoid* and  $\omega\text{B97X-D}$  predict *gauche* conformation. Experimental photolysis followed by UV and IR spectroscopy studies demonstrated directly that a mixture of *gauche* and *anti* conformers of  $\text{Si}_4$  is present in a nitrogen matrix [36, 37, 38], indicating thus, that  $\omega\text{B97X-D}$  functional performs best.

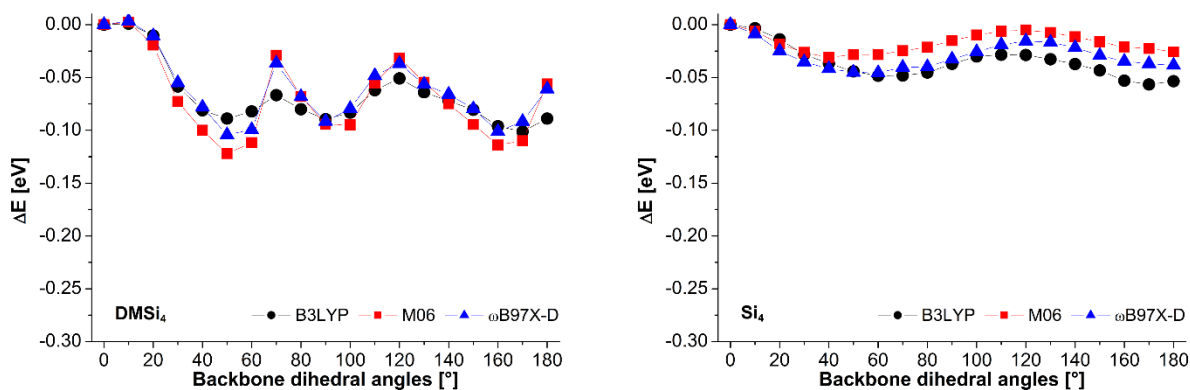


**Fig. 2** Molecular energy differences of  $\text{DMSi}_4$  (left) and  $\text{Si}_4$  (right) calculated with B3LYP, M06 and  $\omega\text{B97X-D}$ .

Fig. 3 is divided into two graph window panels corresponding to conformational energy dependence of  $\text{MPSi}_4$  and  $\text{MPC}_4$  in the  $\omega$  range from  $0^\circ$  to  $180^\circ$ . Again here, the conformational energy profile is symmetrical according to a point  $\omega = 180^\circ$ . Two local minima of potential energy can be observed at  $\omega = 70-80^\circ$  and  $170-190^\circ$  for  $\text{MPSi}_4$  corresponding to *gauche* and *anti* conformers, respectively.  $\text{MPSi}_4_{70}$  and  $\text{MPSi}_4_{80}$ , are the most energetically favourable arrangements of a backbone according to B3LYP and  $\omega\text{B97X-D}$  although the latter method predicts bigger energy gain for transition from *eclipsed* conformation to *anti*. The use of M06 resulted into nearly the same

energy of *anti* as for *gauche*. However, the *anti* conformation is not viable at any in long PMPSi chain. In these molecules, the difference between B3LYP and M06 and  $\omega$ B97X-D is the largest, in numbers 0.07 and 0.05 eV, or even 0.1 eV for MPSi<sub>4</sub>\_170, respectively. Significant stabilization by phenyl-phenyl interaction is observed due to their mutual positions typical for attractive interactions. On the other hand, local energy maxima are related to MPSi<sub>4</sub>\_120 (*eclipsed*) because repulsive phenyl interactions contribute to destabilization of this conformers as manifested by the higher energy difference obtained by M06 and  $\omega$ B97X-D in contrast to B3LYP. These results show that approximately *gauche* conformation of a kink is the most favourable arrangement of MPSi<sub>4</sub> and therefore is suitable for occurrence in PMPSi chains as folding element [29].

The second graph in Fig. 3 shows MPC<sub>4</sub> which is carbonaceous analogue of MPSi<sub>4</sub>. This molecule stand for the case which contains the same side groups, however  $\sigma$ -conjugation related with Si atoms is cancelled. On the first sight, the energy difference scale is much larger than for all other molecules. Energy barriers exceed 1 eV testifying for much larger steric strain than observed for tetrasilylenes. Similarly to MPSi<sub>4</sub>, *gauche* and *transoid* conformations can be found as the most stable however, long range interactions do not contribute to stabilization of these molecules but make the sterically demanding structure (due to shorter C-C bonds than Si-Si) more flexible most likely due to decrease of energy barriers between the two stable conformers [14]. The contribution can be estimated roughly as 0.1 eV. Also here, *syn* and *eclipsed* conformations are the least favourable.

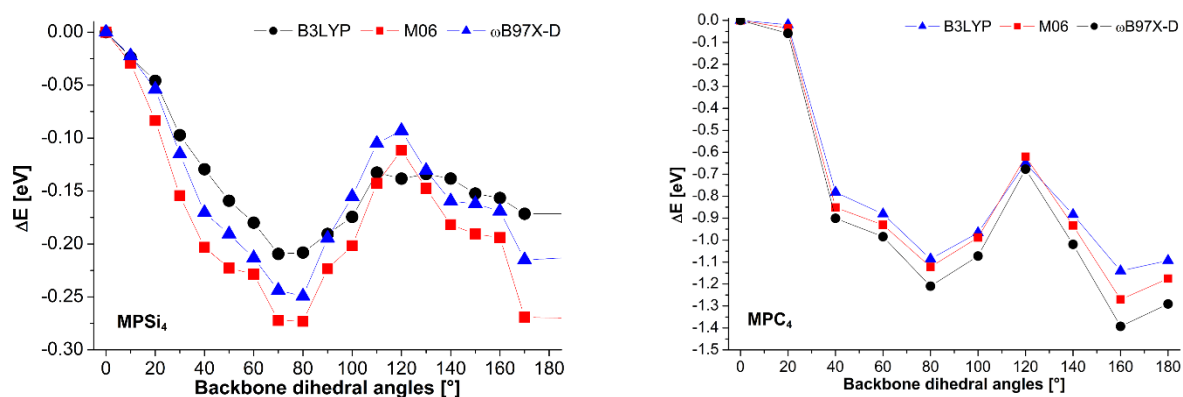


**Fig. 3** Molecular energy differences of MPSi<sub>4</sub> (left) and its carbonaceous analogue MPC<sub>4</sub> (right) calculated with B3LYP, M06 and  $\omega$ B97X-D

The graph in Fig. 4 shows results of calculations performed with conformers of cyc-HMSi<sub>4</sub> that represent the analogue of MPSi<sub>4</sub>, however it carries cyclohexyl groups instead phenyl groups. Thus cyc-HMSi<sub>4</sub> provides a model molecule, which does not contain aromatic groups in its structure but at the same time the side groups are of approximate size as phenyl groups having both six membered carbon ring. On the other hand, the cyclohexyl group contains 10 hydrogen atoms making it bigger than phenyl group with 5 hydrogen atoms

only. Therefore these groups cause not exactly the same steric barriers but no better model is at hand. Interestingly, the most energetically unfavourable geometry was found for *cyc-HMSi<sub>4</sub>\_20* which serves as the reference for  $\Delta E$  calculations. The energy profile evidences for viability of the *syn* conformation whose local minimum is predicted to be more than two times deeper using M06 and  $\omega$ B97X-D than B3LYP. Both dispersion involving functionals predict nearly the same values of  $\Delta E$  for each tested  $\omega$  value. It can be explained by similar efficiency of both functionals in accounting of long range interactions involved exactly in this kind of molecule. All three functionals predict the same for  $\omega$  in the range 140–180° where the most stable conformation is *transoid*. The biggest difference between B3LYP and M06 and  $\omega$ B97X-D can be found for  $\omega = 40^\circ$ . It is evident, that while B3LYP predicts local energy minimum for *ortho* conformation the other two functionals predict broad flat-bottomed minimum with most favourable geometry for *cisoid* *cyc-HMPSi<sub>4</sub>\_40* conformer which is shown in the image in the right panel of Fig. 4.

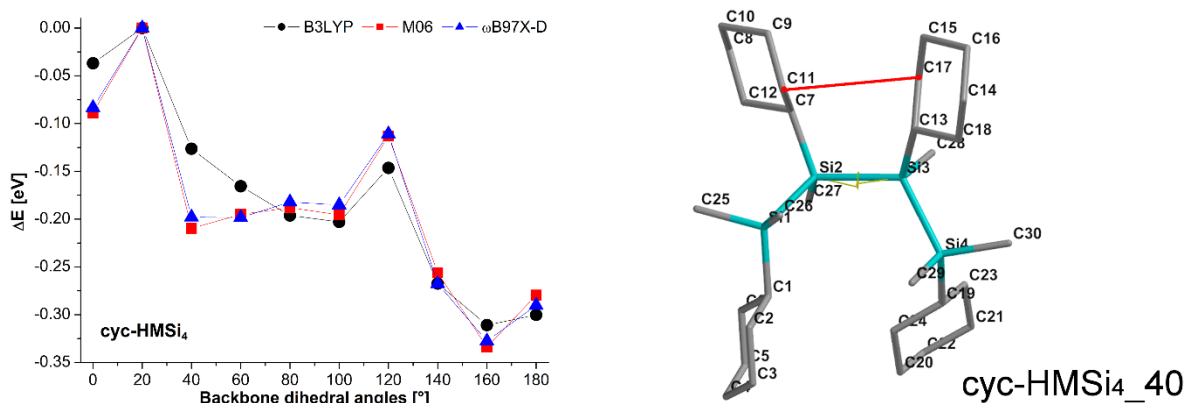


**Fig. 4** Molecular energy differences of *cycHMSi<sub>4</sub>* (left) calculated with B3LYP, M06 and  $\omega$ B97X-D and molecule of *cyc-HMSi<sub>4</sub>\_40* with highlighted shortest distance between cyclohexyl groups

Cyclohexyl substituents attached to second and third Si atoms of the tetrasilene backbone come into closer contact during rotation of the Si-Si bond from  $\omega = 100^\circ$  to  $\omega = 40^\circ$ . B3LYP which does not account dispersive forces that much as the other two functionals predict increase of conformational energy in the sense of increasing pushing of adjacent cyclohexyl side groups. The cyclohexyl ring in chair conformation is relatively locked and has restricted free rotation of CH<sub>2</sub> groups which makes possible more intimate contact between these groups than one would expect for their linear aliphatic analogues. Indeed, the distance between carbon atoms C11-C17 in the *cyc-HMPSi<sub>4</sub>\_40* conformer is 3.734 Å that is the smallest among all other conformers. This behaviour can be ascribed to larger importance of Van der Waals interactions in stabilization of the molecular conformation which is in compliance with well-known difference of cyclohexane and hexane boiling points [39].

## Conclusion

Performed calculations corroborated with available experimental and theoretical literature confirmed that long range interactions are very important when polysilylenes are described and they should not be ignored despite the fact that their conformational barriers are lower by order of magnitude than the barriers of carbonaceous analogues as molecules with carbon skeleton have much larger steric strain than their silicon counterparts. Comparison of the calculation and experiment revealed  $\omega$ B97X-D, which includes long range correction and empirical dispersion terms, to be the best performing functional in the prediction of polysilylene conformational dependencies regardless the type of the tested side groups (H, methyl, phenyl, cyclohexyl). Van der Waals and  $\pi$ - $\pi$  interactions are employed significantly in stabilization of conformers of described molecules.  $\text{Si}_4$  molecule can be characterised by extremely shallow energy barriers between stable conformers *gauche* and *anti* that can be associated to high flexibility of its chain. In comparison with  $\text{Si}_4$ ,  $\text{DMSi}_4$  molecule is more suitable for formation of a stable conformers that corresponds to its deeper minima on the energy profile with  $\omega = 50^\circ$  (*gauche*) and  $\omega = 160^\circ$  (*transoid*). This leads to conclusion that *gauche* conformation of  $\text{DMSi}_4$ , which is a model for a kink in the polysilylene backbone, can be expected in polymer-size (dimethyl)silylene chains. Similarly in  $\text{MPSi}_4$ , *gauche* conformer is energetically favourable as well as dispersion stabilized and therefore viable as a kink defect in PMPSi backbones, which is in accordance with our previous studies. Beside *gauche* conformer of  $\text{MPSi}_4$ , *transoid* conformation represents another energy minimum that can be also found in PMPSi as an optimal defectless conformation of the main chain resulting in its helical secondary structure. Study on  $\text{MPC}_4$  served for comparison of  $\text{MPSi}_4$  with its carbonaceous analogue. Generally, the energy barriers between conformers and the depth of local energy minima obtained for  $\text{DMSi}_4$  and  $\text{Si}_4$  are significantly lower than those calculated for  $\text{MPSi}_4$ .

Besides PMPSi, poly[cyclohexyl(methyl)silylene] belongs to the most important solution processable polysilanes which invoked investigation of cyc-HMSi<sub>4</sub>. This tetrasilylene evinces surprisingly strong stabilization in *cisoid* and *gauche* conformation that is assigned to Van der Waals interactions between cyclohexyl groups as this molecule represents non-aromatic case of the investigated set of tetrasilylenes.

## Acknowledgement

This work was supported by the Ministry of Education, Youth and Sports of the Czech Republic – Program NPU I (LO1504).

## References

- [1] Tsuji H, Michl J, Tamao K (2003) Recent experimental and theoretical aspects of the conformational dependence of UV absorption of short chain peralkylated oligosilanes. *J Organomet Chem.* Doi:10.1016/S0022-328X(03)00162-1
- [2] Tsuji H, Fogarty HA, Ehara M et al (2014) Electronic transitions in conformationally controlled tetrasilanes with a wide range of SiSiSiSi dihedral angles. *Chem Eur J.* Doi:10.1002/chem.201403495
- [3] Tsuji H, Toshimitsu A, Tamao K (2001) UV, MCD, and LD spectra of a conformationally constrained *ortho*-tetrasilane: Support for the avoided crossing model of conformational effects on excited states. *J Phys Chem A.* Doi:10.1021/jp010792z
- [4] Fogarty HA, Ottosson C-H, Michl J (2000) Conformations of oligosilanes with ethyl and methyl substituents. *J Mol Struct.* Doi:10.1016/S0022-2860(00)00656-6
- [5] Kirtman B, Hasan M (1992) Linear and nonlinear polarizabilities of trans-polysilane from ab initio oligomer calculations. *J Chem Phys.* Doi:10.1063/1.462483
- [6] Urbanek P, Kuritka I (2015) Thickness dependent structural ordering, degradation and metastability in polysilane thin films: A photoluminescence study on representative  $\sigma$ -conjugated polymers. *J Lumin.* Doi:10.1016/j.jlumin.2015.08.022
- [7] Urbanek P, Kuritka I, Danis S et al (2014) Thickness threshold of structural ordering in thin MEH-PPV films. *Polymer.* Doi:10.1016/j.polymer.2014.05.054
- [8] Mirzov O, Scheblykin IG (2006) Photoluminescence spectra of a conjugated polymer: From films and solutions to single molecules. *Phys Chem Chem Phys.* Doi:10.1039/b612073c
- [9] Nguyen TQ, Martini I, Liu J et al (2000) Controlling interchain interactions in conjugated polymers: The effects of chain morphology on exciton-exciton annihilation and aggregation in MEH-PPV films. *J Phys Chem B.* Doi:10.1021/jp993190c
- [10] Overney RM, Buenviaje C, Luginbuhl R et al (2000) Glass and structural transitions measured at polymer surfaces on the nanoscale. *J Therm Anal Cal.* Doi:10.1023/A:1010196214867
- [11] Benight SJ, Knorr Jr. DB, Johnson LE et al (2012) Nano-engineering lattice dimensionality for a soft matter organic functional material. *Adv Mater.* Doi:10.1002/adma.201104949
- [12] Eshaghi A, Graeli A (2014) Optical and electrical properties of indium tin oxide (ITO) nanostructured thin films deposited on polycarbonate substrates "thickness effect". *Optik.* Doi:10.1016/j.ijleo.2013.09.011
- [13] Gedelian CA, Rajanna KC, Premerlani B et al (2014) Photoluminescence properties of poly (p-phenylene vinylene) films deposited by chemical vapor deposition. *J Lumin.* Doi:10.1016/j.jlumin.2013.07.042

- [14] Karatsu T (2008) Photochemistry and photophysics of organomonosilane and oligosilanes: Updating their studies on conformation and intramolecular interactions. *J Photoch Photobio C*. Doi:10.1016/j.jphotochemrev.2008.06.001
- [15] Despotopoulou MM, Frank CW, Miller RD et al (1990) Role of the restricted geometry on the morphology of ultrathin poly(di-n-hexylsilane) films. *Macromolecules*. Doi:10.1021/ma00123a042
- [16] Teramae H, Matsumoto N (1996) Theoretical study on gauche-kink polysilane polymer.. *Solid State Commun*. Doi:10.1016/0038-1098(96)00333-X
- [17] Michl J, West R (2000) Conformations of linear chains. Systematics and suggestions for nomenclature. *Account Chem Res*. Doi:10.1021/ar0001057
- [18] Imhof R, Antic D, David DE et al (1997) Conformational effects in photoelectron spectra of tetrasilanes, *J Phys Chem. A*. Doi:10.1021/jp970693e
- [19] Imhof R, Teramae H, Michl J (1997) Conformational effects in UV absorption spectra of tetrasilanes. *Chem Phys Lett*. Doi:10.1016/S0009-2614(97)00405-3
- [20] Crespo R, Piqueras MC, Michl J (2007) Electronic excitation in a syn-tetrasilane: 1,1,2,2,3,3,4,4-octamethyltetrasilacyclopentane. *Theor Chem Acc*. Doi:10.1007/s00214-007-0246-1
- [21] Piqueras MC, Crespo R, Michl J (2008) Interpretation of the electronic spectra of four disilanes. *J Phys Chem A*. Doi:10.1021/jp804677v
- [22] Fogarty HA, Imhof R, Michl J (2004) Magnetic circular dichroism of peralkylated tetrasilane conformers. *PNAS*. Doi:10.1073/pnas.0403209101
- [23] Hanulikova B, Kuritka I (2014) Manifestations of conformational defect in electronic spectra of polysilanes – A Theoretical Study. *Macromol Symp*. Doi:10.1002/masy.201300143
- [24] Hanulikova B, Kuritka I (2014) Theoretical study of polaron binding energy in conformationally disrupted oligosilanes. *J Mol Model*. Doi:10.1007/s00894-014-2442-y
- [25] Hanulikova B, Kuritka I, Urbanek P (2016) Effect of backbone conformation and its defects on electronic properties and assessment of the stabilizing role of  $\pi$ - $\pi$  interactions in aryl substituted polysilylenes studied by DFT on deca[methyl(phenyl)silylene]s. *Chem Cent J*. Doi:10.1186/s13065-016-0173-0
- [26] Fujiki M (2003) Switching handedness in optically active polysilanes. *J Organomet Chem*. Doi:10.1186/s13065-016-0173-0
- [27] Fogarty HA, Ottosson C-H, Michl J (2000) The five favored backbone conformations of n-Si<sub>4</sub>Et<sub>10</sub>: cisoid, gauche, ortho, deviant, and transoid. *J Mol Struct-Theochem*. Doi:10.1016/S0166-1280(00)00416-4
- [28] Nespurek S (199) Thin polysilylene films. Their electronic and photoelectrical properties. *Mat Sci Eng C*. Doi: 10.1016/S0928-4931(99)00089-2
- [29] Hanulikova B, Kuritka I (2016) Contribution of non-bonding interactions to stabilization of aryl-substituted polysilylene chains conformational disorder examined by DFT on tetra[methyl(phenyl)silylene] model molecule. *Submitted to J Mol Model*

[30] Civalleri B, Zicovich-Wilson CM, Valenzano L et al (2008) B3LYP augmented with an empirical dispersion term (B3LYP-D\*) as applied to molecular crystals. CrystEngComm. Doi:10.1039/b715018k

[31] Chai J-D, Head-Gordon M (2008) Long-range corrected hybrid density functionals with damped atom–atom dispersion corrections. Phys Chem Chem Phys. Doi:10.1039/b810189b

[32] Walker M, Harvey AJA, Sen A et al (2013) Performance of M06, M06-2X, and M06-HF density functionals for conformationally flexible anionic clusters: M06 functionals perform better than B3LYP for a model system with dispersion and ionic hydrogen-bonding interactions. J Phys Chem A. Doi:10.1021/jp408166m

[33] Chai J-D, Head-Gordon (2008) Systematic optimization of long-range corrected hybrid density functionals. J Chem Phys. Doi:10.1063/1.2834918

[34] Shao Y, Molnar LF, Jung Y et al (2006) Advances in methods and algorithms in a modern quantum chemistry program package. Phys Chem Chem Phys. Doi:10.1039/b517914a

[35] Fogarty HA, Ottosson H, Michl J (2006) Calculation of relative energies of permethylated oligosilane conformers in vapor and in alkane solution. J Phys Chem B. Doi:10.1021/jp064643y

[36] Piqueras MC, Merchán M, Crespo R (2002) Conformational effects on the ultraviolet absorption spectrum of *n*-tetrasilane: multistate complete active space second-order perturbation theory treatment. J Phys Chem A. Doi:10.1021/jp020460+

[37] Albinsson, B, Teramae, H, Plitt HS et al (1996) Matrix-isolation IR and UV spectra of Si<sub>3</sub>H<sub>8</sub> and Si<sub>4</sub>H<sub>10</sub>: Isomers and conformers of oligosilanes. J Phys Chem. Doi:10.1021/jp9537318

[38] Albinsson, B, Teramae, H, Downing JW et al (1996) Conformers of saturated chains : matrix isolation, structure, IR and UV spectra of n-Si(4)Me(10). Chem Eur J. Doi:10.1002/chem.19960020512

[39] Speight JG (2011) Handbook of industrial hydrocarbon processing. Elsevier



## Online Resource 1

Molecular energy data of studied  $\text{DMSi}_4$ ,  $\text{Si}_4$ ,  $\text{MPSi}_4$ ,  $\text{MPC}_4$ ,  $\text{cyc-HMSi}_4$  calculated by DFT with B3LYP, M06 and  $\omega\text{B97X-D}$  functionals and 6-31G\* basis set. Energies are dependent on the Si-Si-Si-Si dihedral angle  $\omega$  that was in calculation constrained by step of  $10^\circ$  or  $20^\circ$  from  $0^\circ$  through  $180^\circ$ .

*Table A1 Molecular energy of  $\text{DMSi}_4$  and  $\text{Si}_4$*

<b>DMSi<sub>4</sub></b>	<b>B3LYP</b>	<b>M06</b>	<b><math>\omega\text{B97X-D}</math></b>
0	-42374.3801	-42361.5086	-42369.4099
10	-42374.3792	-42361.5076	-42369.4063
20	-42374.3904	-42361.5254	-42369.4164
30	-42374.4387	-42361.5785	-42369.4664
40	-42374.4612	-42361.6125	-42369.4928
50	-42374.4690	-42361.6285	-42369.5147
60	-42374.4622	-42361.6202	-42369.5089
70	-42374.4468	-42361.5294	-42369.4398
80	-42374.4602	-42361.5786	-42369.4749
90	-42374.4696	-42361.6094	-42369.5041
100	-42374.4634	-42361.5988	-42369.4882
110	-42374.4422	-42361.5600	-42369.4562
120	-42374.4310	-42361.5404	-42369.4455
130	-42374.4441	-42361.5622	-42369.4615
140	-42374.4524	-42361.5884	-42369.4761
150	-42374.4607	-42361.6022	-42369.4847
160	-42374.4763	-42361.6243	-42369.5133
170	-42374.4813	-42361.6179	-42369.5016
180	-42374.4690	-42361.5612	-42369.4698
<b>Si<sub>4</sub></b>	<b>B3LYP</b>	<b>M06</b>	<b><math>\omega\text{B97X-D}</math></b>
0	-31673.5547	-31669.8743	-31671.0672
10	-31673.5581	-31669.8794	-31671.0740
20	-31673.5686	-31669.8928	-31671.0897
30	-31673.5829	-31669.9009	-31671.1003
40	-31673.5914	-31669.9044	-31671.1076
50	-31673.5989	-31669.9026	-31671.1120
60	-31673.6031	-31669.9053	-31671.1151
70	-31673.6028	-31669.8992	-31671.1086
80	-31673.6001	-31669.8957	-31671.1055
90	-31673.5918	-31669.8897	-31671.1012
100	-31673.5848	-31669.8836	-31671.0922
110	-31673.5832	-31669.8807	-31671.0859
120	-31673.5834	-31669.8813	-31671.0843
130	-31673.5874	-31669.8850	-31671.0862
140	-31673.5920	-31669.8867	-31671.0897
150	-31673.5980	-31669.8896	-31671.0940
160	-31673.6077	-31669.8953	-31671.1026
170	-31673.6113	-31669.8970	-31671.1053
180	-31673.6082	-31669.8982	-31671.1045

Table A2 Molecular energy of  $MPSi_4$  and  $MPC_4$

<b>MPSi<sub>4</sub></b>	<b>B3LYP</b>	<b>M06</b>	<b>wB97X-D</b>
0	-63243.7477	-63215.1785	-63231.9518
10	-63243.7714	-63215.2093	-63231.9754
20	-63243.7936	-63215.2654	-63232.0077
30	-63243.8449	-63215.3360	-63232.0675
40	-63243.8771	-63215.3856	-63232.1240
50	-63243.9069	-63215.4072	-63232.1420
60	-63243.9276	-63215.4075	-63232.1635
70	-63243.9571	-63215.4525	-63232.1977
80	-63243.9558	-63215.4535	-63232.2014
90	-63243.9383	-63215.4049	-63232.1451
100	-63243.9221	-63215.3826	-63232.1100
110	-63243.8803	-63215.3268	-63232.0544
120	-63243.8860	-63215.2933	-63232.0451
130	-63243.8817	-63215.3306	-63232.0789
140	-63243.8859	-63215.3686	-63232.1092
150	-63243.9001	-63215.3794	-63232.1144
160	-63243.9043	-63215.3833	-63232.1193
170	-63243.9192	-63215.4479	-63232.1636
<b>MPC<sub>4</sub></b>	<b>B3LYP</b>	<b>M06</b>	<b>wB97X-D</b>
0	-35874.6076	-35846.9739	-35864.4320
20	-35874.6272	-35847.0092	-35864.4911
40	-35875.3897	-35847.8253	-35865.3326
60	-35875.4887	-35847.9051	-35865.4164
80	-35875.6933	-35848.0955	-35865.6417
100	-35875.5741	-35847.9624	-35865.5044
120	-35875.2577	-35847.5943	-35865.1091
140	-35875.4912	-35847.9076	-35865.4515
160	-35875.7478	-35848.2443	-35865.8246
180	-35875.7007	-35848.1491	-35865.7227

Table A3 Molecular energy of *cyc*- $HMSi_4$

<b>cyc-<math>HMSi_4</math></b>	<b>B3LYP</b>	<b>M06</b>	<b>wB97X-D</b>
0	-63637.8187	-63608.9788	-63628.3597
20	-63637.7818	-63608.8900	-63628.2764
40	-63637.9084	-63609.0985	-63628.4743
60	-63637.9474	-63609.0850	-63628.4748
80	-63637.9780	-63609.0780	-63628.4585
100	-63637.9847	-63609.0856	-63628.4616
120	-63637.9282	-63609.0031	-63628.3873
140	-63638.0492	-63609.1461	-63628.5440
160	-63638.0927	-63609.2238	-63628.6040
180	-63638.0820	-63609.1696	-63628.5667

## **Research Paper V:**

**HANULIKOVA, Barbora** and Ivo KURITKA.

Theoretical study of polaron binding energy in conformationally disrupted oligosilanes

*Journal of Molecular Modeling*. 2014, vol. 20, no. 10, pp. 2442-2450.



# Theoretical study of polaron binding energy in conformationally disrupted oligosilanes

Barbora Hanulikova · Ivo Kuritka

Received: 9 June 2014 / Accepted: 26 August 2014 / Published online: 24 September 2014  
© Springer-Verlag Berlin Heidelberg 2014

**Abstract** Density functional theory was used for a quantum chemical study of oligo[methyl(phenyl)silylene] structures containing a conformational defect: a kink in the silicon backbone. Oligomers were studied in the neutral state as well as in the form of positive ( $P^+$ ) and negative ( $P^-$ ) polaron quasiparticles. Computations performed using the B3LYP model and the 6-31G(d) basis set revealed that the charge distribution is not influenced by the presence of the kink, but the positive charge on the Si backbone differs slightly in  $P^+$  and  $P^-$  quasiparticles. On the other hand, the spin density is significantly shifted away from the chain part that contains the kink, and this effect is more intense in  $P^-$  polarons. Changes in electron density are also evident from the frontier molecular orbital distribution. The deformation energy (which is associated with the relaxation of polarons) decreases with the number of atoms in the oligomer backbone in  $P^+$  but shows the opposite behavior for  $P^-$  quasiparticles.

**Keywords** Oligo[methyl(phenyl)silylene] · Polaron · Spin density · Charge · Density functional theory

## Introduction

Polymers that contain silicon (Si) atoms as the structural units in their backbones show remarkable and unique electron properties. Electrons are delocalized along the chain since the vicinal and geminal Si orbitals overlap, enabling the formation of a continuous space that can be occupied by  $\sigma$

electrons. This  $\sigma$  conjugation is similar and often compared to  $\pi$  conjugation in compounds with carbon backbones, even though they have different origins [1–3]. Poly[methyl(phenyl)silylene] (PMPSi) is a commonly studied polymer of this type because it is attainable, processable, and presents both  $\sigma$  and  $\pi$  bonds on the backbone and aromatic substituent, respectively. Further, PMPSi is a semicrystalline polymer with properties that are influenced by both the backbone conformation and the presence of substituents [4]. Generally, the conformations of polysilylenes are described by the values of dihedral angles, each of which is defined by the relative positions of four successive silicon atoms [5]. The ideal conformation is all-*anti*, meaning that the silicon chain is stretched, all dihedral angles are equal to  $180^\circ$ , electrons are regularly delocalized, and  $\sigma$  conjugation is maximized [6]. However, the presence of a bulky substituent such as a phenyl group discourages this arrangement, leading to the formation of a left- or right-handed helix structure with dihedral angles close to the *deviant* ( $150^\circ$ ) or *transoid* ( $165^\circ$ ) conformation [7, 8]. The difference between these two conformations is depicted visually in Fig. 1.

Some backbone deformations or defects, such as bends in the chains and disruptions to the ideal conformation, can appear in the chains. As would be expected, such backbone defects influence the properties of the polymer that are related to electron delocalization, such as the absorption maximum ( $\lambda_{\max}$ ) or the course of the excitation process itself, since it can disrupt the overlaps between orbitals. We performed a theoretical investigation of such a defect—a kink consisting of four silicon atoms in an approximately *gauche* conformation, which was introduced into oligo[methyl(phenyl)silylene] chains—in our previous work [9]. It was discovered that  $\lambda_{\max}$  shifted to shorter wavelengths as the position of the kink was moved towards the center of the oligomer. Moreover, when the chain was divided into a longer and a shorter part by the

B. Hanulikova (✉) · I. Kuritka  
Centre of Polymer Systems, University Institute, Nad Ovcimou  
3685, 76001 Zlín, Czech Republic  
e-mail: hanulikova@ft.utb.cz

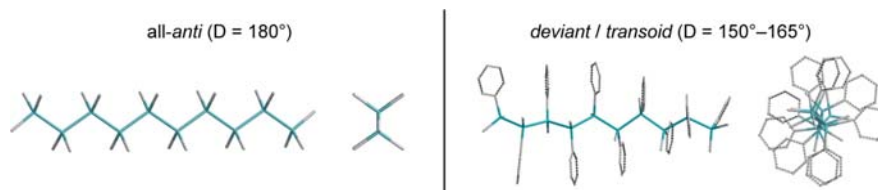


**Fig. 1** Ideal deca(dimethylsilylene) (*all-anti*) and real deca[(methyl)phenylsilylene] (*deviant/transoid*) conformations of a decasilane chain ( $D$  dihedral angles in the silicon backbone)

kink, the frontier molecular orbitals were delocalized more on the longer part of the chain.

Another deeply investigated area of poly/oligosilylene molecules is their ability to form polaron quasiparticles. A polaron quasiparticle is a relaxed system with either a positive or a negative excess charge. It can be considered a (macro)molecule that alters the positions of its atoms in order to minimize its potential energy when a charge carrier is present [10]. Theoretical research in this field (primarily on equilibrium geometries, charge distributions, and polaron binding energies) is described in [10–15]. Si–Si bonds in both positive and negative polaron quasiparticles are longer than those found in the neutral geometry. Bond angles are smaller, and dihedral angles are similar in positive polarons and neutral molecules [10]. On the other hand, the bond angles are stretched in negatively charged polarons [11]. In addition, excess charge is accumulated on the attached substituents, whereas the spin density is greatest on the backbone [10–14]. Changes in energy between neutral and charged states of a molecule can be expressed via the polaron binding energy  $E_p$ , which consists of a deformation energy part and an electron–photon energy part. The former represents, on average, 90 % of the  $E_p$  of a polymer molecule, because the process of relaxation involves a significant change in the macromolecular conformation (i.e., shifts in the equilibrium positions of the atoms). The latter is obtained from the difference in the vibrational frequencies of the neutral molecule and the relaxed molecule [10]. Experimentally,  $E_p$  is found to have a value of 0.29 eV [16–19], which is in good agreement with theoretically calculated values, which are 0.20 eV on average [12]. All of these results were obtained from theoretical studies of oligomer-sized chains in the *all-anti* conformation. However, there were no reported studies of molecules with both a chain defect (a kink) and a polaron, so the present paper investigates such systems. Even though the *all-anti* conformation is an ideal case, kinks are conformational defects that are responsible for polymer chain folding or coil formation in real materials.

Therefore, the aim of the work reported in this paper was to describe the influence of a kink in an oligo[methyl(phenyl)silylene] chain in the form of a positive ( $P^+$ ) or a negative ( $P^-$ ) polaron quasiparticle. Equilibrium geometries, spin densities, charges, and deformation energies were investigated using density functional theory (DFT) and

the B3LYP hybrid model with the 6-31G(d) basis set. This level of theory and this model were chosen because they have already been successfully employed to perform calculations similar to those of interest to us in the present work (see, for instance, [10–13, 20]).

### Computational methods

Oligo[methyl(phenyl)silylene] (OMPS $_n$ ) molecules were investigated via quantum chemical calculations performed in the Spartan '08 software (Wavefunction, Inc., Irvine, CA, USA) [21]. Oligomers ranging from two to ten repeated units in length were studied by DFT with the B3LYP (Becke–3-parameter–Lee–Yang–Parr) hybrid model and the 6-31G(d) basis set. Each end of the Si backbone was capped with a methyl group, and no geometric constraints were placed on the calculation. The molecules were treated as isolated in a vacuum environment.

Each molecule of OMPS $_n$  was optimized with the theory described above. Structures of approximately *transoid* conformation were attained in the first step of the calculation. Afterwards, a set of semi-empirical PM3 calculations was performed to obtain energy profiles of the oligosilane conformers ( $n \geq 4$ ) with different values of the dihedral angle representing the kink which, in the ideal case, adopts the *syn* ( $0^\circ$ ) conformation. Using a plot of energy against dihedral angle, the most suitable conformers containing the kink were chosen and set as initial guesses for another structural optimization by DFT/B3LYP 6-31G(d) in order to obtain a new energy minimum, as well as to establish the geometry of the required kink more precisely. To ensure that the most appropriate results were obtained (i.e., to get the smallest kink angle possible and the true potential energy minimum), several geometry optimizations were run for each oligomer from different initial values of the kink angle. After optimization, this dihedral angle was measured virtually, which yielded values of 50–60° for all oligosilylenes, i.e., a kink with an approximately *gauche* conformation was formed.

Further, positive and negative polaron quasiparticles were created from the optimized structures in the cationic or anionic state, respectively. Firstly, the calculations were performed using the single point energy to obtain the oligomer [10] in the hot (i.e., unrelaxed) state. Finally, the polaron geometry

was optimized, which led to the formation of the relaxed structure. The unrestricted B3LYP model was used for these calculations, as it is suitable for open-shell systems. All other settings were kept the same.

## Results and discussion

### Geometry

The results of geometry optimization of neutral oligomers by DFT B3LYP/6-31G(d) are depicted in Fig. 2. As can be seen, the oligomer chain can adopt several conformations that differ in the position of the kink. Ten Si atoms in the chain enable the creation of four different structures with a kink. The number of potential kink positions is dependent on the number of silicon atoms in the backbone. For oligomers containing four or more units, the number of possible kink positions increases by one every two monomers added to the backbone. Figure 2 also provides information about the designation of the kink location in oligomers. The value (**10**) represents the size of the oligomer and the letter (**A**) shows where the first atom of the kink is located.

The dihedral angle for the kink was measured for each oligomer. The average value was  $54.7^\circ$ , irrespective of the direction in which the angle was measured. This angle increased during positive polaron ( $P^+$ ) formation to  $69.0^\circ$  but remained unchanged during negative quasiparticle ( $P^-$ ) formation ( $54.7^\circ$  on average).

Our investigation of the Si–Si bonds revealed (see Fig. 3) that these bonds lengthened during polaron relaxation. This effect was slightly more intense for  $P^+$  than for  $P^-$ . The longest bonds in molecules without the kink were found in the central part of the structure for all neutral ( $P^0$ ),  $P^+$ , and  $P^-$  oligomers. Another interesting fact can be ascertained from the lengths of the kink bonds. Each kink contains three bonds that are inconsistent in length when compared with the defectless

chain. The next adjacent bond right after the kink shows the longest length, which is significantly above average. The exception to this rule is the **10D** oligomer, where the longest bond is part of the kink. Similar trends can be observed for both the  $P^+$  and  $P^-$  structures.

A comparison of the bond lengths in other investigated  $OMPSi_n$  also revealed that the changes in bond lengths are greater in very short chains (2–4 units long). This may be due to the fact that atoms in short chains are less limited by the presence of other atoms and functional groups.

Bond angles are shown in Fig. 4. The angles in a defectless  $P^-$  decamer chain are about  $7^\circ$  higher than those in the neutral form, and they are highest in the central part of the backbone. Negative polarons are therefore more open structures. On the contrary,  $P^+$  structures without the kink have angles that are  $5^\circ$  smaller and the largest angles occur at the edges of the chain (as in the neutral case). These results are in agreement with those reported in the literature, as described in the “Introduction.” The insertion of a kink, however, caused the bond angles to change again. As can be seen in **10A–10D** of  $P^0$  and  $P^+$ , the largest bond angle is reached at the location of the kink. More precisely, the largest bond angle is the first angle in **10A–10C** and the second angle in **10D**, as the kink consists of two angles. This suggests that the part containing the defect stretches more than the rest of the chain, the angles of which are closer to those seen in the defectless chain. The situation is more complicated in  $P^-$ , as the highest angles are located furthest from the kink. Therefore, the part of the chain that is close to the kink contracts, as the angles are smaller than in the defectless chain. On the other hand, the remainder of the backbone is significantly stretched, as the angles are higher than in the no-kink chain.

### Charge and spin distribution

Other monitored properties of oligosilanes are connected to the electron density distribution before and after polaron

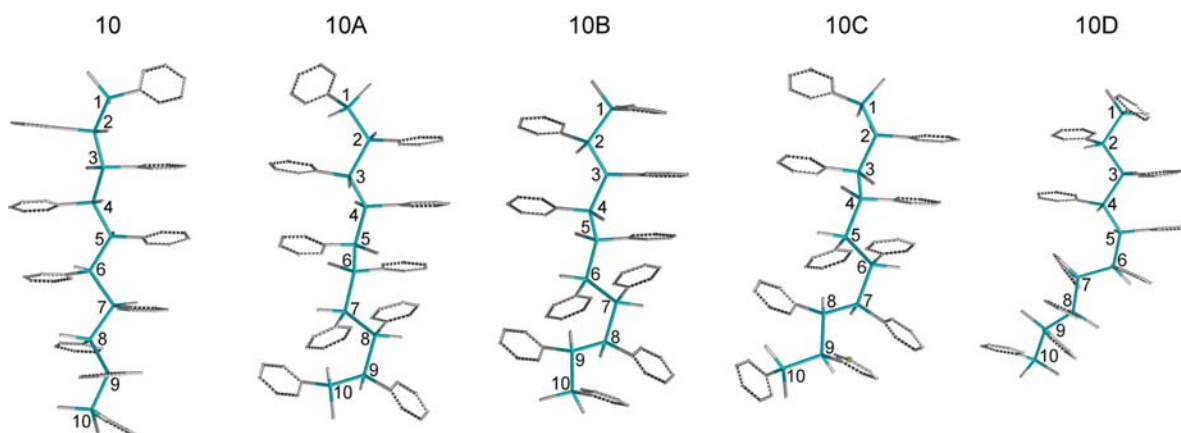
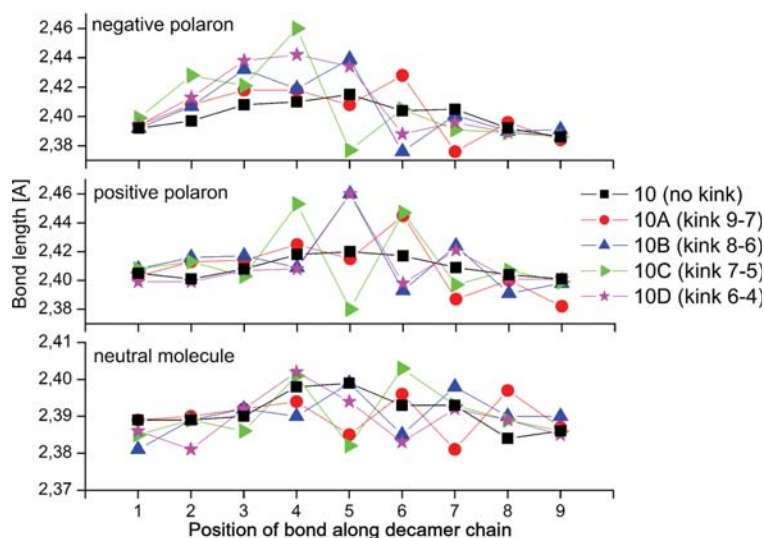


**Fig. 2** Optimized structures (DFT B3LYP/6-31G(d)) of  $OMPSi_{10}$ , with atom numbering and molecule designation shown (H atoms are omitted)

**Fig. 3** Bond lengths (Si–Si) in the decamer chain, as calculated with DFT B3LYP/6-31G(d)



formation. Figure 5 shows the distribution of natural charge along the backbone of the decamer. The results for the  $P^0$ ,  $P^+$ , and  $P^-$  molecular states are displayed and compared. All Si chains are positively charged, with the highest charges seen on the edge atoms. This is probably due to Coulomb repulsion, which pushes the positive charge to the edges. The  $P^+$  state carries more charge, approximately  $0.05 e$ , than the neutral structure. If marginal atoms are not considered, the central part of the  $P^+$  decamer is the area with the highest charge. On the other hand, the  $P^-$  decamer carries a slightly lower charge (average difference  $0.05 e$ ) than the neutral molecule. Again, the lowest charge can be found at the center of the decamer. Figure 5 also presents a similar plot for carbon atoms from the methyl group and phenyl ring. The group of carbon atoms

attached to a particular silicon atom (Si number 4 for example) is indicated by a rectangle. Methyl carbons carry a negative charge of around  $-1.17 e$ , carbons that link the Si chain to the phenyl ring have a charge of  $-0.48 e$ , and other carbons in the phenyl ring carry a charge of  $-0.23 e$ . The charges on structures containing the kink were compared with these curves, and their dependencies are shown in Fig. 6. However, this did not lead to any new insight as the differences between particular molecules are very slight. Therefore, it can be said that the kink does not cause any significant change in the charge distribution.

Figure 7 shows the spin distribution along the decamer backbone. The left graph shows the spin distributions for  $P^+$  quasiparticles and the right graph shows the distributions for

**Fig. 4** Bond angles (Si–Si–Si) in the decamer chain, as calculated with DFT B3LYP/6-31G(d)

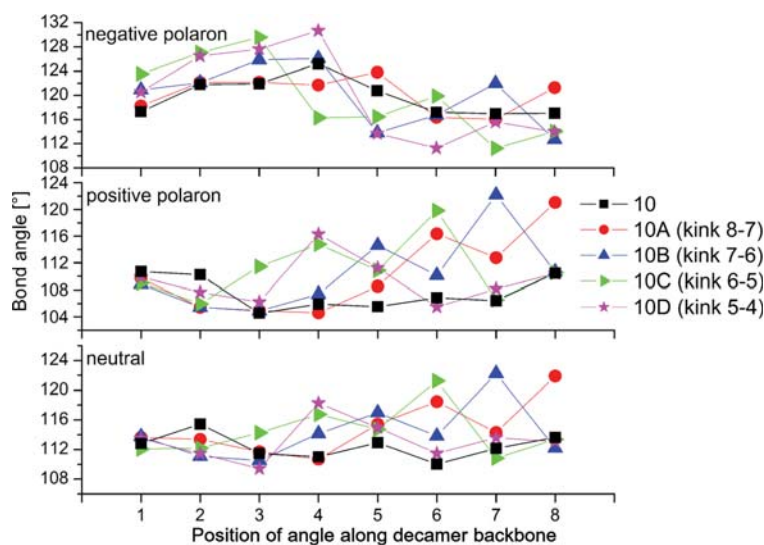
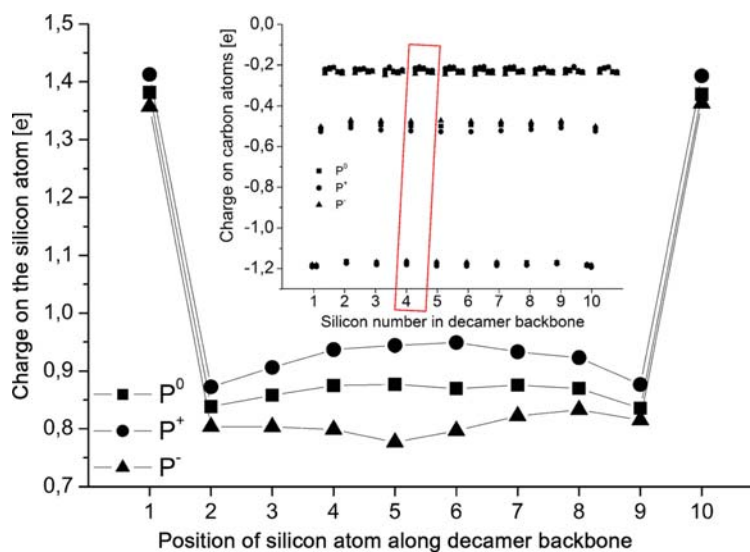




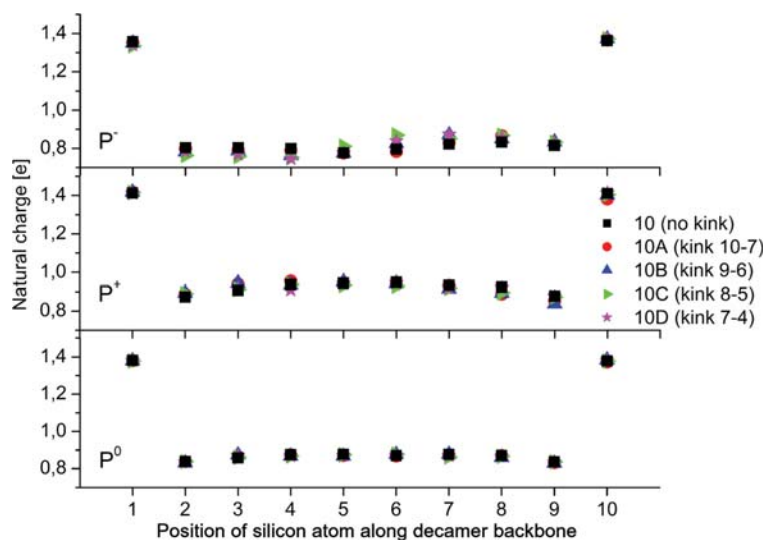
**Fig. 5** Natural charge distribution along the silicon chain and on the carbon atoms in decamer **10**, as calculated with DFT B3LYP/6-31G(d)



$P^-$  quasiparticles. In both of the defectless cases, the highest spin density is located in the central part of the backbone, which is in agreement with [11]. At the same time, the difference between the spin densities for  $P^-$  and  $P^+$  is about  $0.07 e/\text{au}^3$  at most. Further, introducing a kink significantly influences the spin density distribution. As can be observed in the plots for **10A–10D**, the spin density changes when the position of the kink in the chain is altered. The  $\sigma$ -orbital conjugation is disrupted by this conformational anomaly, which is displayed in the form of Kohn–Sham orbitals in Fig. 8. Therefore, the spin density is shifted away from the kink region to the regular parts of the oligomers, where it reaches its maximum.

As mentioned above and depicted in Fig. 8, the presence of a defect in the chain (the kink as well as the polaron) impacts on the delocalization of the HOMO (the highest occupied molecular orbital) and the LUMO (the lowest unoccupied molecular orbital). In neutral molecules (such as **10**), the HOMO and LUMO are regularly delocalized along the whole Si backbone. When the kink is introduced and the chain is divided by its presence into longer and shorter parts, the HOMO shifts to the longer part of the backbone. At the same time, the more symmetrical the division of the backbone by the kink, the more regularly the HOMO is delocalized. The LUMOs are concentrated in the central parts of the oligosilane chains on silicon atoms as well as on three adjacent phenyl

**Fig. 6** Natural charge along the Si backbone for all decamer structures in  $P^0$ ,  $P^+$ , and  $P^-$  form, as calculated with DFT B3LYP/6-31G(d)



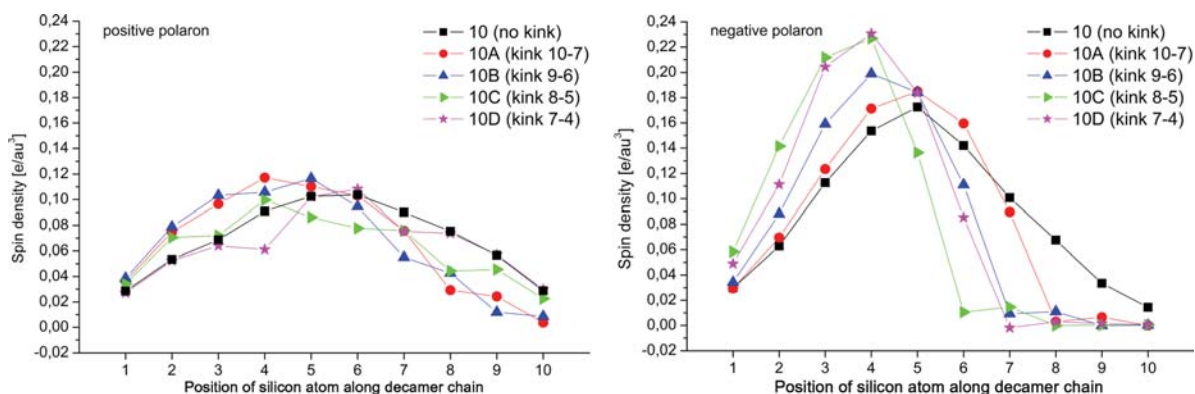


**Fig. 7** Spin distribution along the silicon decamer chain, as calculated with DFT B3LYP/6-31G (d). *Left panel:* positive polaron structures. *Right panel:* negative polaron structures

rings.  $P^+$  quasiparticles show a similar trend in the HOMO distribution to that seen for neutral molecules. However, they differ in the delocalization of the HOMOs, which are also present on the phenyl rings that are close to the kink. The LUMOs are only distributed in the center of

the chain on two or three phenyl rings that are attached to Si numbers 4, 5, and 6.

Finally, the HOMOs of negative polaron molecules alter considerably when a kink is inserted. These orbitals are delocalized on the Si atoms and they are located on the longer

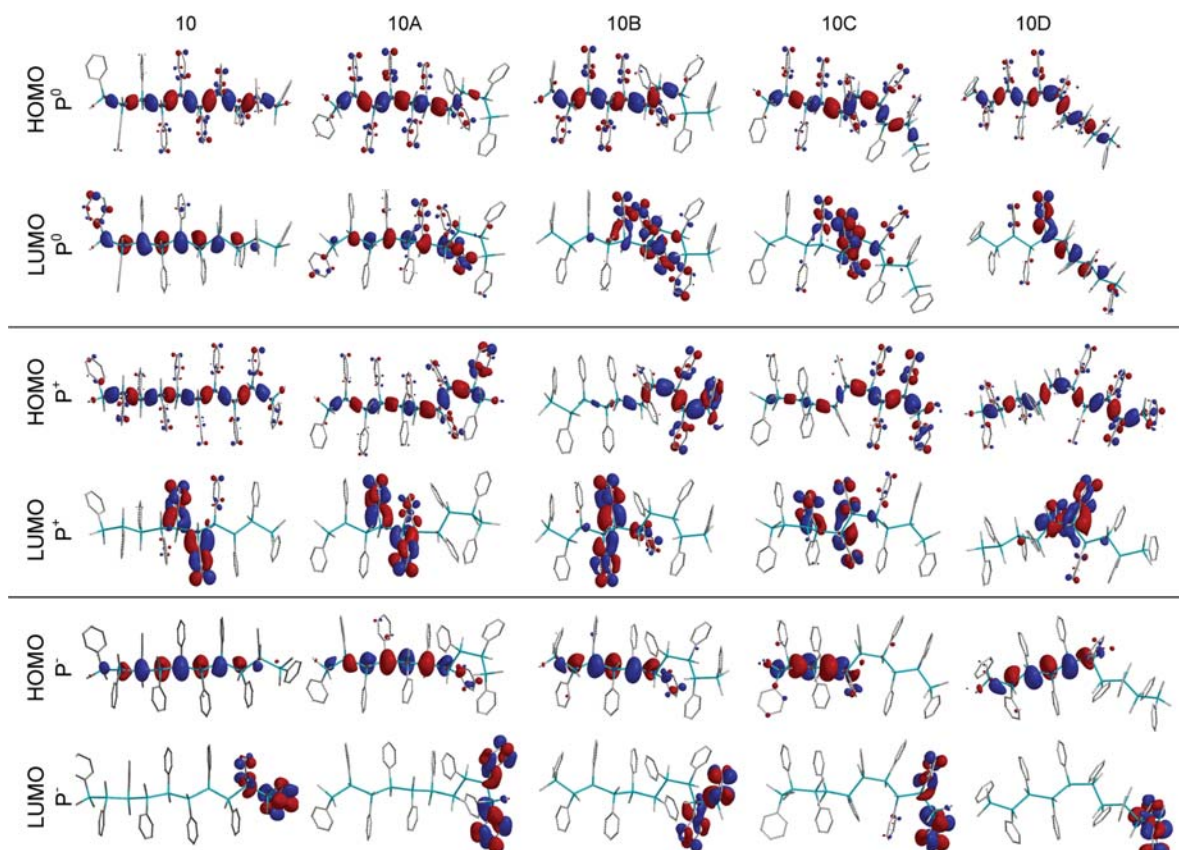
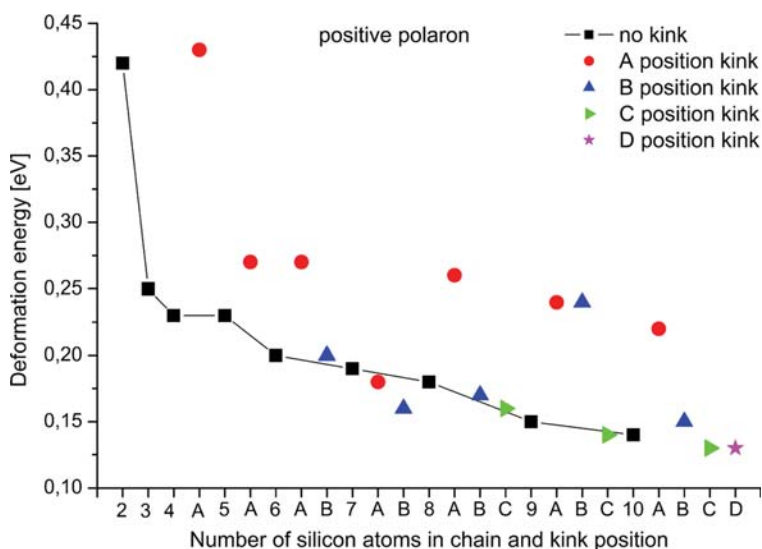


**Fig. 8** Frontier molecular orbital (HOMO and LUMO) delocalization in  $P^0$ ,  $P^+$ , and  $P^-$  molecules, as calculated with DFT B3LYP/6-31G(d)

**Fig. 9**  $E_{\text{def}}$  of each  $\text{OMPSi}_n$  in the form of a positive polaron



parts of kinked chains. Even in the symmetrical case (**10D**), the HOMO is located only on one part of the backbone. The LUMOs of  $\text{P}^-$  are also strictly localized on the phenyl ring, as in  $\text{P}^+$  molecules, but they are located at different positions. They are distributed on the phenyls attached to Si numbers 9 and 10, and they ignore the presence of the kink and its position.

Polaron binding energy and deformation energy

The polaron binding energy ( $E_p$ ) consists of two terms: the deformation energy ( $E_{\text{def}}$ ) and the electron-photon energy

( $E_{\text{el-ph}}$ ). Since segments can move relatively easily in oligomer molecules,  $E_{\text{def}}$  comprises most of  $E_p$  (about 90 %) for such molecules. Therefore,  $E_{\text{def}}$  was plotted for the positive and negative polaron quasiparticles derived from all of the studied oligomers, and these are displayed in Figs. 9 and 10, respectively. First, let us consider  $\text{OMPSi}_n$  without the kink defect. As can be seen, both graphs can be divided into parts associated with very short oligomers (2–4 units) and with longer chains. For  $\text{P}^+$ ,  $E_{\text{def}}$  decreases rapidly with oligomer length until the pentamer, after which the decrease in  $E_{\text{def}}$  is much more gradual. Our investigation of geometries revealed that there is a significant influence of the relaxation process on

**Fig. 10**  $E_{\text{def}}$  of each  $\text{OMPSi}_n$  in the form of a negative polaron

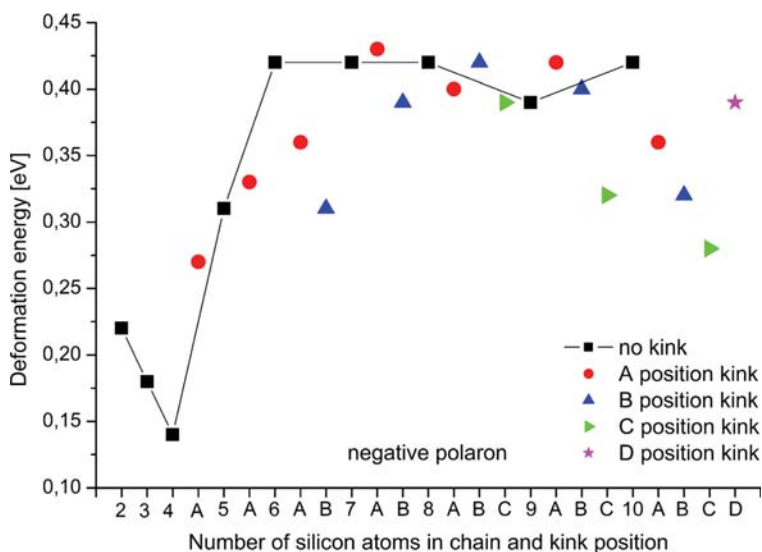


**Table 1** Values of  $E_{\text{def}}$ ,  $E_{\text{el-ph}}$ , and  $E_{\text{p}}$  in eV, as calculated according to [10] (estimated values are shown in italics)

Molecule	$\text{P}^+$			$\text{P}^-$		
	$E_{\text{p}}$	$E_{\text{def}}$	$E_{\text{el-ph}}$	$E_{\text{p}}$	$E_{\text{def}}$	$E_{\text{el-ph}}$
<b>2</b>	0.43	0.42	0.01	0.37	0.22	0.15
<b>3</b>	0.26	0.25	0.01	0.31	0.18	–
<b>4</b>	0.23	0.23	–0.01	0.27	0.14	–
<b>4A</b>	0.44	0.43	0.01	0.40	0.27	–
<b>5</b>	0.21	0.23	–0.02	0.45	0.31	0.14
<b>5A</b>	0.27	0.27	0.00	0.48	0.33	0.15
<b>6</b>	0.17	0.20	–0.03	0.54	0.42	0.12
<b>6A</b>	0.25	0.27	–0.02	0.47	0.36	0.11
<b>6B</b>	0.18	0.20	–0.02	0.42	0.31	0.11
<b>7</b>	<i>0.19</i>	0.19	–	0.55	0.42	0.13
<b>7A</b>	<i>0.17</i>	0.18	–	0.55	0.43	–
<b>7B</b>	<i>0.19</i>	0.16	–	0.56	0.39	–
<b>8</b>	<i>0.27</i>	0.18	–	0.52	0.42	–
<b>8A</b>	<i>0.18</i>	0.26	–	0.55	0.39	–
<b>8B</b>	<i>0.17</i>	0.17	–	0.53	0.42	–
<b>8C</b>	<i>0.16</i>	0.16	–	0.55	0.39	–
<b>9</b>	<i>0.25</i>	0.15	–	0.52	0.39	–
<b>9A</b>	<i>0.25</i>	0.24	–	0.52	0.42	–
<b>9B</b>	<i>0.15</i>	0.24	–	0.55	0.40	–
<b>9C</b>	<i>0.15</i>	0.14	–	0.53	0.32	–
<b>10</b>	<i>0.23</i>	0.14	–	0.45	0.42	–
<b>10A</b>	<i>0.16</i>	0.22	–	0.55	0.36	–
<b>10B</b>	<i>0.14</i>	0.15	–	0.49	0.32	–
<b>10C</b>	<i>0.14</i>	0.13	–	0.45	0.28	–
<b>10D</b>	<i>0.19</i>	0.13	–	0.41	0.39	–

the geometries of short oligomers. Hence, the higher values of  $E_{\text{def}}$  can be explained by this considerable change in geometry (e.g., bond lengths).

Negative polarons show a different trend in  $E_{\text{def}}$  with oligomer length. Surprisingly (considering the conclusion of the previous paragraph), in this case the longer oligomers show higher deformation energies. However, the bond angles must be also taken into account when describing the geometry, and it is worth noting that (as depicted in Fig. 4) the highest difference between the neutral molecule and the  $\text{P}^+$  decamer is  $6^\circ$ , whereas the highest difference between the  $\text{P}^0$  and  $\text{P}^-$  OMPSi<sub>10</sub> is  $15^\circ$  (bond number 6).

Hence,  $\text{P}^-$  relaxation greatly affected some bond angles, and these particular changes in geometry were probably more influential than the changes in bond lengths, leading to an increased  $E_{\text{def}}$  for the longer oligomers.

Table 1 summarizes all of the computed  $E_{\text{p}}$ ,  $E_{\text{def}}$ , and  $E_{\text{el-ph}}$  values. It is clear that the difference between  $E_{\text{p}}$  and  $E_{\text{def}}$  is given by  $E_{\text{el-ph}}$ , which seems to have a similar value for all oligomers (although many of the  $E_{\text{el-ph}}$  values for the longer oligomers were not computed due to the excessive computational time required to do so). The average value for positive

polarons is  $|0.01|$  eV and that for negative polarons is  $|0.13|$  eV. Note that  $E_{\text{def}}$  for  $\text{P}^-$  quasiparticles is no smaller than  $E_{\text{def}}$  for  $\text{P}^+$  quasiparticles, but  $E_{\text{p}}$  for  $\text{P}^-$  quasiparticles is significantly higher than  $E_{\text{p}}$  for  $\text{P}^+$  quasiparticles, which means that the  $E_{\text{el-ph}}$  contribution for  $\text{P}^-$  quasiparticles is much higher than the corresponding contribution for  $\text{P}^+$  quasiparticles. To summarize the whole situation for  $E_{\text{p}}$ , Table 1 also displays estimated  $E_{\text{p}}$  values (in italics) for the molecules for which  $E_{\text{el-ph}}$  could not have been computed. They were estimated by adding 0.01 eV to  $E_{\text{def}}$  for  $\text{P}^+$  and adding 0.13 eV to  $E_{\text{def}}$  for  $\text{P}^-$ , respectively.

## Conclusions

A computational investigation of oligo[methyl(phenyl)silylene]s into which a kink was introduced, leading to the disruption of the backbone conformation, revealed that this defect exerts a significant influence on the relaxation processes of positive and negative polaron quasiparticles. In particular, the spin density distribution is sensitive to the presence of the conformational anomaly.

Overlaps between molecular orbitals and the delocalization of these orbitals are disturbed, which has a direct impact on the electron distribution. When the kink is inserted such that it divides the chain into longer and shorter parts, the delocalized HOMOs are shifted towards the longer part. The LUMOs are only delocalized on the phenyl rings in the  $P^+$  and  $P^-$  quasiparticles, and this delocalization is seemingly independent of the presence of a kink. In the  $P^+$  quasiparticles, the LUMOs are located on the central phenyls, whereas they are on the edge phenyls in the  $P^-$  quasiparticles.

While the spin distribution is significantly affected, the charge distribution is only slightly influenced by the introduction of a kink. There are differences between  $P^0$ ,  $P^+$ , and  $P^-$  in the central region of the backbone. However, the introduction of the kink does not cause a substantial charge redistribution.

The change in the deformation energy, which is the change in energy associated with the process of relaxation from the neutral molecule to the polaron quasiparticle, was found to present opposite trends for  $P^+$  and  $P^-$ . This is because the change in deformation energy is related to changes that occur to the geometry of the oligosilylene. Nevertheless, the shorter chains can easily adjust their geometries during the relaxation process, whereas longer chains can undergo larger changes in geometry but those changes only occur to a particular part of the chain.

**Acknowledgments** This work was supported by the Internal Grant Agency of Tomas Bata University in Zlín (grant no. IGA/FT/2014/006). This paper was written with the support of the Operational Program Research and Development for Innovations, co-funded by the European Regional Development Fund (ERDF) and the national budget of the Czech Republic, within the framework of the Centre of Polymer Systems (reg. number: CZ.1.05/2.1.00/03.0111) project, and with the support of the Operational Program Education for Competitiveness, co-funded by the European Social Fund (ESF) and the national budget of the Czech Republic, within the framework of the Advanced Theoretical and Experimental Studies of Polymer Systems (reg. number: CZ.1.07/2.3.00/20.0104) project.

## References

- Demchenko YV, Klimovic J, Nespurek S (2004) Optical spectroscopy of poly silylene films. *Macromol Symp* 212:461–466
- Nespurek S, Wang G, Yoshino K (2005) Polysilanes—advanced materials for optoelectronics. *J Optoelectron Adv M* 7:223–230
- Semenov VV (2011) Preparation, properties and applications of oligomeric and polymeric organosilanes. *Russ Chem Rev* 80:313–339
- Mark JE, Allcock HR, West R (2005) *Inorganic polymers*. Oxford University Press, New York
- Michl J, West R (2000) Conformations of linear chains. Systematics and suggestions for nomenclature. *Acc Chem Res* 33:821–823
- Fogarty HA, Ottosson C-H, Michl J (2000) The five favoured backbone conformations of  $n$ -Si<sub>4</sub>Et<sub>10</sub>: *cisoid*, *gauche*, *ortho*, *deviant* and *transoid*. *J Mol Struct THEOCHEM* 506:243–255
- Fujiki M (2003) Switching handedness in optically active polysilanes. *J Organomet Chem* 685:15–34
- Karatsu T (2008) Photochemistry and photophysics of organo monosilane and oligosilanes: updating their studies on conformation and intermolecular interactions. *J Photochem Photobiol C* 9:111–137
- Hanulikova B, Kuritka I (2014) Manifestation of conformational defect on electronic spectra of polysilanes—a theoretical study. *Macromol Symp* 339:100–111
- Nozar J, Nespurek S, Sebera J (2012) Polaron binding energy in polymers: poly[methyl(phenyl)silylene]. *J Mol Model* 18:623–629
- Toman P, Nespurek S, Jang JW, Lee CE (2002) Conformation changes of polysilanes during the polaron formation. *Curr Appl Phys* 2: 327–330
- Nespurek S, Kochalska A, Nozar J, Kadashchuk A, Fishchuk II, Sworakowski J, Kajzar F (2010) Feature of polaronic charge carriers in polysilanes: experimental and theoretical approach. *Mol Cryst Liq Cryst* 521:72–83
- Toman P (2000) Quasiparticle in  $\sigma$ -conjugated polymers. *Synth Met* 109:259–261
- Nespurek S, Nozar J, Kadashchuk A, Fishchuk II (2009) Polaronic transport in polysilanes. *J Phys Conf Ser* 193:012108
- Nespurek S, Kadashchuk A, Fishchuk II, Arkhipov VI, Emelianova EV (2005) Polarons in polysilanes: theoretical background and experimental detection. In: *Proc Int Symp Electrets (ISE-12)*, Salvador, Brazil, 11–14 Sept 2005, pp 216–219
- Nespurek S, Valerian V, Eckhardt A, Herden V, Schnabel V (2001) Charge carrier transport in poly[methyl(phenyl)silylene]: the effect of additives. *Polym Adv Technol* 12:306–318
- Nespurek S, Eckhardt A (2001) Poly(silylene)s: charge carrier photogeneration and transport. *Polym Adv Technol* 12:427–440
- Nespurek S, Sworakowski J, Kadashchuk A, Toman P (2003) Poly silylenes: charge carrier transport and photogeneration. *J Organomet Chem* 685:269–279
- Nespurek S, Schauer F, Kadashchuk A, Fishchuk II (2007) Polarons in wide-band-gap molecular materials: polysilanes. *J Non-Cryst Solids* 353:4474–4478
- Hehre WJ (2003) *A guide to molecular mechanics and quantum chemical calculations*. Wavefunction, Inc., Irvine
- Shao Y, Molnar LF, Jung Y, Kussmann J, Brown ST, Ochsenfeld C, Gilbert ATB, Slipchenko LV, Levchenko SV, O'Neill DP, DiStasio RA Jr, Lochan RC, Wang T, Beran GJO, Besley NA, Herbert JM, Lin CY, Van Voorhis T, Chien SH, Sodt A, Steele RP, Rassolov VA, Maslen PE, Korambath PP, Adamson RD, Austin B, Baker J, Byrd EFC, Dachselt H, Doerksen RJ, Dreuw A, Dunietz BD, Dutoi AD, Furlani TR, Gwaltney SR, Heyden A, Hirata S, Hsu C-P, Kedziora G, Khalliulin RZ, Klunzinger P, Lee AM, Lee MS, Liang WZ, Lotan I, Nair N, Peters B, Proynov EI, Pieniazek PA, Rhee YM, Ritchie J, Rosta E, Sherrill CD, Simmonett AC, Subotnik JE, Woodcock HL III, Zhang W, Bell AT, Chakraborty AK, Chipman DM, Keil FJ, Warshel A, Hehre WJ, Schaefer HF, Kong J, Krylov AI, Gill PMW, Head-Gordon M (2006) Advances in methods and algorithms in a modern quantum chemistry program package. *Phys Chem Chem Phys* 8:3172–3191